UNIVERSIDAD MICHOACANA DE SAN NICOLÁS DE HIDALGO

INSTITUTO DE INVESTIGACIONES QUÍMICO BIOLÓGICAS

LABORATORIO DE BIOTECNOLOGÍA MICROBIANA

"Participación del sistema ISC en el daño oxidativo y la disfunción mitocondrial dependiente de Fe en *Saccharomyces cerevisiae*"

TESIS que presenta el:

M.C. Mauricio Gómez Gallardo

Para obtener el grado de:

Doctor en Ciencias Biológicas, Opción Biología Experimental

Asesor: D.C. Jesús Campos García

Co-asesor: D.C. Christian Cortés Rojo

Morelia, Michoacán, Agosto de 2020

RESUMEN

Muchas proteínas dependen de cofactores para ser funcionales, estos pueden ser compuestos orgánicos o inorgánicos unidos de manera covalente o no covalente a motivos de secuencias específicas. Entre los cofactores mas conservados y versátiles están los grupos Hemo y los centros Fe-S, que intervienen en una gran variedad de procesos y funciones, o en algunos casos simplemente estabilizan la estructura de las proteínas. Lo anterior, gracias a la reactividad y la capacidad del hierro para alternar entre los estados de oxidación (II), (III) y (IV) que lo hacen extremadamente útil para llevar a cabo diversas reacciones, que incluyen activación de sustratos, transferencia de electrones y reacciones de oxidación-reducción. De manera que, mediante la coordinación con otras biomoléculas se controla la solubilidad del hierro y se atenúa su reactividad, evitando así su precipitación en soluciones acuosas.

El hierro es necesario para la biosíntesis de cofactores Hemo y centros Fe-S, para su formación e inserción en las apoproteínas. En los organismos eucariontes, la biosíntesis de grupos Hemo se lleva a cabo dentro de las mitocondrias, donde también se ensamblan los centros Fe-S. El hierro desempeña un papel central en una amplia gama de procesos metabólicos, principalmente durante la respiración aeróbica, en el ciclo de Krebs y a nivel de la Cadena de Transporte de Electrones (CTE).

Los centros Fe-S son más simples que los grupos Hemo. Mientras que el Hemo es una mezcla de componentes orgánicos (protoporfirina) e inorgánicos (hierro), los grupos Fe-S son estrictamente inorgánicos. Los centros de Fe-S existen en una variedad de configuraciones dependiendo de su número respectivo de átomos de hierro y azufre, las tres formas más comunes son: 2Fe-2S, 3Fe-4S y 4Fe-4S. La producción de los centros de Fe-S debe estar altamente regulada para evitar reacciones no deseadas de hierro y azufre libres. Existen tres vías generales conocidas para la formación de centros de Fe-S: el sistema mitocondrial de ensamble de centros hierro azufre (ISC), el sistema citosólico de ensamble de centros hierro azufre (CIA) y la vía de asimilación de azufre (SUF). Estas vías proporcionan los centros de Fe-S para la mayoría de las proteínas Fe-S en casi todos los organismos.

Debido a la gran importancia del Fe en diversas funciones biológicas, es nuestro interés determinar su participación en la generación de Especies Reactivas de Oxígeno (ERO) y la disfunción de la CTE, utilizando como modelo células de la levadura *Saccharomyces cerevisiae*. El metabolismo aerobio facultativo de esta levadura permite el estudio de mutantes en el sistema ISC sin comprometer su viabilidad.

Palabras Clave: Proteínas Fe-S, Grupos Hemo, Función Mitocondrial, Estrés oxidativo.

ABSTRACT

Many proteins depend on cofactor molecules for its functionality. Cofactors can be either organic or inorganic compounds, covalently or non-covalently linked to specific sequence motifs. Hemo groups and the Fe-S centers are two of the most conserved and versatile cofactors that participate in a wide variety of processes and functions, including the stabilization of protein structures. This is related to the ability of iron to alternate between the oxidation states Fe (II), (III) and (IV), that make it extremely useful for carrying out various reactions, including substrate activation and multiple redox reactions. By its coordination with other biomolecules, both the solubility and reactivity of iron is modulated, thus avoiding its precipitation in aqueous solution and the occurrence of uncontrolled damaging reactions.

Iron is necessary for the biosynthesis of Heme and Fe-S cofactors, and for its insertion into apoproteins. In eukaryotes, Heme group biosynthesis is carried out inside the mitochondria. Iron plays a central role in a wide range of metabolic processes, including the aerobic respiration though tricarboxylic acids cycle and the electron transport chain (ETC).

Fe-S centers are structurally simpler than Heme groups. While Heme groups are constituted by organic (protoporphyrin) and inorganic (iron) components, the Fe-S groups are strictly inorganic. The Fe-S centers exist in a variety of configurations depending on their respective number of iron and sulfur atoms, the three most common forms are: 2Fe-2S, 3Fe-4S and 4Fe-4S. The synthesis of Fe-S centers must be highly regulated to avoid unwanted reactions of both free iron and sulfur. There are three known general pathways for the formation of Fe-S centers: the mitochondrial iron sulfur cluster assembly (ISC) system, the cytosolic iron sulfur assembly (CIA) system and the sulfur assimilation pathways (SUF). These pathways provide the Fe-S centers for most of the Fe-S proteins in almost all organisms.

Due to the importance of iron in diverse biological functions, is our interest determines its participation in Reactive Oxygen Species (ROS) generation and ETC dysfunction using the budding yeast *Saccharomyces cerevisiae* with mutations in the ISC system. The aerobic facultative metabolism of this yeast allows the study of ISC mutants without compromising the cell viability.

Keywords: Fe-S Proteins, Heme Groups, Mitochondrial Function, Oxidative Stress.

1. INTRODUCCIÓN.

1. 1 Importancia biológica del hierro

El hierro es un elemento traza, clave para prácticamente todos los organismos; funciona como un cofactor esencial en varios procesos celulares centrales, tales como la respiración, biosíntesis de metabolitos, síntesis y reparación de ADN, biogénesis de los ribosomas y el transporte de oxígeno en los vertebrados. Aunque el hierro es muy abundante, su biodisponibilidad es baja debido a su escasa solubilidad en condiciones ambientales. Por lo tanto, todas las células han desarrollado sistemas eficientes de absorción de hierro para satisfacer sus demandas. Estos niveles deben equilibrarse con delicadeza, ya que el hierro es una fuente de Especies Reactivas de Oxígeno (ERO) y, por lo tanto, un elemento tóxico a concentraciones altas **[Lyons y Eide, 2007]**. Para mantener los niveles adecuados de hierro y evitar su sobrecarga, las células han desarrollado sistemas para lograr la homeostasis de este elemento **[Mühlenhoff et al., 2015]**.

Ya que el hierro es esencial para la vida, su distribución coordinada entre los compartimentos intracelulares y la adaptación de su absorción a las demandas celulares son fundamentales para garantizar su autorregulación (homeostasis). Las mitocondrias ocupan un lugar central en el metabolismo del hierro ya que albergan las dos principales vías que utilizan este elemento: la síntesis de grupos Hemo y la biogénesis de las proteínas hierro-azufre (Fe/S) **[Mühlenhoff et al., 2015]**. En concordancia con este papel central, las mitocondrias también son reguladores críticos de la homeostasis del hierro celular, pues influyen directamente en la captación de hierro intracelular y el estado de los procesos metabólicos que lo utilizan, a través de cofactores dependientes de hierro o mediante el control de la expresión génica. Durante la última década, se han realizado progresos considerables con respecto a la caracterización funcional de la adquisición de hierro mitocondrial y la identificación de los transportadores involucrados. El organismo modelo *Saccharomyces cerevisia*e ha sido especialmente útil para ello.

A nivel celular, este equilibrio se logra a través de un acoplamiento estricto de la captación celular de hierro a nivel de la membrana plasmática, con las demandas de hierro intracelular y una distribución equilibrada entre los compartimentos celulares implicados en su utilización y almacenamiento; ya que la alteración o la sobreexpresión de las moléculas relacionadas con el hierro pueden tener importantes consecuencias para la sobrevivencia celular **[Mühlenhoff et al., 2015]**. Se ha observado que los defectos de proteínas de mamíferos implicadas en el transporte, la regulación o la utilización del hierro en las mitocondrias, se asocian frecuentemente con trastornos degenerativos recesivos crónicos, como la anemia crónica o la sobrecarga sistémica de hierro. En el último caso, los efectos citotóxicos de niveles elevados de hierro intracelular dan como resultado un daño tisular progresivo crónico y, en última instancia, una falla de los órganos involucrados **[Heeney y Andrews, 2004; Muñoz et al., 2011; Papanikolaou et al., 2005]**.

En los organismos eucariontes, las mitocondrias son el principal sitio de utilización de hierro, por lo que son importantes consumidores al albergar abundantes y variadas proteínas dependientes de este elemento, que desempeñan papeles esenciales en la Cadena Transportadora de Electrones (CTE) (complejos I-IV), el ciclo de los ácidos tricarboxílicos (aconitasa y succinato deshidrogenasa) y la biosíntesis de aminoácidos y vitaminas (lipoato sintasa). Tanto las reacciones iniciales de la biosíntesis de grupos Hemo, así como el paso final (la inserción de hierro ferroso en la protoporfirina IX) se llevan a cabo en el interior de las mitocondrias. Además, las mitocondrias albergan el sistema mitocondrial ISC (Iron Sulfur Cluster) y los sistemas de exportación que son esenciales para la maduración de todas las proteínas con cofactores Fe/S, ya sea en las propias mitocondrias, el citosol o el núcleo **[Lill et al., 2014; Rouault, 2012; Lill et al., 2015]**. Del mismo modo la maduración de proteínas extramitocondriales requiere la exportación de un pequeño soluto que es producido por el sistema mitocondrial ISC y se exporta a través del transportador mitocondrial ABC Atm1 al citosol, donde es utilizado por el sistema de ensamblaje de proteínas citosólicas Fe/S (CIA) para la formación de todas las proteínas Fe/S citosólicas y nucleares **[Lill et al., 2014; Netz et al., 2014; Paul y Lill, 2015; Sharma et al., 2010]**. Varias de estas proteínas

desempeñan papeles esenciales en la traducción de proteínas, síntesis y reparación de ADN y otros aspectos en la estabilidad del genoma nuclear.

1.2 Regulación de la homeostasis del hierro

Las mitocondrias son esenciales en la regulación de la homeostasis del hierro, comunican activamente el estado de disponibilidad de hierro mitocondrial a los sistemas reguladores de hierro citosólico, con el fin de equilibrar el transporte y el almacenamiento con las demandas intracelulares. De manera que, la alteración del sistema de ensamblaje ISC y exportación CIA mitocondrial están asociados con una remodelación dramática de la homeostasis del hierro celular, que es en muchos aspectos, similar a la observada en las células carentes de hierro **[Kaplan y Kaplan, 2009; Lill et al., 2012].**

El vínculo entre el ensamblaje mitocondrial de centros Fe/S y la regulación de los factores de transcripción sensibles al hierro, se ha estudiado en las levaduras *S. cerevisiae* y *Schizosaccharomyces pombe*. Ambas levaduras utilizan reguladores sensibles al hierro, funcional y estructuralmente no relacionados. En *S. cerevisiae*, los activadores transcripcionales parálogos Aft1 y Aft2 controlan la expresión de genes del regulón de hierro, un conjunto de ~40 genes que codifican para transportadores de hierro en la membrana celular, sistemas de captación, sideróforos y proteínas involucradas en la distribución y utilización intracelular de hierro **[Courel et al., 2005; Rutherford et al., 2003]**. Aft1 se trasloca entre el citosol y el núcleo de una manera sensible al hierro y actúa como activador transcripcional en condiciones limitantes del hierro. Otro modelo que proporciona una explicación simple de cómo la expresión génica sensible a hierro está relacionada con la capacidad del ensamblaje mitocondrial ISC, se basa en la suposición de que los factores de transcripción fúngicos que responden a hierro son proteínas Fe/S. Su cofactor Fe/S se ensambla de una manera dependiente de Grx4, lo cual se apoya en el hecho de que las monotiol glutaredoxinas desempeñan un papel central en el metabolismo del hierro citosólico, y transfieren fácilmente su propio centro Fe/S a las apoproteínas diana *in vitro* **[Muhlenhoff et al., 2010; Rouhier et al., 2010]**.

En los hongos, el grupo Hemo desempeña solo un papel menor en la regulación del metabolismo del hierro celular, que se relaciona principalmente con la adaptación de los sistemas celulares de captación de hierro a la hipoxia **[Crisp et al., 2003]**. El estado del sistema respiratorio mitocondrial tampoco tiene un impacto significativo en la regulación del hierro ya que las células rho^0 de levadura (que carecen de ADN mitocondrial) muestran una homeostasis celular normal del hierro. Sin embargo, las condiciones de pérdida aguda de ADNmt que están asociadas con cambios drásticos en el metabolismo mitocondrial y la composición de los complejos respiratorios inducen cambios transitorios masivos en todos los aspectos de la homeostasis del hierro, incluida la inducción de la respuesta transcripcional a la privación de hierro **[Veatch et al., 2009]**. Una inducción similar de los sistemas de captación de hierro celular se observa durante la respuesta al estrés oxidativo en *S. cerevisiae* y células de mamíferos. Sin embargo, esta respuesta es el resultado del daño oxidativo de los componentes involucrados en la detección de hierro en el citosol, como el Aft1 en *S. cerevisiae* y el IRP1 de mamíferos, y muy probablemente no relacionado directamente con las mitocondrias **[Castells-Roca et al., 2011; Eisenstein, 2000; Mueller y Pantopoulos, 2002]**. El impacto del sistema mitocondrial ISC sobre la regulación del hierro se restringe a los miembros del sistema central ISC que es esencial para la maduración de todas las proteínas Fe/S. Estos componentes están implicados en la síntesis *de novo* de los centros Fe/S por la proteína de andamiaje Isu1, o en la transferencia de los centros Fe/S asistida por la chaperona monotiol glutaredoxina 5 (Grx5). Defectos en los factores ISC de acción tardía que son específicamente requeridos para la maduración de las proteínas [4Fe-4S] no afectan significativamente la regulación del **hierro [Gelling et al., 2008; Muhlenhoff et al., 2011; Sheftel et al., 2012]**.

1.3 La cadena de transporte de electrones (CTE)

Las mitocondrias desempeñan una serie de funciones vitales en las células eucariontes, entre las cuales la más importante es la producción de ATP mediante la fosforilación oxidativa. Desde el descubrimiento de los citocromos por Keilin **[Keilin D, 1925]**, seguido por la elucidación de la secuencia de eventos que conducen a la fosforilación oxidativa **[Chance y Williams, 1955]** y posteriormente la

identificación de los complejos enzimáticos implicados en el proceso **[Chance y Williams, 1955; Hatefi et al., 1962]**, la organización estructural y funcional de la CTE ha sido un tema de gran debate y diversos estudios. La catálisis del NADH y el $FADH_2$ generados durante la glucólisis, la oxidación de ácidos grasos y en el ciclo de los ácidos tricarboxílicos son los sustratos de la CTE, generando la transferencia de electrones entre los distintos complejos respiratorios (formados por enzimas multiméricas) incrustados en la membrana mitocondrial interna, mediada a su vez, por dos componentes mas pequeños: la ubiquinona y el citocromo *c*, estos difunden entre los complejos respiratorios, permitiendo el flujo de electrones que finalmente permitirá producir agua a partir de oxígeno molecular **[Boumans et al., 1998]**. Las membranas internas fuertemente plegadas de las mitocondrias llamadas crestas, contienen muchas copias de los componentes de la CTE, los complejos respiratorios I, II, III y IV, que junto con la ATP sintasa forman la maquinaria para la producción de ATP. Los complejos respiratorios son enzimas que en conjunto generan un gradiente electroquímico de protones a través de la membrana mitocondrial interna que es utilizado por la F_1F_o (complejo V - ATP sintasa) para producir ATP a través de la fosforilación oxidativa, donde solamente el complejo II no es capaz de bombear protones **[Chaban et al., 2013]** al espacio intermembrana. La organización de los complejos respiratorios ha sido objeto de intenso debate, partiendo de numerosos estudios realizados para dilucidar su organización molecular, donde se han considerado varios modelos funcionales (**Fig. 1**).

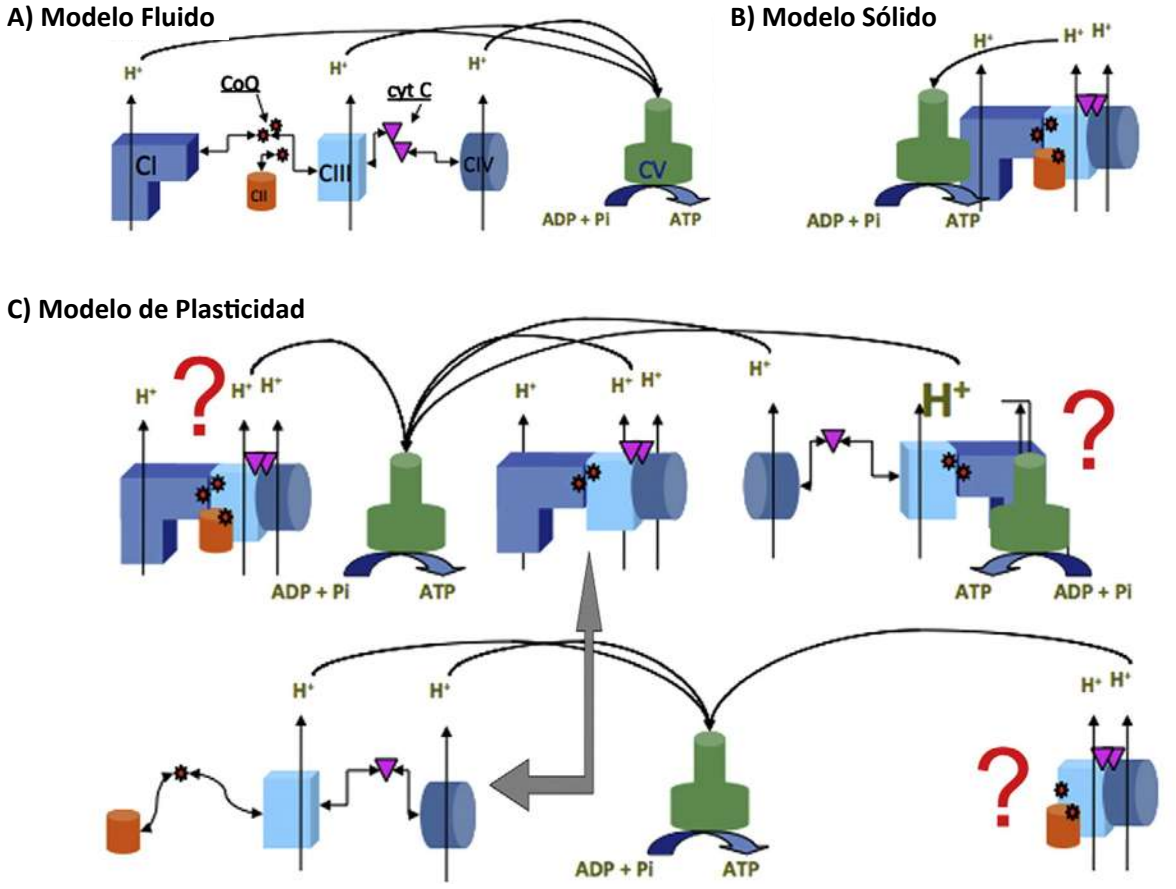

Fig. 1. Representación esquemática de los diferentes modelos propuestos de la CTE. (A) Modelo de colisión aleatoria de Hackenbrock o modelo fluido, (B) Modelo sólido propuesto por Schägger, y (C) Modelo de plasticidad. La forma y el código de color para representar los complejos individuales se pueden ver en el panel A; la coenzima Q se representa como pequeñas estrellas rojas y el citocromo *c* como triángulos morados. Solo un complejo de cada tipo está representada en las diferentes asociaciones de supercomplejos, aunque la estequiometría real puede variar. El signo de interrogación indica asociaciones putativas o supercomplejos cuya existencia no está completamente confirmada. Los supercomplejos que contienen los complejos I a IV también se denominan respirasomas, ya que pueden transferir directamente electrones de NADH a oxígeno. Modificado de **Acín-Pérez et al., 2008**.

Inicialmente, el primer modelo consideraba una estructura rígida que implicaba el desarrollo de reacciones redox secuenciales, donde los componentes respiratorios se empaquetaban estrechamente para garantizar el acceso y, por lo tanto, una alta eficiencia en el transporte de electrones **[Keilin y Hartree, 1947; Slater, 2003]** (**Fig. 1B**). Posteriormente se consideró que los componentes de la CTE son libres de difundirse lateral e independientemente el uno del otro en el plano de la membrana, y la transferencia de electrones se acoplaba a las colisiones basadas en la difusión libre entre estos componentes, ya que estos se encontraban formando una "poza", es decir, se hallan siempre en cantidades disponibles. Esto implica que los portadores móviles regulan la transferencia de electrones entre los complejos respiratorios. Bajo este esquema, los componentes respiratorios estarían dispuestos como un conjunto o cadena macromolecular ordenada, pues inicialmente se reportaron numerosas observaciones, que indicaron la posibilidad de aislar unidades multicomplejas. Para el caso de mitocondrias de *Saccharomyces cerevisiae* en condiciones iónicas fisiológicas, ni la ubiquinona ni el citocromo *c* funcionan como una "poza", indicando que, al menos en la levadura, los complejos de la CTE forman una unidad respiratoria funcional **[Boumans et al., 1998]**. Sin embargo, faltarían estudios paralelos en células completas para comprender la dinámica de los complejos y su relevancia funcional. Además, la pregunta sobre sí los portadores de electrones móviles están atrapados dentro de conjuntos que se han definido como "canales de difusión", aún permanecía sin respuesta **[Boumans et al., 1998]**.

El siguiente modelo presentado por Green y Tzagaloff argumentaba que, por el contrario, la ubiquinona y el citocromo *c* actúan como portadores de electrones móviles entre complejos inmóviles unidos a la membrana **[Green y Tzagoloff, 1966]** (**Fig. 1A**). En este modelo apoyado por Kröger y Klingenberg **[Kroger y Klingenberg, 1973a; Kroger y Klingenberg, 1973b]**, la CTE estaría compuesta por complejos unidos a la membrana y lanzaderas de electrones que se distribuyen aleatoriamente dentro de la membrana interna y el espacio intermembrana de las mitocondrias. Extensos estudios realizados por Hackenbrock y sus colegas sobre las propiedades de difusión de los diferentes actores de la CTE, en particular del citocromo *c*, aportaron evidencias convincentes para un modelo fluido o de colisión aleatoria **[Hackenbrock et al., 1986]**. En este modelo, los complejos respiratorios se ven como entidades independientes incrustadas en la membrana interna, donde la ubiquinona y el citocromo *c* actúan como portadores móviles que difunden libremente en la membrana lipídica **[Trouillard et al., 2011]**.

Sin embargo, la aparición de nuevas técnicas de aislamiento de los componentes de la membrana, junto con estudios de análisis de control del flujo en mitocondrias de levadura y de mamíferos, demostraron que era posible purificar asociaciones estables de estos complejos respiratorios **[Schägger y Pfeiffer, 2000; Cruciat et al., 2000]**. Esto dio pie a una reformulación del modelo respiratorio, donde los complejos se organizan en estructuras más grandes (supercomplejos, SC), permitiendo un transporte de electrones más eficiente. Partiendo de la caracterización por Schägger y Pfeiffer de estos nuevos "supercomplejos" que contienen citocromo bc_1 y citocromo *c* oxidasa (CcOx), en diversas proporciones estequiométricas **[Schagger y Pfeiffer, 2000]**, fomentó la reformulación de que las propiedades funcionales de la CTE están conformadas por su organización ultraestructural. Se ha demostrado que la composición y abundancia de los supercomplejos caracterizados bioquímicamente, varían durante el crecimiento y/o las condiciones fisiológicas **[Rosca et al., 2008; Gómez et al., 2009]**. Todas las propuestas anteriores han llevado finalmente al modelo de plasticidad (**Fig. 1C**), que conjunta los modelos sólido y fluido al considerar la organización de los complejos respiratorios como una red de diferentes asociaciones, así como complejos individuales. De acuerdo con esta visión, los estudios cinéticos de control de flujo metabólico también pueden discriminar entre el modelo de colisión aleatoria (fluido) y el sólido (**Fig. 1**). Por lo tanto, en el primero, cada enzima sería el factor limitante, mientras que en el segundo, el sistema completo se comportaría como una sola unidad donde la inhibición de cualquiera de sus componentes afectaría a toda la vía **[Acín-Pérez y Enriquez, 2014]**.

1.4 Complejos respiratorios mitocondriales

1.4.1 Complejo I

El Complejo I o NADH:ubiquinona oxidorreductasa, es la enzima más grande de la CTE y tiene forma de L característica con una parte extensa que se incrusta en la bicapa lipídica y un hombro más

pequeño que sobresale en la matriz mitocondrial. Este complejo une el sustrato NADH y transfiere dos electrones, uno a la vez, a través del FMN y siete centros de Fe/S a la ubiquinona. La reducción de la ubiquinona induce cambios conformacionales en el dominio membranal que producen la translocación de cuatro protones al espacio intermembrana.

1.4.2 Complejo II

La succinato deshidrogenasa (SDH, complejo II), también conocida como succinato:ubiquinona oxidorreductasa, es un complejo heterotetramérico integral de membrana de aprox 120 kDa, que cataliza la oxidación de dos electrones dependiente de FAD y del succinato para obtener fumarato, junto con la reducción de la ubiquinona a ubiquinol. La SDH es la única enzima que acopla el ciclo de los ácidos tricarboxílicos a la CTE, aunque a diferencia de otros complejos respiratorios, no hay transferencia de protones a través de la membrana acoplada con su actividad. Los dos electrones extraídos de la deshidrogenación del succinato se canalizan a la CTE, desde el FAD hasta la ubiquinona, a través de los cofactores [2Fe-2S], [4Fe-4S], [3Fe-4S] y posiblemente el hemo *b* (**Fig. 2**). Sin embargo, la participación del hemo *b* como parte de la cadena de transferencia de electrones no se ha establecido claramente **[Lemire y Oyedotun, 2002; Lancaster, 2002; Lemos et al., 2002; Rutter et al., 2000]**. La SDH está compuesta en general de cuatro polipéptidos distintos designados Sdh1-4 en levadura (SDHA-D en bacterias y humanos). Los tres centros Fe/S están contenidos en la subunidad Sdh2 y actúan como un cable de electrones que conecta el FAD al sitio de unión de la ubiquinona. El dímero catalítico Sdh1-Sdh2 está orientado exclusivamente en el lado de la matriz de la membrana interna en eucariontes, mientras que Sdh3-Sdh4 anclan el dímero catalítico a la membrana. Se ha sospechado de un segundo sitio de unión a la ubiquinona en la SDH, donde un exceso de flujo de electrones podrían ser transferidos al sitio Qd mediado por el hemo *b*. Esto aumenta la posibilidad de que el hemo pueda funcionar de manera alterna entregando los electrones al segundo sitio Qd. Inclusive el hemo *b* podría estar involucrado en la prevención de las ERO durante la transferencia de electrones, actuando como un condensador cuando hay un alto flujo de electrones **[Yankovskaya et al., 2003]**, minimizando el nivel de semiquinona con un flujo inverso de electrones del ubiquinol.

1.4.3 Complejo III

El complejo ubiquinol:citocromo *c* oxidoreductasa (citocromo bc_1, complejo III) es un componente central de las CTE respiratorias y fotosintéticas implicadas en la fosforilación oxidativa. En eucariontes, el complejo existe como un dímero, incrustado en la membrana interna de las mitocondrias. La función del complejo III es mediar la transferencia de electrones al citocromo *c* mediante la oxidación del ubiquinol localizado en la membrana. Esta reacción está acoplada a la translocación de protones a través de la bicapa lipídica al espacio intermembrana. Todos los complejos bc_1 contienen tres subunidades con grupos prostéticos redox conocidos como las subunidades centrales: un citocromo *b* (Cob) di-hemo que contiene tanto el b_H de alto potencial (*b*562) como el b_L de bajo potencial (*b*565); el hemo c_1 de tipo *c* asociado con la subunidad Cyt1; y una proteína hierro-azufre (ISP, Rip1) con un centro 2Fe-2S (**Fig. 2**), además de contener hasta ocho subunidades supernumerarias por monómero, no requeridas para el flujo de electrones o la translocación de protones, pero sí para su estabilización. La proteína Cob es la única subunidad bc_1 codificada por el genoma mitocondrial de la levadura y sirve como la proteína fundamental en la biogénesis del complejo. Las otras subunidades están codificadas por el genoma nuclear y deben importarse a la mitocondria. La proteína Rip1 se entrelaza entre los monómeros adyacentes del complejo, por lo tanto, la transferencia de electrones solo puede ocurrir cuando el complejo se ensambla como un dímero. El dímero del complejo III forma **supercomplejos** de orden superior con el complejo IV en levadura y con los complejos I y IV en eucariotas superiores **[Kim et al., 2012]**.

1.4.4 Complejo IV

La citocromo *c* oxidasa (CcO) es la enzima terminal de la CTE. Miembro de la superfamilia de las hemo-cobre oxidasas, ésta enzima cataliza la reducción total del oxígeno molecular formando agua, acoplado a la translocación de protones a través de la membrana mitocondrial interna que contribuye a la formación del gradiente electroquímico de protones utilizado para generar ATP.

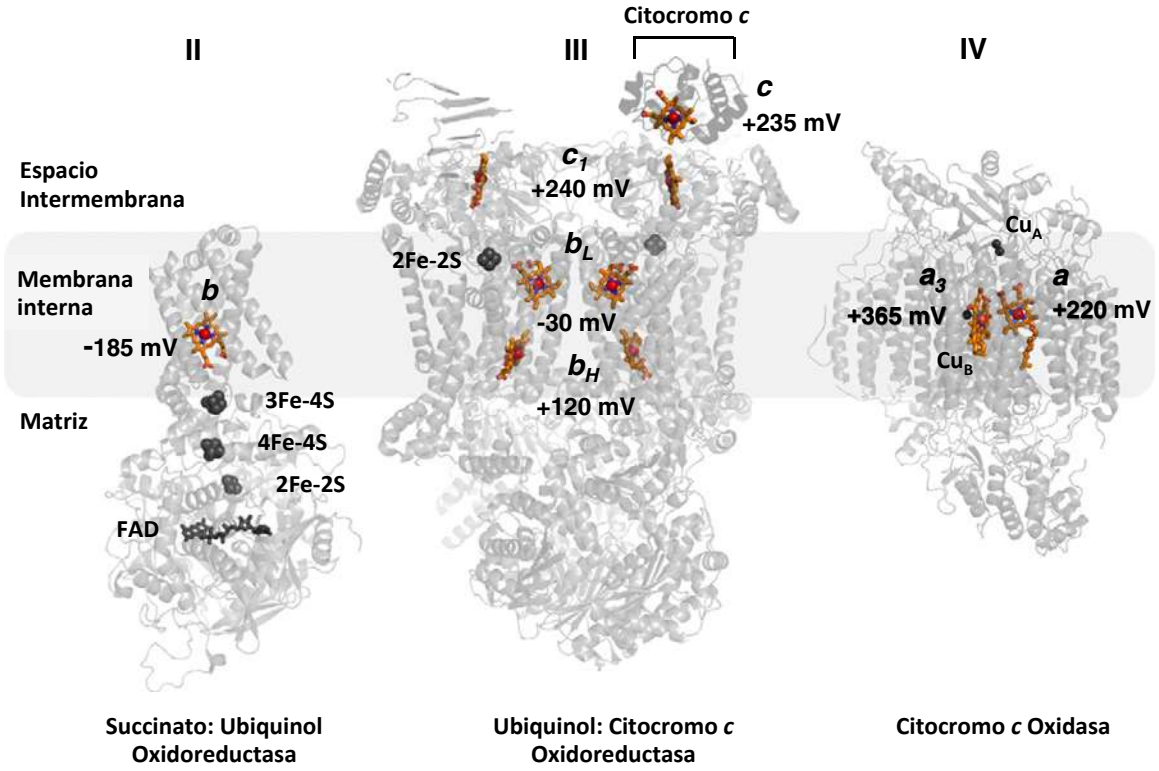

Fig. 2. Distribución de los hemos *b*, *c* y *a*, con sus respectivos potenciales de punto medio, en los complejos respiratorios II, III y IV en mitocondrias de *Saccharomyces cerevisiae*. Obsérvese la tendencia general de aumentar el potencial redox del hemo *b* del Complejo II al hemo a_3 del Complejo IV (el sitio terminal receptor de electrones y donde ocurre la reducción de O_2). Otros cofactores en los complejos están en gris. Complejo II: FAD, [2Fe-2S], [4Fe-4S], [3Fe-4S]; Complejo III: Rieske 2Fe-2S; Complejo IV: binuclear Cu_A, Cu_B. El complejo III se muestra como un dímero con el citocromo *c* acoplado a una de las subunidades. Modificado de **[Kim et al., 2012]**.

Este complejo consiste en 11 subunidades en levaduras y 13 en mamíferos; sin embargo, el núcleo catalítico de la enzima está formada por las tres proteínas más grandes, Cox1, Cox2 y Cox3, las cuales muestran un grado significativo de conservación a lo largo de la evolución **[Khalimonchuk y Rödel, 2005]**. Las tres subunidades centrales están codificadas en el ADN mitocondrial, mientras que las subunidades adicionales son productos del genoma nuclear **[Mick et al., 2011; Soto et al., 2012]**. Cox1 contribuye tanto al bombeo de protones como a las reacciones de reducción de oxígeno. Por su parte Cox 3 es importante para la estabilidad del núcleo catalítico y modula las vías de bombeo de protones en Cox1 **[Varanasi y Hosler, 2011]**.

Los sitios redox de la CcO están representados por los iones de cobre y los cofactores del Hemo *a* que juntos forman cofactores únicos que se encuentran solo en oxidasas terminales. La subunidad Cox2 contiene el centro binuclear Cu_A ubicado dentro del espacio intermembrana, y los otros cofactores redox están presentes en Cox1, que contiene dos moléculas de hemo, donde el segundo está dentro de un centro heterobimetálico formado por cobre (denominado Cu_B) y hemo a_3. Los electrones del citocromo *c* reducido ingresan a la CcO a través del centro Cu_A ubicado cerca del sitio de acoplamiento de Cox2, posteriormente la transferencia de electrones continua del Cu_A al hemo *a* (sin la traslocación de protones) y posteriormente al centro heterobimetálico hemo a_3: Cu_B donde se produce la reducción del oxígeno (**Fig. 2**). La hemilación de Cox1 es uno de los eventos clave en la biogénesis de CcO. Se requiere del hemo *a* para la estabilidad y el plegamiento de la subunidad Cox1 **[Nobrega et al., 1990; Steinrücke y Ludwig, 1993; Williams et al., 2004]**. Además, el hemo *a* no es sólo un sitio reactivo sino también una "unidad estructural" de Cox1. Es posible que la inserción del hemo pueda ser necesaria para la formación y/o estabilización del intermediario **[Barros et al., 2002]**.

1.5 Supercomplejos Respiratorios

Hasta el final del siglo pasado, la visión más aceptada del sistema de fosforilación oxidativa en las mitocondrias preveía una organización aleatoria de los complejos de la CTE de acuerdo con el modelo de difusión aleatoria de Hackenbrock. El año 2000 representó un cambio drástico que cambió el entendimiento actual, a una organización en ensamblajes supramoleculares llamados supercomplejos o respirasomas (**Fig. 3**). Mediante el análisis de una multitud de datos en la literatura obtenida por electroforesis en geles azules nativos (BN-PAGE) se observó que los complejos implicados en la asociación supramolecular son las tres enzimas translocadoras de protones: los complejos I, III y IV. Los supercomplejos llegan a presentar diversas configuraciones y estequiometrías en las mitocondrias en diferentes organismos de estudio **[Schägger y Pfeiffer, 2000; Schägger y Pfeiffer, 2001]**. Además, se ha sugerido que pueden existir incluso niveles más altos de organización (macrocomplejos o "redes" respiratorias).

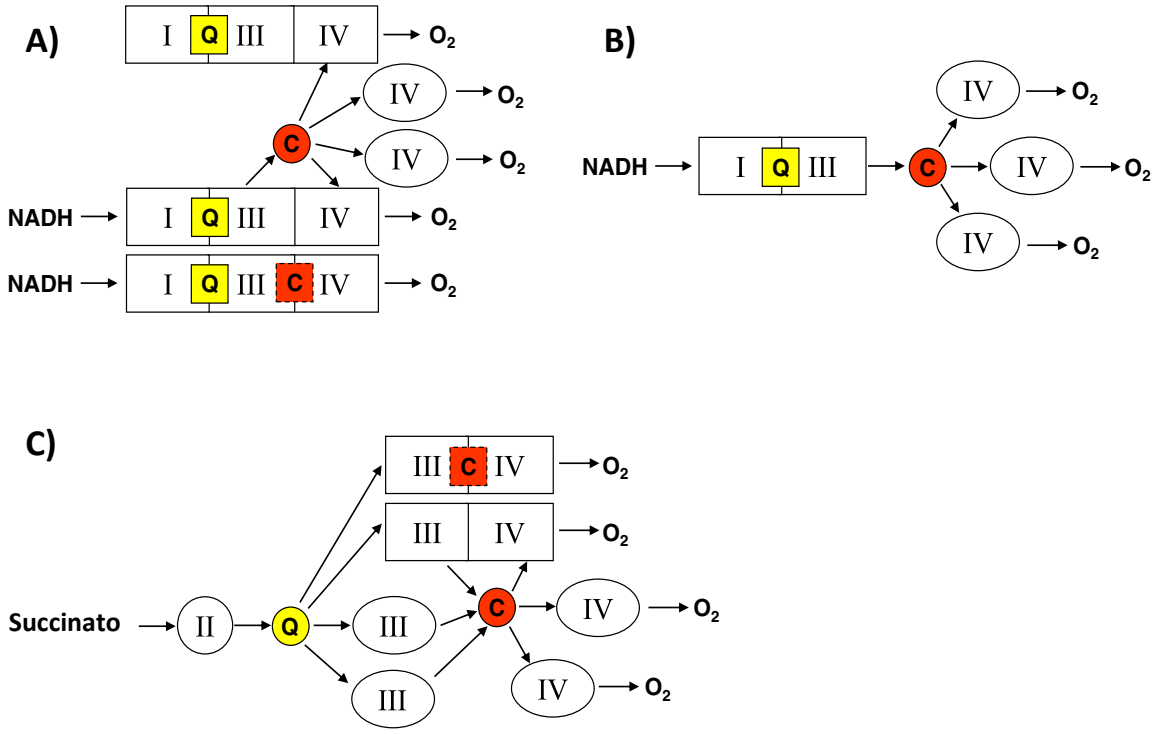

Fig. 3. Organización postulada de las CTE en las mitocondrias de mamíferos. (A) Están representados los respirasomas (I-III-IV) y las moléculas de citocromo *c* oxidasa (IV) libres; La transferencia de electrones entre CI y CIII siempre se produce por la canalización de CoQ (Q), mientras que la disociación rápida del citocromo *c* (C) de CIII también puede permitir la transferencia de electrones por colisiones aleatorias del citocromo *c* libre con el CIV, ya sea libre o unida en otros respirasomas. **(B)** Se muestra un esquema de la posible función del supercomplejo formado por el CI y el CIII; en este caso, se postula que el citocromo *c* libre choca con unidades de CIV libres. **(C)** Se describe el mecanismo de transferencia de electrones desde el succinato a través de el CII libre y el conjunto de CoQ. Este modelo también puede aplicarse a otras enzimas que alimentan electrones al grupo de CoQ, que interactúa con asociaciones libres de CIII o de CIII/CIV. Modificado de **[Genova y Lenaz, 2014]**.

La primera demostración experimental de los supercomplejos obtenida mediante BN-PAGE después de la solubilización leve de las mitocondrias con digitonina **[Schägger y Pfeiffer, 2000; Schägger y Pfeiffer, 2001]**, evidenció que existen varios tipos de asociación entre los complejos I, III y IV. Entre ellos la combinación $I_1III_2IV_1$ denominada "respirasoma", porque se consideró la unidad mínima para realizar la respiración completa desde el NADH hasta el oxígeno. Estas unidades presentan actividad en gel para cada uno de los complejos individuales, sin embargo, la primera demostración de que son efectivamente funcionales y capaces de una actividad completa provino del aislamiento cromatográfico de un respirasoma funcional de *P. denitrificans* **[Stroh et al., 2004]** y la actividad respiratoria de un respirasoma aislado de mitocondrias de mamíferos reportada por Acín-Pérez et al **[Acín-Pérez et al.,**

2008], cuyos resultados demostraron que las bandas de BN-PAGE que contienen tanto la subunidad CoQ9 (el principal homólogo de CoQ en roedores) como el citocromo *c* mostraron actividad completa de NADH oxidasa. Este estudio demostró que los supercomplejos no solo son entidades reales, sino que son competentes en la respiración y, por lo tanto, su papel debe ser coherente con su actividad, es decir, deben proporcionar alguna ventaja en la transferencia de electrones.

Inmediatamente después del descubrimiento de los supercomplejos, se propuso que la consecuencia natural de tales conjuntos es la canalización de los sustratos o la catálisis mejorada en la transferencia de electrones entre complejos. La canalización de los sustratos es la transferencia directa de un intermedio entre los sitios activos de dos enzimas que catalizan reacciones consecutivas **[Ovàdi, 1991]**, en el caso de la transferencia de electrones, esto significa la transferencia directa entre dos enzimas consecutivas mediante la reducción sucesiva y la reoxidación del intermediario sin su difusión en el medio. En tal caso, la transferencia de electrones entre complejos se vuelve indistinguible de la transferencia de electrones intracomplejos, por lo que los llamados intermediarios móviles (ubiquinona y citocromo c), se predice que mostrarán un comportamiento similar a un sustrato en la vista clásica del modelo de colisión aleatoria, que estarían situados en la interfaz entre los dos complejos consecutivos. La evidencia de este tipo de canalización proviene de la estructura tridimensional del supercomplejo mitocondrial $I_1III_2IV_1$, cuya disposición única de los tres complejos indica las vías a lo largo de las cuales la ubiquinona y el citocromo *c* pueden viajar para transportar electrones entre sus respectivas proteínas asociadas **[Althoff et al., 2011]**. En el modelo mencionado anteriormente, los sitios de unión a la Coenzima Q en el Complejo I y en el Complejo III se enfrentan entre sí y están separados por un espacio de 13 nm dentro del núcleo de la membrana del supercomplejo. Es probable que la coenzima Q recorra una trayectoria a través de esta brecha que supuestamente está llena de lípidos de membrana.

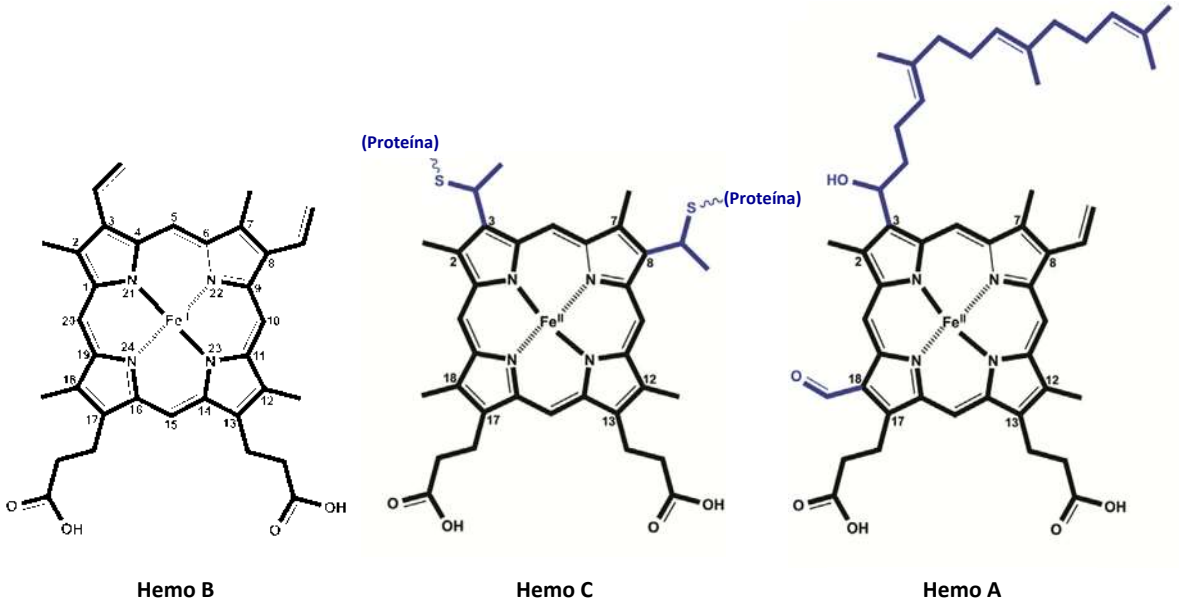

Fig. 4. Estructura del hemo. El sistema de numeración estándar 1-24 IUPAC se usa para numerar los átomos de carbono del tetrapirrol en la molécula hemo original (hemo B), las diferencias se muestran en azul. Tomado y modificado de **Barupala et al., 2016**.

1.6 Proteínas y cofactores dependientes de hierro

El hierro es el cuarto elemento más abundante en la corteza terrestre **[Crichton et al., 2001]**, por lo que su alta prevalencia durante la evolución ha sido factor determinante para su presencia ubicua en la naturaleza. La reactividad y capacidad del hierro para alternar entre distintos estados de oxidación lo hacen extremadamente útil para llevar a cabo diversas reacciones, que incluyen: activación de sustratos, transferencia de electrones y reacciones de oxido-reducción **[Wrighting y Andrews, 2008]**.

Mediante la coordinación con otras biomoléculas, la solubilidad del hierro es controlada y su reactividad atenuada, evitando así su precipitación en soluciones acuosas **[Boukhalfa y Crumbliss, 2002]**. El flujo secuencial de electrones en la CTE, desde un sustrato de bajo potencial de reducción hasta el O_2, está mediado por cofactores redox unidos a proteínas. En las mitocondrias, los grupos Hemo (**Fig. 4**) junto con los cofactores de flavina, los centros Fe/S (**Fig. 5**) y de cobre, median esta transferencia de múltiples electrones entre los complejos respiratorios. Los grupos Hemo, en tres formas diferentes (citocromo *a*, *b* y *c*) se usan como un grupo prostético unido a los complejos II, III y IV. Así mismo, los centros Fe/S se encuentran en los complejos I, II y III como subunidades catalíticas necesarias en la CTE, estos grupos se caracterizan por la presencia fundamental de hierro en sus estructuras **[Barupala et al., 2016]**.

Las células captan el hierro a través de la transferrina o mediante un transportador de membrana directo (DMT1) **[Johnson y Smith, 2011]**. Una vez en la célula, el hierro importado puede unirse a las proteínas reguladoras del hierro que regulan su concentración, puede almacenarse dentro del complejo de ferritina, ser exportado o incorporado como cofactor en las apoproteínas. En los seres humanos, la mayor parte del hierro en el cuerpo (más del 75%) está dirigida hacia la biosíntesis de cofactores hemo y Fe/S (**Fig. 4 y 5**) **[Johnson y Smith, 2011]**. En los eucariontes, la biosíntesis de grupos hemo se inicia y se completa dentro de las mitocondrias.

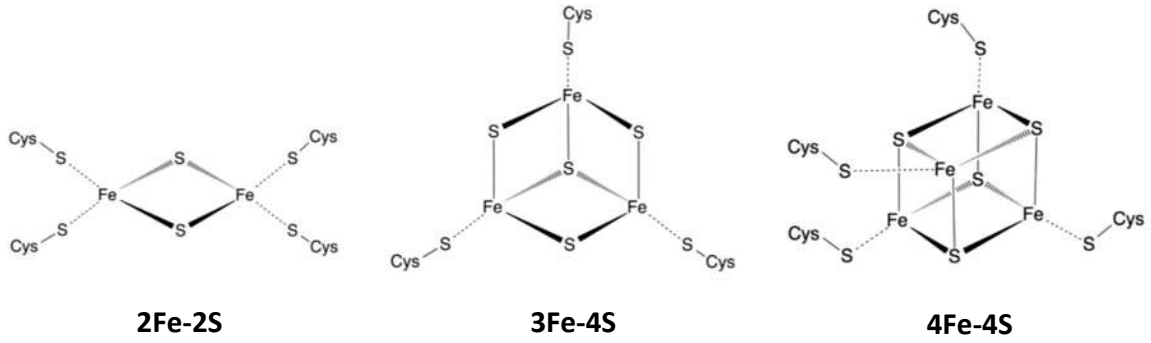

Fig. 5. Estructura de las 3 formas más comunes de centros Fe-S: 2Fe-2S, 3Fe-4S y 4Fe-4S. Tomado y modificado de **Barupala et al., 2016**.

1.6.1 Biogénesis de los grupos Hemo

En la naturaleza, el grupo Hemo es uno de los más abundantes ya que se encuentran en un amplio espectro de organismos, y son necesarios en muchos procesos biológicos vitales incluyendo, la fotosíntesis, el transporte de oxígeno, la oxidación y reducción biológica, entre otros. La mayor parte del contenido total de hierro en el cuerpo humano se incorpora a las proteínas que contienen grupos Hemo, tales como hemoglobina, mioglobina, catalasas, peroxidasas, óxido nítrico sintasas y citocromos **[Tsiftsoglou et al., 2013]**. Las modificaciones de la molécula básica del grupo Hemo permiten la diversidad de funciones encontradas en la naturaleza, donde el grupo hemo *b*, sirve como plataforma en cada caso: cit *a* y cit *b* (**Fig. 4**). La unidad de tetrapirrol del grupo Hemo consiste en cuatro unidades de pirrol unidas por cuatro puentes metilo, además un átomo de nitrógeno de cada pirrol coordina el enlace del hierro en el centro del anillo de tetrapirrol, mientras que las distorsiones del plano en la molécula pueden ser críticas para la función y la reactividad de este **[Arnone, 1974; Fenna et al., 1995]**. Dado que el grupo Hemo sirve como un cofactor esencial para varias proteínas involucradas en los procesos metabólicos centrales, todos los organismos han establecido una vía biosintética conservada para sintetizar este cofactor. El proceso de ensamblaje general consta de cuatro etapas: 1) la síntesis de un solo pirrol, 2) el ensamblaje de cuatro pirroles para hacer que el anillo de tetrapirrol, 3) la modificación de las cadenas laterales y 4) la inserción del hierro en el anillo **[Barupala et al., 2016]**.

El primer paso en la biosíntesis del Hemo es la formación mitocondrial del ácido 5-aminolevulínico (ALA), que es el precursor que sirve como la única fuente de átomos de carbono y

nitrógeno necesarios para construir la unidad básica del hemo. La enzima ALA sintasa (ALAS) que reside en el lado de la matriz de la membrana mitocondrial interna cataliza la condensación de la glicina y el succinil-CoA. Tras su formación, el ALA sale de la mitocondria para servir como sustrato para las conversiones subsiguientes por cuatro enzimas que se encuentran en el citosol (**Fig. 6**). Una vez exportado al citosol, el ALA sirve como el bloque de construcción para sintetizar uroporfirinógeno III siguiendo tres pasos consecutivos. El primer paso consiste en la condensación de dos moléculas de ALA para formar porfobilinógeno (PBG) por acción de la porfobilinógeno sintasa (PBGS), también conocida como ALA dehidratasa (ALAD). Posteriormente cuatro moléculas de porfobilinógeno se someten a polimerización para formar 1-hidroximetilbilano en una reacción catalizada por la porfobilinógeno desaminasa (PBGD). Este tetrapirrol inestable sirve como sustrato para la uroporfirinógeno sintasa (UROS), la enzima que sintetiza el uroporfirinógeno III. Este intermediario cíclico se convierte en coproporfirinógeno III, un producto que carece de cuatro grupos funcionales ácidos. Los siguientes pasos de descarboxilación son llevados a cabo por la uroporfirinógeno descarboxilasa (UROD) dentro del citosol para producir cuatro grupos metilo en lugar de las cadenas laterales acéticas. Tres enzimas asociadas con la membrana interna mitocondrial completan los pasos terminales. En el primero de ellos, el coproporfirinógeno III se somete a una descarboxilación oxidativa de sus cadenas laterales de propionilo en dos anillos de pirrol para formar el protoporfirinógeno IX por la coproporfirinógeno III oxidasa (CPO), una enzima localizada en el espacio intermembrana mitocondrial. En el siguiente paso, el protoporfirinógeno IX se oxida a protoporfirina IX, después de la eliminación de seis átomos de hidrógeno del anillo de porfirinógeno, para proporcionar una estructura de doble enlace alterno al macrociclo; esta reacción es catalizada por la protoporfirinógeno IX oxidasa (PPO).

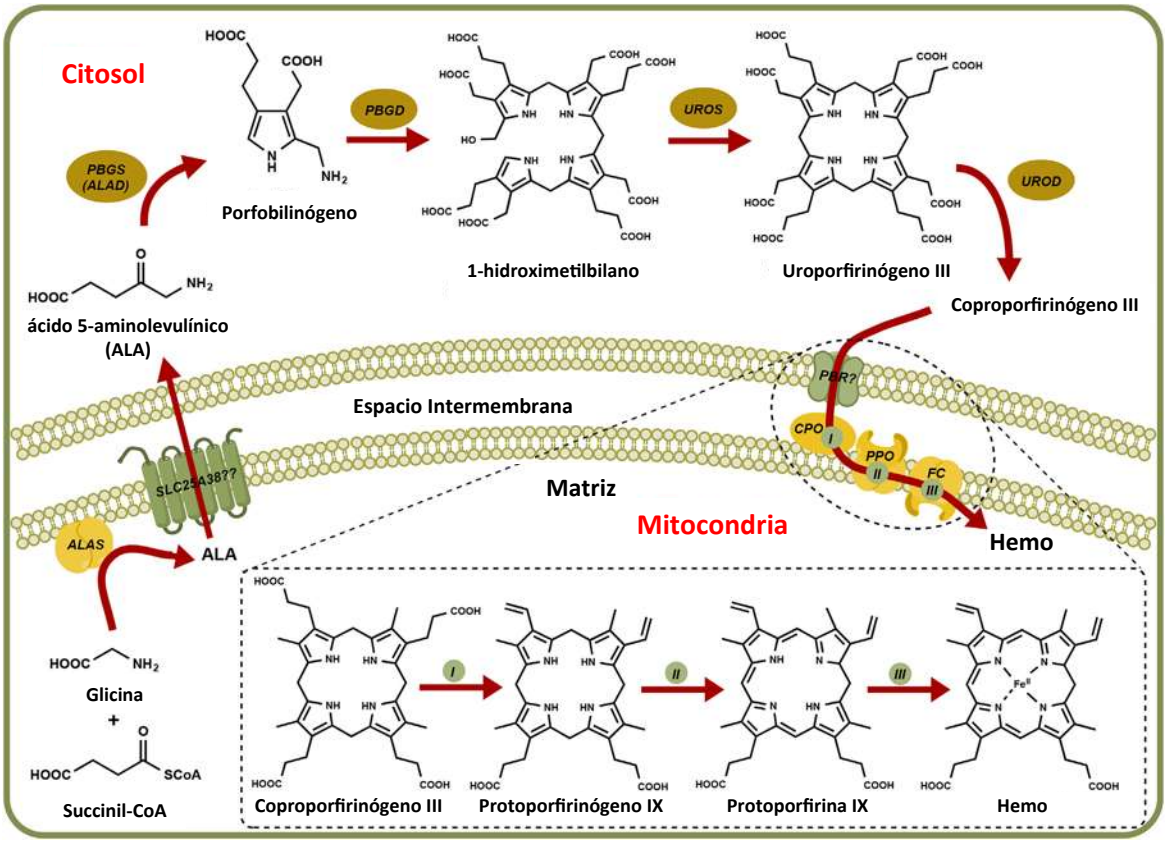

Fig. 6. Vía de biosíntesis de hemo. ALA: ácido 5-aminolevulínico, ALAS: ALA sintasa, PBGS: porfobilinógeno sintasa, ALAD: ALA deshidratasa, PBGD: porfobilinógeno desaminasa, UROS: uroporfirinógeno sintasa, UROD: uroporfirinógeno descarboxilasa, PBR: receptor de ovario, fosfato de peróxido de fosfato de potasio., PPO: protoporfirinógeno IX oxidasa, FC: ferroquelatasa. Tomado y modificado de **Barupala et al., 2016**.

Por último, la ferroquelatasa (FC) es responsable de la inserción del hierro ferroso en la protoporfirina IX para formar Fe-protoporfirina IX o Hemo. La FC funciona como un homodímero y cada monómero contiene un clúster 2Fe-2S cuya función aún es desconocida **[Barupala et al., 2016]**. Una vez sintetizado, el grupo Hemo puede sufrir modificaciones en la cadena lateral (por ejemplo, síntesis de hemo *a* y hemo *b*) o enlaces covalentes (por ejemplo, hemo *c* en la biogénesis del citocromo *c*) para producir tipos de Hemo adicionales dependiendo de las necesidades celulares (**Fig. 4**).

Dentro de una proteína de andamiaje, el Hemo puede llevar a cabo el transporte de O_2 **[Antonini, 1971]**, detectar el óxido nítrico y monóxido de carbono **[Rodgers, 1999]**, llevar a cabo reacciones de oxigenasa **[Sono et al., 1996]**, regular la actividad enzimática **[Mense y Zhang, 2006; Hu et al., 2008]** y el transporte de electrones **[Gray y Winkler, 1996]**. Esta última función es central en el mecanismo asociado con la fuerza protonmotriz en la fosforilación oxidativa. En las células eucariotas, siete grupos Hemo de diferente arquitectura (hemos *b*, *c* y *a*) están incrustados en las proteínas de la CTE, y se reducen y oxidan aumentando los potenciales de reducción para transferir cuatro electrones para reducir en última instancia al O_2. Estos "pigmentos celulares" o citocromos dan lugar a bandas de absorción espectrales del grupo hemo *b* del complejo II, hemo *b* del complejo III, hemos *a* del complejo IV y hemos c_1 de complejo III y el mediador de electrones soluble, citocromo *c*. El complejo I contiene cofactores de flavina y Fe/S, pero carece de Hemos **[Kim et al., 2012]**. Las proteínas de andamiaje también se usan para proporcionar una modificación al macrociclo del Hemo y se unen mediante la combinación de tres interacciones: 1) la interacción entre un ligando axial y el hierro Hemo; 2) interacciones hidrofóbicas entre la proteína y el macrociclo de porfirina; y 3) interacciones polares entre la proteína y los ácidos propiónicos del macrociclo **[Reedy y Gibney, 2004]**.

1.6.2 Biogénesis de Centros Fe/S

Por otro lado, los centros Fe/S son más simples que los grupos Hemo. Mientras que el grupo Hemo es una mezcla de componentes orgánicos (protoporfirina) e inorgánicos (hierro), los centros Fe/S son estrictamente inorgánicos. Los átomos de hierro en los centros Fe/S interactúan directamente con los residuos de las proteínas y los átomos de azufre unen los átomos de hierro vecinos. Los centros Fe/S existen en una variedad de configuraciones dependiendo de su número respectivo de átomos de hierro y azufre, las tres formas más comunes son: 2Fe-2S, 3Fe-4S y 4Fe-4S (**Fig. 5**). Sin embargo, también se han observado centros Fe/S más complejos, incluyendo los centros 7Fe-8S y 8Fe-8S identificados en ferredoxinas de *Desulfovibrio africanus* **[George et al., 1989]**. Una de las principales características de los átomos de Fe dentro del grupo Fe/S, es que pueden existir tanto en su forma férrica como ferrosa y el ciclo entre estos estados redox permite la transferencia de electrones para llevar a cabo reacciones redox, esta tendencia del centro Fe/S oxidado a ganar un electrón se denomina "potencial de reducción".

La producción de centros Fe/S debe ser altamente regulada para evitar reacciones no deseadas tanto del hierro libre como del azufre. De forma similar a las proteínas Hemo, las proteínas Fe/S se sintetizan en su estado de apoproteína y obtienen su cofactor a partir de una vía de formación de centros Fe/S. En la actualidad, existen tres vías generales conocidas para la formación de centros Fe/S: el sistema mitocondrial de ensamblaje de centros hierro azufre (ISC), el sistema citosólico de ensamblaje de centros hierro azufre (CIA) y las ruta de asimilación del azufre (SUF). Estas tres vías proporcionan los centros Fe/S para la mayoría de las proteínas Fe/S en casi todos los organismos. La maquinaria de ensamblaje ISC es necesaria para la maduración de todas las proteínas dependientes de centros Fe/S en la mitocondria, el citosol y el núcleo, y también está involucrada en la homeostasis de hierro en procariontes y eucariontes **[Barupala et al., 2016]**. El sistema ISC se identificó inicialmente en especies bacterianas, donde los genes ISC están dispuestos en el operón *isc*. El estudio en eucariontes (*Saccharomyces cerevisiae* y proteínas humanas) reveló un sistema altamente homólogo localizado en la mitocondria **[Barupala et al., 2016]**. En *Saccharomyces cerevisiae*, la maquinaria ISC mitocondrial está codificada por los genes NFS1, ISU1, ISU2, ISA1, ISA2, JAC1, SSQ1, YAH1, GRX5 e IBA57 **[Lill et al., 2012; Schilke et al., 2006]**. En la levadura, la chaperona Ssq1 y la proteína Jac1 (co-chaperona) intervienen juntas en la biogénesis de centros Fe/S.

La biogénesis de centros Fe-S en las mitocondrias es iniciado por la cisteína desulfurasa (Nfs-

Isd11), que obtiene el azufre de una cisteína y lo transfiere a las proteínas de ensamble Isu1/Isu2, asistida por Yah1. Esta interacción también implica a la frataxina (Yfh1), que actúa como un donador de hierro. Las proteínas Isu1/Isu2 trasfieren el recién formado centro Fe/S a la proteína Ssq1, que es estimulada por la co-chaperona Jac1 **[Lill et al., 2012; Lill y Muhlenhoff, 2006; Lill, 2009]**. La proteína Isu1 es un sustrato para Ssq1 y Jac1, mientras que Jac1 e Isu1 estimulan cooperativamente la actividad ATPasa de Ssq1 **[Dutkiewicz et al., 2003]**. La posterior transferencia del centro Fe-S a las correspondientes apoproteínas receptoras es asistida por Grx5 **[Lill et al., 2012; Rodríguez-Manzaneque et al., 2002]**. Hasta este punto son incorporados únicamente los centros 2Fe-2S. Posteriormente, las proteínas Isa1 e Isa2 participan en la maduración de apoproteínas mitocondriales que contienen grupos 4Fe-4S tales como la aconitasa, la homoaconitasa y la ácido lipoico sintasa, cuya actividad está mediada por la interacción física con la proteína de ensamblaje Iba57. Las proteínas Isa1/Isa2 son prescindibles para la generación de proteínas mitocondriales [2Fe-2S] y citosólicas [4Fe-4S], porque, aunque las proteínas Isa1 e Isa2 son capaces de unir hierro, éste no se utiliza para el ensamblaje *de novo* de centros [2Fe-2S] junto con las proteínas de ensamblaje general, Isu1/Isu2. De manera que Isa1/Isa2 e Iba57 funcionan como un subsistema de ensamblaje de acción tardía, dedicado específicamente a la maduración de las proteínas mitocondriales [4Fe-4S] **[Mühlenhoff et al., 2011]**.

Los centros Fe-S son cofactores biológicos versátiles que se encuentran en rutas bioquímicas fundamentales, como la aconitasa y la succinato deshidrogenasa que actúan a nivel del ciclo de los ácidos tricarboxílicos y los complejos respiratorios I-III de la cadena de transporte de electrones **[Rouault, 2012]**. Las proteínas nucleares con centros Fe/S también tienen un papel único en el reconocimiento y la reparación del daño del ADN. Varias formas de ADN polimerasa, helicasa, glicosilasa y primasa contienen centros Fe/S **[Paul y Lill, 2015]**. Los centros Fe/S se pueden encontrar en el sitio activo de muchas enzimas esenciales y, por lo general, están involucrados directamente en la catálisis. Al ser estables en una variedad de estados redox, los centros Fe/S son mejor conocidos por su papel como transportadores de electrones, pudiendo acarrear uno o hasta dos electrones y son, posteriormente, estables en varios estados reducidos, como los centros 2Fe-2S, por ejemplo, pueden existir en formas oxidadas (Fe^{3+}/Fe^{3+}) o reducidas (Fe^{3+}/Fe^{2+}) mientras que los grupos 4Fe-4S son estables en las formas oxidada ($Fe^{3+}/Fe^{3+}/Fe^{3+}/Fe^{2+}$), intermedia ($Fe^{3+}/Fe^{3+}/Fe^{2+}/Fe^{2+}$) y reducida ($Fe^{3+}/Fe^{2+}/Fe^{2+}/Fe^{2+}$) **[Johnson et al., 2005]**. De esta manera, el potencial de reducción de un centro Fe/S a menudo se modula mediante las interacciones con residuos de proteínas vecinas, lo que les permite una amplia gama de funciones biológicas. En algunos casos, los centros Fe/S parecen cumplir solamente una función estructural y no participan directamente en procesos catalíticos.

La CTE utiliza numerosos centros Fe/S. Los complejos respiratorios I, II y III de la CTE contienen todos los tipos de centros Fe/S. El complejo I usa una red de 8 agrupaciones Fe/S para la transferencia de electrones **[Vinothkumar et al., 2014]**. De forma similar, la subunidad SDH2 del complejo II contiene un clúster 2Fe-2S, 3Fe-4S y 4Fe-4S **[Janssen et al., 1997]**. Por último, el complejo III utiliza un único centro 2Fe-2S llamado "centro Rieske" (Rip1) **[Silman et al., 1967]**. Las concentraciones mitocondriales de hierro libre deben controlarse estrictamente durante la biogénesis de centros Fe-S para evitar un aumento perjudicial en su concentración. El hierro ferroso (Fe^{2+}) y férrico (Fe^{3+}) catalizan la formación del radical hidroxilo ($OH\cdot$), que es altamente reactivo en presencia de peroxido (H_2O_2) y superoxido (O_2^-) a través del ciclo de Haber-Weiss. En las mitocondrias, estas ERO se producen fisiológicamente como subproductos de la actividad de la CTE. Por lo tanto, la pérdida de la homeostasis de hierro mitocondrial causa daño oxidativo en el ADN, los lípidos y las proteínas a través de la generación de ERO, que a su vez afecta la función de la CTE y conduce a la muerte celular **[Turrens, 2003]**.

Durante la disfunción del sistema de biogénesis ISC, la acumulación de cantidades tóxicas de hierro en la matriz mitocondrial se produce debido a la regulación positiva de los sistemas de transporte de hierro a través de la activación del factor de transcripción Aft1 **[Hoffmann et al., 2011]**. La acumulación de hierro en la levadura requiere la activación de transportadores de hierro vacuolar, así como los transportadores mitocondriales Mrs3/Mrs4, que desempeñan papeles esenciales tanto en la homeostasis del hierro celular como en la síntesis de grupos Hemo y Fe/S al desplazar el hierro a las mitocondrias **[Foury y Roganti, 2002; Xu et al., 2012]**. Por otro lado, las defensas antioxidantes, la

homeostasis del hierro y el reciclado de centros Fe/S son mecanismos importantes para restablecer la función y la integridad de la célula en condiciones oxidativas. Recientemente, en nuestro grupo de trabajo, se ha demostrado que la supresión en *S. cerevisiae* de los componentes genéticos de la maquinaria mitocondrial de ensamblaje ISC aumenta la toxicidad del etanol a través de una mayor generación de ERO, lo que provoca la disminución de la respuesta antioxidante y finalmente inducen apoptosis **[Pérez-Gallardo et al., 2013].**

Debido a la gran importancia del Fe en diversas funciones biológicas, es de nuestro interés determinar su participación en la generación de ERO en mutantes del sistema ISC, empleando como modelo la levadura *Saccharomyces cerevisiae*, que posee un metabolismo aerobio facultativo, permitiendo el estudio en mutantes del sistema ISC y de la CTE sin comprometer su viabilidad.

2. JUSTIFICACIÓN

La disfunción del sistema ISC, incrementa el estrés oxidativo, sobreactivando los sistemas de respuesta antioxidante; sin embargo, se desconoce si se debe solamente a la participación del hierro, o si existe un efecto sinérgico con la disfunción de la CTE. Por lo que es de nuestro interés, determinar que ocurre con el hierro que no es incorporado a las proteínas blanco en mutantes del sistema ISC y de que manera afecta la disfunción del sistema ISC la actividad de la CTE.

3. HIPÓTESIS

La disfunción del sistema **ISC** incrementa la generación de ERO y afecta directamente la actividad de los complejos respiratorios (II, III y IV), alterando la formación de supercomplejos en la **CTE** en *S. cerevisiae.*

4. OBJETIVO GENERAL

Determinar la función del sistema ISC en la actividad de la CTE y la generación de ERO en la levadura *S. cerevisiae*.

4.1 OBJETIVOS ESPECÍFICOS

- Determinar los niveles de hierro libre (Fe^{2+}) y de ERO en condiciones normales y de estrés oxidativo, en cepas mutantes del sistema ISC y en mutantes de la captación de hierro en *S. cerevisiae*.

- Evaluar la actividad de los complejos respiratorios de la CTE, en cepas mutantes del sistema ISC y en mutantes de las subunidades catalíticas de la CTE, en *S. cerevisiae*.

- Determinar la formación de grupos Hemo (Citocromos *a*, *b*, *c*) y centros Fe-S en mutantes del sistema ISC y de la CTE en *S. cerevisiae*.

5. CAPÍTULO I. El mal funcionamiento de la maquinaria de ensamblaje de centros hierro-azufre en *Saccharomyces cerevisiae*, produce estrés oxidativo a través de un mecanismo dependiente de hierro, causando disfunción en los complejos respiratorios.

OPEN ACCESS Freely available online

PLOS ONE

Malfunctioning of the Iron–Sulfur Cluster Assembly Machinery in *Saccharomyces cerevisiae* Produces Oxidative Stress via an Iron-Dependent Mechanism, Causing Dysfunction in Respiratory Complexes

Mauricio Gomez[1], Rocío V. Pérez-Gallardo[1], Luis A. Sánchez[1], Alma L. Díaz-Pérez[1], Christian Cortés-Rojo[2], Victor Meza Carmen[1], Alfredo Saavedra-Molina[2], Javier Lara-Romero[3], Sergio Jiménez-Sandoval[4], Francisco Rodríguez[4], José S. Rodríguez-Zavala[5], Jesús Campos-García[1]*

1 Lab. Biotecnología Microbiana, Instituto de Investigaciones Químico-Biológicas, Universidad Michoacana de San Nicolás de Hidalgo, Morelia, Michoacán, México, **2** Lab. de Bioquímica, Instituto de Investigaciones Químico-Biológicas, Universidad Michoacana de San Nicolás de Hidalgo, Morelia, Michoacán, México, **3** Facultad de Ingeniería Química, Universidad Michoacana de San Nicolás de Hidalgo, Morelia, Michoacán, México, **4** Centro de Investigación y de Estudios Avanzados del IPN, Unidad Querétaro, Querétaro, México, **5** Departamento de Bioquímica, Instituto Nacional de Cardiología, México, D.F., México

Abstract

Biogenesis and recycling of iron–sulfur (Fe–S) clusters play important roles in the iron homeostasis mechanisms involved in mitochondrial function. In *Saccharomyces cerevisiae*, the Fe–S clusters are assembled into apoproteins by the iron–sulfur cluster machinery (ISC). The aim of the present study was to determine the effects of ISC gene deletion and consequent iron release under oxidative stress conditions on mitochondrial functionality in *S. cerevisiae*. Reactive oxygen species (ROS) generation, caused by H_2O_2, menadione, or ethanol, was associated with a loss of iron homeostasis and exacerbated by ISC system dysfunction. *ISC* mutants showed increased free Fe^{2+} content, exacerbated by ROS-inducers, causing an increase in ROS, which was decreased by the addition of an iron chelator. Our study suggests that the increment in free Fe^{2+} associated with ROS generation may have originated from mitochondria, probably Fe–S cluster proteins, under both normal and oxidative stress conditions, suggesting that Fe–S cluster anabolism is affected. Raman spectroscopy analysis and immunoblotting indicated that in mitochondria from *SSQ1* and *ISA1* mutants, the content of [Fe–S] centers was decreased, as was formation of Rieske protein-dependent supercomplex III_2IV_2, but this was not observed in the iron-deficient *ATX1* and *MRS4* mutants. In addition, the activity of complexes II and IV from the electron transport chain (ETC) was impaired or totally abolished in *SSQ1* and *ISA1* mutants. These results confirm that the ISC system plays important roles in iron homeostasis, ROS stress, and in assembly of supercomplexes III_2IV_2 and III_2IV_1, thus affecting the functionality of the respiratory chain.

Citation: Gomez M, Pérez-Gallardo RV, Sánchez LA, Díaz-Pérez AL, Cortés-Rojo C, et al. (2014) Malfunctioning of the Iron–Sulfur Cluster Assembly Machinery in *Saccharomyces cerevisiae* Produces Oxidative Stress via an Iron-Dependent Mechanism, Causing Dysfunction in Respiratory Complexes. PLoS ONE 9(10): e111585. doi:10.1371/journal.pone.0111585

Editor: Janine Santos, National Institute of Environmental Health Sciences, United States of America

Received February 6, 2014; **Accepted** October 6, 2014; **Published** October 30, 2014

Funding: This research was funded by CONACYT (106567), FOMIX-C01-117130, and C.I.C. 2.14/Universidad Michoacana de San Nicolas de Hidalgo (UMSNH) grants. RVPG, MG, and LAS received a scholarship by CONACYT. The funders had no role in study design, data collection and analysis, decision to publish, or preparation of the manuscript.

Competing Interests: The authors have declared that no competing interests exist.

* Email: jcgarcia@umich.mx

Introduction

The iron–sulfur centers (Fe–S) are prosthetic groups in many prokaryote and eukaryote enzymes with redox, catalytic, and regulatory functions. These centers are assembled by the iron–sulfur cluster assembly system (ISC), which has been extensively studied and is known to be involved in the incorporation of the Fe–S centers into apoproteins in both bacteria and eukaryotes [1–5]. In eukaryotes, two main systems of Fe–S-protein biogenesis have been described, the cytosol/nucleus (CIA) and mitochondrial (ISC) machineries. Functionally, the CIA machinery depends on the mitochondrial ISC machinery [6–7]. The ISC assembly machinery for maturation of all cellular Fe–S dependent-proteins (mitochondrial, cytosolic, and nuclear) is also involved in iron homeostasis in prokaryotes and eukaryotes [5,7]. In *Saccharomyces cerevisiae*, the mitochondrial ISC machinery is encoded by the genes *NFS1*, *ISU1*, *ISU2*, *ISA1*, *ISA2*, *JAC1*, *SSQ1*, *YAH1*, *GRX5*, and *IBA57* [5,8]. In yeast, the Ssq1 chaperone and the Jac1 J-protein (co-chaperone) function together to assist in the biogenesis of Fe–S centers of Fe–S-dependent proteins. The Fe–S cluster assembly in mitochondria is initiated by cysteine desulfurase (Nfs-Isd11), which obtains a sulfur group from a cysteine and transfers it to the scaffold proteins Isu1 and its redundant Isu2 protein, assisted by Yah1. This interaction also involves frataxin (Yfh1), which acts as an iron donor or activity regulator. ATPase activity in the Ssq1chaperone is stimulated by the J-type co-chaperone Jac1, during the interaction with the scaffold protein Isu1/Isu2 [5–7]. The protein Isu1 is a substrate for both Ssq1 and Jac1, while Jac1 and Isu1 cooperatively stimulate the ATPase

activity of Ssq1 [3]. The subsequent cluster transference to recipient apoproteins is assisted by glutaredoxin (Grx5) [5,9].

Recently, the participation of the proteins Isa1 and Isa2 in the maturation of mitochondrial apoproteins containing 4Fe–4S clusters such as aconitase, homoaconitase, and lipoic acid synthase was described in *S. cerevisiae*; this activity is mediated by physical interaction with the Iba57 assembly-protein [5,10–12]. In contrast, Isa1/Isa2 proteins are dispensable for the generation of mitochondrial [2Fe–2S] and cytosolic [4Fe–4S] proteins, because, although the Isa1 and Isa2 proteins are able to bind iron, they are not used as donors for *de novo* assembly of the [2Fe–2S] cluster on the general Fe–S scaffold proteins, Isu1/Isu2 [5,12]. Upon depletion of the ISC assembly factor Iba57, which specifically interacts with Isa1 and Isa2, or in the absence of the major mitochondrial [4Fe–4S] protein aconitase, iron is accumulated on the Isa proteins, suggesting that the iron bound to the Isa proteins is required for the *de novo* synthesis of [4Fe–4S] clusters in mitochondria and for their insertion into apoproteins in a reaction mediated by Iba57. Taken together, these findings define Isa1/Isa2 and Iba57 as a specialized, late-acting ISC assembly subsystem that is specifically dedicated to the maturation of mitochondrial [4Fe–4S] proteins [12].

Iron handling by mitochondria during ISC biogenesis must be tightly controlled to avoid a deleterious increase in the concentration of free iron. Ferrous (Fe^{2+}) and ferric (Fe^{3+}) iron catalyze the formation of the highly reactive hydroxyl radical ($OH^{\bullet}$) in the presence of H_2O_2 and $O_2^{\bullet-}$ species through the Haber-Weiss cycle. In mitochondria, these ROS are physiologically produced as by-products of electron transport chain (ETC) activity. Thus, uncontrolled mitochondrial iron homeostasis causes oxidative damage in DNA, lipids, and proteins via the generation of ROS, which in turn further impairs the function of the ETC and leads to cell death [13].

During the dysfunction of the ISC biogenesis system, accumulation of toxic amounts of iron in the mitochondrial matrix occurs due to upregulation of iron transport systems via the activation of the Aft1 transcription factor [14]. Iron accumulation in yeast requires the activation of vacuolar iron transporters as well as the Mrs3/Mrs4 mitochondrial transporters, which play essential roles in both cell iron homeostasis and heme and Fe–S clusters synthesis by shuttling iron into mitochondria [15–17]. The relevance of impaired ISC biogenesis in mitochondrial iron overload and ETC dysfunction is reflected in human diseases like Friedreich's ataxia, sideroblastic anemia, and ISCU myopathy, whose development has been associated with defects in human genes coding for proteins involved in ISC biogenesis, such as Frataxin, Glrx5, and IscU, respectively [18]. In this regard, yeast has been a powerful tool to elucidate key molecular aspects of the pathogenesis of these diseases because several steps of ISC biogenesis and recycling are conserved between yeast and higher eukaryotes [19].

On the other hand, the antioxidant defenses, iron homeostasis and Fe-S recycling are important mechanisms to restore the function and integrity of the cell under oxidizing conditions. We have recently demonstrated that the deletion of genetic components of the mitochondrial ISC assembly machinery in *S. cerevisiae* exacerbates ethanol toxicity via increased ROS generation, provoking depletion of the antioxidant response and leading to apoptosis [20]. Given the central role of mitochondria in iron handling, the role of free iron from Fe–S-containing proteins in ROS production, and the fact that ethanol increases mitochondrial ROS generation, it can be hypothesized that excessive free iron exacerbates the toxicity of ethanol and other stressors in mitochondria by disrupting the functionality of the ETC. To test this hypothesis, we have analyzed the relationship between mitochondrial free iron and the levels of ROS generated by stressors, the amount of Fe–S containing proteins, and their effect on respiratory chain functionality in yeast mutants of the ISC system and affected in mitochondrial iron transport.

Materials and Methods

Yeast strains, growth conditions, and survival tests

The haploid *S. cerevisiae* BY4741 (Mat a, *his3*Δ, *leu2*Δ0, *met15*Δ0, *ura3*Δ0) and its *KanMX4* interruption gene mutants, *ssq1*Δ, *grx5*Δ, *isa1*Δ, *atx1*Δ, *mrs4*Δ, and *aft1*Δ were obtained from Open Biosystems. Growth tests were carried out using yeast extract peptone dextrose (YPD) culture medium. Tubes or flasks were prepared with 10 or 50 mL of YPD culture medium and added stressor (H_2O_2, menadione, or ethanol from Sigma), at the indicated concentrations. Culture medium was inoculated with overnight yeast cultures that had reached an optical density of 0.1 at 600 nm ($OD_{600\ nm}$) and incubated at 30°C with low-speed shaking (50 rpm). Yeast growth (biomass) was spectrophotometrically monitored at $OD_{600\ nm}$. A survival test was carried out in yeast cultures grown on liquid YPD medium, collected in the late exponential growth phase and then adding ethanol 10% (v/v) and 10 mM 1, 10-phenanthroline, incubating at 30°C with low-speed shaking (50 rpm). Cell survival was determined by Trypan blue staining, and yeast counts were performed using a Neubauer chamber [20].

Real-time quantification of ROS in *S. cerevisiae* cultures

Intracellular ROS in yeast cultures or cell suspensions were determined using oxidant-sensitive, cell-permeant fluorescent probes and fluorescence was quantified by flow cytometry [20]. Cell cultures were grown to the late exponential phase and samples (100 µL) were loaded with the appropriate fluorescent probe. For mitochondrial ROS determination (mit-ROS, mainly H_2O_2), yeast suspensions were incubated with 5 µg mL^{-1} of dihydrorhodamine 123 (DHR123; Sigma) and for superoxide ($O_2^{\bullet-}$) determination, yeast were incubated with 5 µg mL^{-1} dihydroethidium (DHE, Molecular Probes, Invitrogen), at 30°C for 2 h in the dark. Then, yeast cell samples were taken to 1 mL with PBS buffer (NaCl 137 mM, KCl 2.7 mM, $Na_2HPO_4{\cdot}2\ H_2O$ 8.1 mM, KH_2PO_4 1.76 mM, at pH 7.4) and the fluorescence was immediately quantified by flow cytometry using a BD Accuri C6 Flow Cytometer (BD Biosciences). The populations of cells for each of the treatments were gated in the forward scatter and side scatter dot plots to eliminate dead cells and cell debris. Populations corresponding to auto- or basal-fluorescence were located in the left quadrant and cells with emission of fluorescence increments of at least one log unit value were located in the right quadrant of the dot plots. In addition, the percentage of fluorescent cells (PFC) and the median fluorescence intensity (FI) were determined in the monoparametric histograms of fluorescence emission obtained from the dot plots and labeled as percentage of cells and as relative units of fluorescence. The equipment was calibrated using Spherotech 8-peak (FL1-FL3) and 6-peak (FL-4) validation beads (BD Accuri). Fluorescence of the DHR123 probe was monitored in the emission fluorescence channel FL1 (533/30 nm), and for the DHE probe, in the FL2 channel (587/40 nm). A minimum of 20,000 cellular events were analyzed for each determination point. For stressor treatments and Fe^{2+} dose-response assays, yeast cultures grown on YPD medium (10 mL) were loaded with the fluorescent probes by incubating for 30–60 min, washed with PBS and supplemented with the respective concentrations of ROS-generator compounds or Fe^{2+} solution [$FeSO_4(NH_4)$ with an equimolar amount of citric acid, Sigma]. At the respective times,

samples (100 µL) were harvested, washed and suspended in PBS, adjusting the volume to 1 mL or 1×10^7 cells mL^{-1} and the fluorescence was determined by flow cytometry.

Real-time quantification of Fe^{2+}

Iron in the yeast suspensions was determined using the fluorescent, cell-permeable indicator for heavy metals Phen green FL (PGFL; Molecular Probes, Invitrogen), which can be used to detect a broad range of ions, including Cu^{2+}, Cu^{+}, Fe^{2+}, Hg^{2+}, Pb^{2+}, Cd^{2+}, Zn^{2+}, and Ni^{2+}. Fluorescence of PGFL disappears after binding of free Fe^{2+}. Therefore, once cells were loaded with the probe, Fe^{2+} was detected by the addition of 1 mM of the chelator 1,10-Phenanthroline. This treatment leads to PGFL-Fe complex dissociation, producing fluorescence [21]. Yeast cells suspensions (1×10^7 cells/mL) were incubated with PGFL (5 µg/mL) at 30°C for 2 h in darkness. Then, yeast cells were harvested, washed once, and re-suspended in PBS. Fe^{2+} quantification in yeast suspensions was performed without and with ROS-generator treatment and fluorescence was quantified by flow cytometry monitoring the emission fluorescence in channel FL1 (533/30 nm).

Confocal microscopy of yeast suspensions

Saccharomyces cerevisiae YPD-grown cultures were harvested and suspended in PBS at 1×10^7 cell/mL and loaded with the fluorescent probe DHE or PGFL as detailed above, incubating with light shaking in darkness. Suspensions were treated with and without ethanol (10%) and incubated for 30 min at 30°C. Afterwards, the cell suspensions were incubated with Rhodamine 123 (Rho123; Sigma) during 30 min for mitochondrial co-localization and analyzed using a confocal microscope (Olympus FV1000). The signal evaluating fluorescence emission was observed between 560–580 nm for DHE, between 405–505 nm for PGFL and between 590–600 nm for Rho123. Images were acquired with different magnifications.

Mitochondria isolation

For the determination of mitochondrial complexes activity, mitochondria of *S. cerevisiae* were isolated from cultures grown in liquid medium YPD at 30°C in a shaking incubator, using a previously described method with light modifications [22], Lyticase from *Arthrobacter luteus* (Sigma-Aldrich) was used instead of zymolyase. Yeast cells were harvested in late exponential growth phase by centrifugation at 2,750× *g* for 15 min at 4°C and washed thrice using distilled water and suspended in digestion solution (sorbitol 1.2 M, EGTA 1 mM, Tris-HCl 50 mM, DTT 10 mM, at pH 7.5); Lyticase was added at 2 mg g^{-1} weight for spheroplast generation. Yeast suspensions were incubated for 60 min at 30°C. Spheroplasts were washed twice with spheroplast washing buffer (sorbitol 1.2 M, EGTA 1 mM, Tris-HCl 50 mM, DTT 10 mM, at pH 7.5). Then, spheroplasts were suspended in homogenizing buffer (sorbitol 0.6 M, HEPES-KOH 20 mM, DTT 10 mM, at pH 7.4) and lysed in a Potter-Elvehjem pestle and glass tube and washed thrice with the same buffer. The unruptured cells were removed by centrifugation at 2,500× *g* for 10 min at 4°C, and yeast mitochondria were harvested from the supernatant by centrifugation at 9,600× *g* for 10 min at 4°C and suspended in homogenizing buffer.

Determination of *in situ* mitochondrial oxygen consumption rate

Cells (25 mg wet weight) of *S. cerevisiae* were placed in 2.5 mL of MES-TEA buffer (pH 6.0) in a sealed glass chamber with constant stirring. The oxygen consumption rate (OCR) was measured with a Clark-type oxygen electrode coupled to a biological oxygen monitor (YSI 5300). Basal oxygen consumption (state 4), was induced by adding 20 mM glucose as substrate, and 3 min later, 5 µM of the uncoupling agent carbonyl cyanide m-chlorophenyl hydrazone (CCCP) was added to stimulate maximal OCR (uncoupled (U) state). To discriminate the mitochondrial oxygen consumption from unspecific-cytosolic oxygen utilization, the mitochondrial ETC was inhibited with 1 µg antimycin A and a further addition of 0.5 mM KCN [23].

Determination of the ETC complexes activity

Detergent solubilization of mitochondria for determination of ETC activities was carried out by mixing 250 µL of intact mitochondria (10 mg of protein) plus 750 µL of hypotonic buffer (KCl 100 mM, $MgCl_2$ 10 mM, Tris-base 10 mM, pH 7.5, and Triton X-100 (0.02%) with vigorous shaking in a vortex for 15 sec. This solution was centrifuged at 18,600× *g* for 15 min at 4°C. Supernatants were discarded and the pellets suspended in buffer composed of 50 mM KH_2PO_4, pH 7.6 and protein was quantified by the Biuret method. These suspensions of permeabilized mitochondria were used to determine the activity of the ETC complexes, as described below.

Determination of complex II activity. The activity of complex II was evaluated by measuring the succinate-DCIP oxidoreductase activity of solubilized mitochondria [22]. The reaction mixture contained 0.1 mg/mL permeabilized mitochondria, 1 µg antimycin A and 0.75 mM KCN in a final volume of 1 mL 50 mM KH_2PO_4 buffer (pH 7.6). After 5 min of incubation with ETC inhibitors, the determination was started by adding 80 µM 2,6 dichlorophenolindophenol (DCIP) and the basal absorbance at 600 nm was determined for 1 min. Then, the reaction was started by adding 10 mM sodium succinate and the changes in absorbance were further followed for 5 min. The rate of DCIP reduction was calculated from the slopes of the absorbance plots using a molar extinction coefficient for DCIP of 21 mM^{-1} cm^{-1}.

Determination of complex III activity. For this purpose, the activity of antimycin A-sensitive succinate-cytochrome *c* oxidoreductase was measured, which is representative of complex III activity, using endogenous ubiquinol-6 as substrate [24]. Solubilized mitochondria (0.1 mg/mL) were resuspended in 50 mM KH_2PO_4 buffer (pH 7.6) and incubated for 5 min with 0.75 µM KCN. Then, 1.5 mg oxidized cytochrome *c* was added and the basal absorbance was recorded at 550 nm. After 1 min, 10 mM succinate was added, and the reduction of cytochrome *c* was recorded for 3 min. The reaction was stopped by adding antimycin A (1 µg). The rate of cytochrome *c* reduction was determined from the slopes of the absorbance plots, using a molar extinction coefficient for cytochrome *c* of 19.1 mM^{-1} cm^{-1} [22]. Alternatively, complex III activity was measured with 10 mM glycerol, instead of succinate, to bypass electron transfer at complex II and eliminate the possibility that impaired electron transfer at complex II level might mask defects in electron transfer at complex III.

Determination of the complex IV activity. Cytochrome *c* oxidase activity was measured in 0.1 mg/mL solubilized mitochondria suspended in 50 mM KH_2PO_4 buffer (pH 7.6), incubated for 5 min with 1 µg antimycin A. The reaction was started by adding dithionite-reduced cytochrome *c* (250 µg) and the changes in the absorbance at 550 nm were followed during 1 min. The reaction was stopped with 0.75 mM KCN. The rate of cytochrome *c* oxidation was determined from the slope of the

absorbance plots using a molar extinction coefficient for cytochrome *c* of 19.1 mM^{-1} cm^{-1} [22].

Determination of lactate-cytochrome c oxidoreductase. This activity was measured in 1 mg/mL freeze-thawed mitochondria re-suspended in 50 mM KH_2PO_4 buffer incubating for 5 min with 0.75 µM KCN. Basal absorbance at 550 nm during 1 min was registered, and then the reaction was started by adding 10 mM D-lactic acid. Then, the changes in the absorbance were recorded for 5 min. The rate of cytochrome *c* reduction was determined from the slopes of the absorbance plots using a molar extinction coefficient for cytochrome *c* of 19.1 mM^{-1} cm^{-1}.

Determination of *cis*-aconitase activity

Aconitase activity was determined as described by Henson and Cleland (1967) [25]; 100 µg of mitochondrial protein was suspended in lysis buffer (Tris-HCl 50 mM, Triton X-100 0.02%, pH 7.4) with vigorous shaking and incubated for 5 min. Extracts were centrifuged at 9,900× *g* for 5 min at 4°C, and supernatants obtained were used for *cis*-aconitase determinations. Eighty micrograms of protein from the supernatants were used for enzymatic determination in reaction buffer (Tris-HCl 90 mM, isocitrate 20 mM, pH 7.4) with light agitation; the absorbance at 240 nm was immediately recorded.

Mitochondrial membrane potential

Membrane potential in the mitochondrial suspensions was determined using the fluorescent, cell-permeable indicator Rho123. Mitochondrial suspensions (1×10^7 mitochondria/mL) were loaded with Rho123 (5 µg/mL) and incubated at 30°C for 30 min in darkness. Suspensions were harvested, washed once and re-suspended in PBS. Membrane potential in suspensions was determined by fluorescence generation and quantified by flow cytometry, monitoring the emission fluorescence in channel FL1 (533/30 nm).

Raman spectroscopy of mitochondria

Suspensions of intact mitochondria (250 µg) from yeast cultures grown on YPD were subjected to Raman spectroscopy. Raman analysis was performed using a microRaman spectrometer (Dilor model LabRam) equipped with a confocal microscope with 50× amplification, using He-Ne laser emitting at 632.8 nm and 30 mW at sample point for excitation. Mitochondrial dried-pellets were collocated in a cooper plate and laser impacted into a spot of 2 µm with an integration time of 60 s; a 256×1024 pixel charge-coupled device (CCD) was used as a photon detector. The spectra showed correspond to the average of spectra overlapped by 60 s of recording; measurements were carried out at room temperature with sample preparation as described elsewhere [26].

Native Gel Electrophoresis and western blot

For Blue Native gel electrophoresis, samples of 100 µg of mitochondrial protein were solubilized using buffer A containing dodecylmaltoside (1 g/g), triton X-100 (2.4 g/g), and digitonin (3 g/g) as described [27], and separated by native polyacrylamide gel electrophoresis on 8% Bis-tris gels (BN-PAGE); mitochondrial complexes were identified as described [28–30]. For immunodetection assay 50 µg of mitochondrial protein were run in SDS-PAGE 12% polyacrylamide gels and transferred to polyvinylidene difluoride (PVDF) membranes. Membranes were blocked using dry milk in PBS-T and blotted with the *S. cerevisiae* anti-Rip1 antibody as first antibody in blocking medium at a 1:20000 dilution for 2 h at 4°C [4]; after washing, the membrane was incubated with the secondary antibody, a monoclonal anti-mouse IgG HRP-conjugate (Promega), in blocking medium at a 1:5000 dilution for 2 h at 4°C; the membrane was washed with PBS-T and developed using Supersignal West Pico Luminol (Pierce) and exposing in light-sensitive films. Assays were conducted by triplicate and representative images are shown. Bands intensities in gels or films were quantified using the Image J software.

Results

ROS susceptibility of *S. cerevisiae* is exacerbated by mutations in the *ISC*

In order to verify whether the dysfunction in the ISC system is related to a parallel increase in the sensitivity to oxidative damage, the susceptibility to several ROS-generating compounds was tested using three *ISC* mutants, whose disrupted genes encode proteins that play important roles in assembly of Fe–S centers. In addition, control *S. cerevisiae* strains that display a severe imbalance in iron homeostasis were used; these included *atx1*Δ mutants, which are impaired in high affinity iron-depleted medium, as this gene is involved in copper trafficking and delivery to Fet3p, which oxidizes Fe^{2+} to Fe^{3+} for uptake by Ftr1p [31] and *mrs4*Δ mutants, which show cellular iron accumulation and sensitivity to H_2O_2 and menadione, as this gene is co-regulated with the iron regulon, and encodes the Mrs4 Fe^{2+} iron transporter at the inner mitochondrial membrane under conditions of iron deprivation [15–17]. *aft1*Δ mutant shows increased ROS sensitivity and iron accumulation by inducing iron-sensing genes under iron depletion conditions [32]. All these yeast strains show iron-dependence when grown in the presence of phenanthroline, which induces iron-depletion, and which was improved with iron addition in the culture media (Figure S1). *aft1*Δ mutant is more sensitive to iron depletion than *mrs4*Δ mutant, which in turn correlates with the exacerbated sensitivity of the *aft1*Δ mutant to ROS inducers (Fig. 1). Of the *ISC* mutants, *ssq1*Δ, *grx5*Δ, and *isa1*Δ mutants showed a significantly impaired growth rate compared to WT, displaying severely compromised growth at concentrations in the range of 6.25–12.5 mM H_2O_2. *grx5*Δ mutants were the least sensitive at all concentration of H_2O_2 (Fig. 1b–c). The susceptibility to menadione (a superoxide generator), followed a similar pattern to that observed with H_2O_2 treatments: at 80 µM menadione, *ISC* mutants showed a moderate but significant inhibition in their growth kinetics, with respect to the WT strain (Fig. 1d), while at 150 µM menadione, also with ethanol (8%), the growth of all *ISC* mutants was drastically affected (Fig. 1e–f); again, *grx5*Δ was the least sensitive *ISC* mutant to the stressor. As expected, *atx1*Δ and *mrs4*Δ mutants (which show imbalanced iron homeostasis), showed similar behavior to the WT under iron sufficiency, except in YPD supplemented with 12.5 mM H_2O_2 (Fig. 1c), in which delayed growth was observed. In contrast, the hypersensitive *aft1*Δ mutant exhibited a marked sensitivity to H_2O_2, menadione, and ethanol treatments (Fig. 1b–f).

Increment in ROS generation correlates with a dysfunctional ISC assembly system

To elucidate whether the enhanced sensitivity to ROS generators was correlated with increased mitochondrial ROS generation due to *ISC* mutations, real-time quantification of ROS was performed by flow cytometry, using the fluorescent ROS indicators DHE and DHRH123 to detect mitochondrial $O_2^{\bullet-}$ and H_2O_2, respectively. ROS generation was determined as the percentage of fluorescent cells (PFC), corresponding to cells that produced ROS level increments of at least one log unit. All mutants displayed a significant increment in the PFC generating $O_2^{\bullet-}$ or H_2O_2 when ROS induction was conducted using H_2O_2,

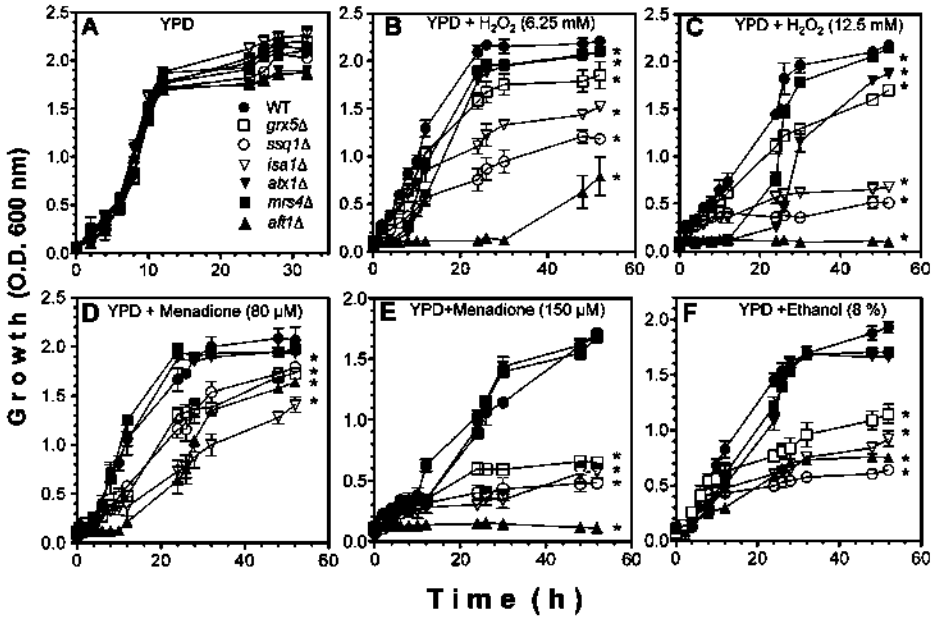

Figure 1. Growth kinetics of *S. cerevisiae ISC* mutants in the presence of ROS generators. A–E) Yeast cultures were grown on YPD liquid medium as follows: A) no addition, B) H_2O_2 6.25 mM, C) H_2O_2 12.5 mM, D) menadione 80 μM, E) menadione 150 μM, and F) ethanol 8% (v/v). Cultures were incubated at 30°C with light shaking and growth (biomass) was determined by measuring O.D. at 600 nm. Values representing the mean and standard errors of the mean (SEM) are indicated as bars (n = 3), one-way ANOVA with Bonferroni's post-hoc test was used to compare mutants versus controls. Significant differences ($p<0.05$) are indicated with (*).
doi:10.1371/journal.pone.0111585.g001

menadione, or ethanol (Fig. 2, continuous lines), compared to untreated strains (Fig. 2, dotted lines). PFC values in yeast suspensions without ROS-inducers were approximately 10%, while in treatments with ROS-inducers the PFC increased to 40–90%. Moreover, *ssq1*Δ, *isa1*Δ, and *grx5*Δ mutants showed higher PFC values than the WT in all ROS-inducer treatments (Fig. 2), indicating that *ISC* mutations caused increased ROS generation compared to WT yeast. Importantly, ethanol treatment exacerbated H_2O_2 generation in *ISC* mutants, but decreased H_2O_2 generation in *atx1*Δ, *mrs4*Δ, and *aft1*Δ iron- transport mutants, compared to *ISC* mutants (Fig. 2f). In addition, *atx1*Δ, *mrs4*Δ, and *aft1*Δ mutants exhibited higher levels of superoxide than H_2O_2 (Fig. 2c and 2f). *grx5*Δ mutants, concordant with their lowest sensitivity to oxidants among *ISC* mutants (Fig. 1), also produced the lowest amounts of ROS, except $O_2^{\bullet-}$, under treatment with 10% ethanol (Fig. 2). In addition, $O_2^{\bullet-}$ production in *aft1*Δ mutants was higher than in all other *ISC* mutants, concordant with its higher sensitivity to stressors (Fig. 1). Interestingly, when ethanol was used as the ROS generator, the *ISC* mutants produced higher levels of H_2O_2 than the iron-transport mutants, (Fig. 2f). These results indicated that the $O_2^{\bullet-}$ and H_2O_2 generation are increased by treatment with ROS inducers in *S. cerevisiae* and are enhanced by the *ISC* mutation in a time-dependent manner, as in the defective iron-transport mutants *atx1*Δ, *mrs4*Δ, and *aft1*Δ.

Increment in ROS generation correlates with Fe^{2+} release and is increased by *ISC* mutations

To evaluate whether the increment in ROS following treatment with oxidant agents was correlated with the functionality of ISC assembly system and the level of the free iron pool, *in vivo* real-time free Fe^{2+} quantification was performed using flow cytometry. Cell suspensions of *ssq1*Δ, *grx5*Δ, and *isa1*Δ mutants showed a significant, time-dependent increment in levels of free Fe^{2+} compared to the WT strain, independent of the presence or absence of oxidants (Fig. 3). As expected, yeast suspensions treated with toxic concentrations of H_2O_2 (12.5 mM), menadione (80 μM), or ethanol (10%) exhibited higher iron- and time-dependent fluorescence increments than untreated yeast strains, leading to a 2–5 fold augmentation of the quantity of free Fe^{2+} in *ISC* mutants after 6 h of treatment. Notably, *ssq1*Δ and *isa1*Δ mutants showed higher levels of Fe^{2+} than *grx5*Δ mutants. In addition, Fe^{2+} release was higher in *atx1*Δ mutants than in *aft1*Δ and *mrs4*Δ mutants, and in these mutants, free Fe^{2+} was also increased when they were treated with oxidant agents (Fig. 3). However, *aft1*Δ and *mrs4*Δ mutants showed behavior intermediate between the WT strain and *ISC* mutants; these cells showed higher free Fe^{2+} than WT, but lower free Fe^{2+} than *ISC* and *atx1*Δ mutants (Fig. 3b–c). When the Fe^{2+} release data were analyzed following 6 h of treatment with ethanol, a significant increment in fluorescence values was observed for *ssq1*Δ, *grx5*Δ, and *isa1*Δ strains, but not for the iron-transport defective strains *atx1*Δ, *mrs4*Δ, and *aft1*Δ. However, in the absence of ethanol, only *ssq1*Δ and *isa1*Δ mutants showed significant differences in free Fe^{2+} release values (Fig. 3d). As mentioned above, with ethanol treatment, the free Fe^{2+} value was significantly increased in all strains, compared to untreated yeast cultures.

In addition, microscopic analysis showed that ethanol treatment caused an increment in superoxide generation, associated with release of free Fe^{2+} and being exacerbated in *ISC* mutants (Fig. 4). For example, in both WT cells and *ssq1*Δ mutants, $O_2^{\bullet-}$ levels were higher under treatment with ethanol than with glucose; this

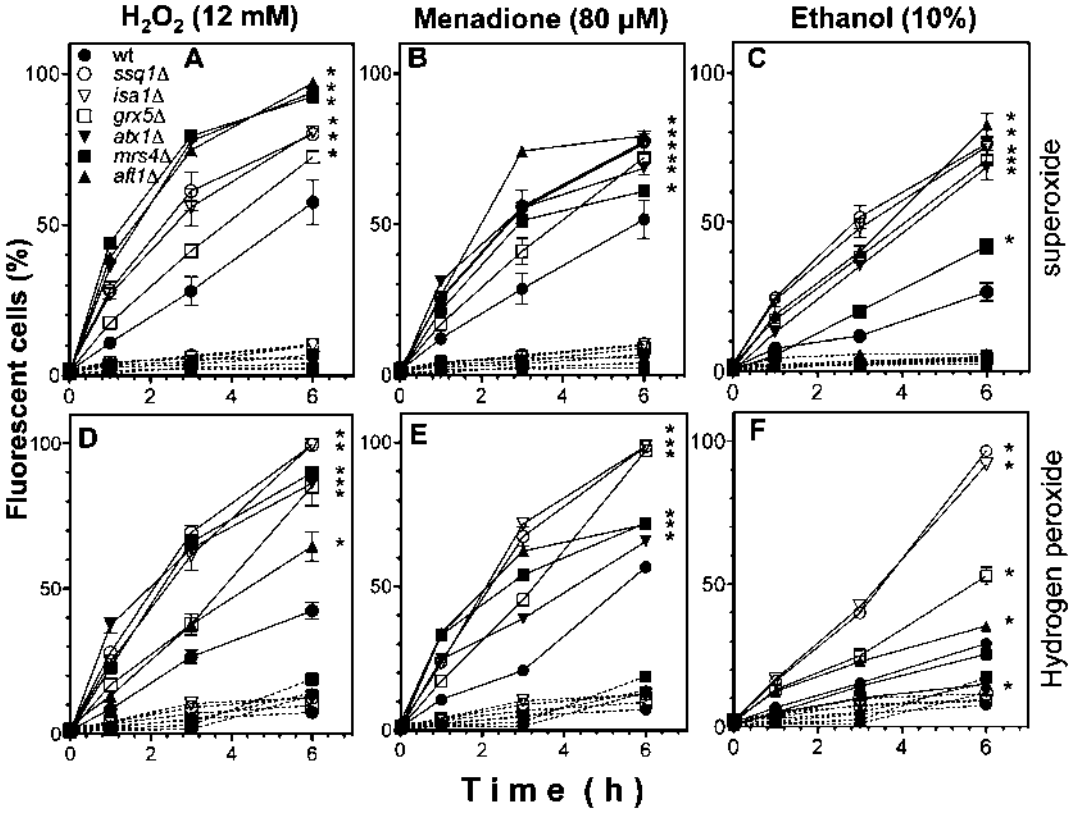

Figure 2. Kinetics of ROS generation in suspensions of *S. cerevisiae ISC* mutants treated with stressors. Yeast cultures were grown in liquid YPD medium without stressors and harvested in late exponential growth phase. Yeast YPD-grown cultures were incubated for 2 h with the respective ROS probe; then, the suspensions were treated with and without stressor (H_2O_2 12 mM, menadione 80 μM, and ethanol 10%), incubated at 30°C with light shaking. Samples (100 μL) were taken and suspended in PBS buffer for determination of intracellular ROS levels by real-time analysis in a flow cytometer. A–F) Results represent the percentage of cells that showed positive fluorescence. Yeast suspensions without a stressor (dashed lines) and with a stressor treatment (continuous lines). The ROS fluorescent probes DHE ($O_2^{\bullet-}$ indicators) and DHR123 (mitochondrial ROS in general, mainly a H_2O_2 indicator) were used. A–C) Fluorescence determination using DHE probe, D–F) fluorescence determination using DHR123 probe. Values are the mean of three independent experiments with 20,000 cells counted by flow cytometry per each point. SEM values are indicated as bars (n = 3), one-way ANOVA was used to compare mutants versus to WT. Significant differences ($p<0.05$) are indicated with (*).
doi:10.1371/journal.pone.0111585.g002

response was exacerbated in *ssq1*Δ mutants, consistent with iron-fluorescence levels determined using the PGFL probe, indicating that it was associated with free Fe^{2+} release (Fig. 4a–h). Interestingly, in the WT strain grown on glucose, $O_2^{\bullet-}$ production and free Fe^{2+} were co-localized in mitochondrial structures (Fig. 4a–b), which were defined by high fluorescence in the *ssq1*Δ mutants or in yeast treated with ethanol (Fig. 4c–h). Further co-localization assays were performed, using rhodamine 123 as an indicator of the mitochondrial membrane potential (Δ*p*). Images showed that in the WT strain, free Fe^{2+} fluorescence was observed in all cells, but with greatest intensity in mitochondrial structures, co-localized with $O_2^{\bullet-}$ generation; interestingly, high-intensity fluorescence was observed inside the cytoplasmic membrane, a response that intensified under ethanol treatment (Fig. 4i–l). As expected, in *ssq1*Δ mutants, which showed affected respiration and Δ*p* behavior (see below), high free Fe^{2+} fluorescence was observed, but it was not co-localized with mitochondrial activity; however, it was probably associated with vacuolar structures (Fig. 4m–n). These results suggest that at least in the WT, the $O_2^{\bullet-}$ generation and free Fe^{2+} release occurred in the mitochondria, although other cellular compartments may also have been involved in this effect. Co-localization assays were performed to analyze $O_2^{\bullet-}/Fe^{2+}$ levels in *ISC* and iron-transport mutants. In both *ssq1*Δ, *atx1*Δ and *aft1*Δ mutants, increased levels of fluorescence corresponding to $O_2^{\bullet-}$ generation and free Fe^{2+} release were observed; in yeast strains, these increased levels were co-localized in possible mitochondrial structures, around some hyper-structures that may correspond to vacuoles (Fig. 4o–t). These results confirm that *ISC* mutations cause an increase in free iron, which was enhanced by treatment with ROS inducers such as ethanol, and which was preferentially associated with mitochondrial structures; interestingly, in *ISC* and iron-transport mutants as well as in WT under ethanol treatment, a clear swelling of vacuolar structures was observed.

To confirm that enhanced ROS generation was correlated with the free Fe^{2+} content, real-time quantification of ROS by flow cytometry in a medium containing sufficient iron was performed using Fe^{2+}dose-response tests (Fig. 5). As expected, all yeast strains displayed a significant, dose-dependent increment in levels of fluorescence (indicating $O_2^{\bullet-}$ and H_2O_2 generation) when treated

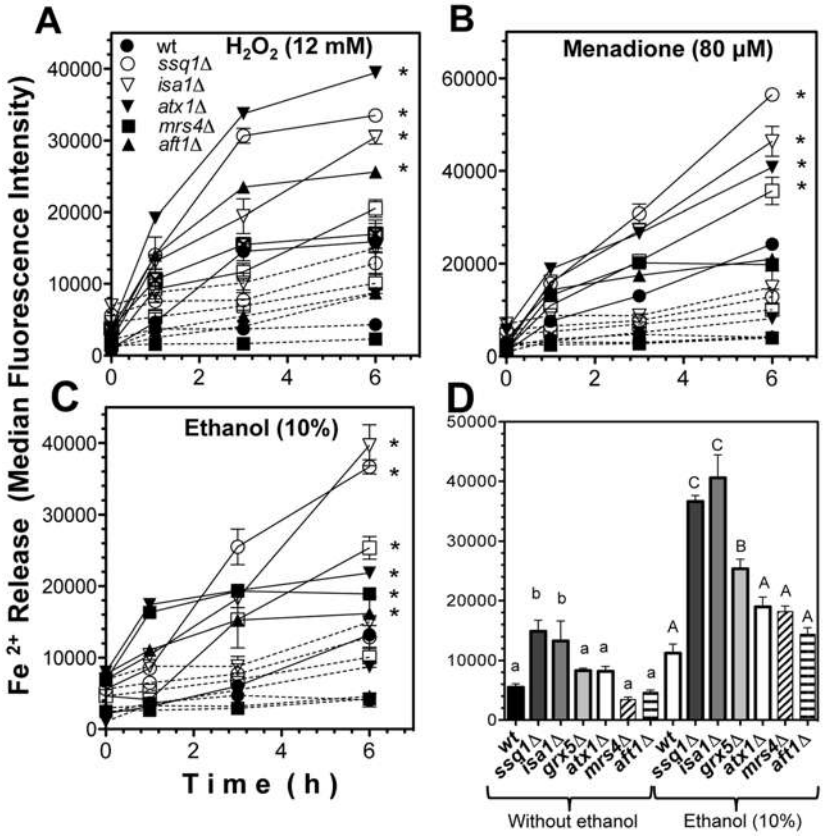

Figure 3. Determination of Fe^{2+} release in *S. cerevisiae ISC* mutants. Yeast cultures were grown in liquid YPD medium, harvested and suspended in YPD at 1×10^7 cells/mL and charged with the fluorescent probe PGFL and incubated for 2 h at 30°C with light shaking in darkness. Then, yeast suspensions were treated with and without a stressor and incubated at 30°C with light shaking. Samples (100 μL) were collected, suspended in PBS buffer, and the fluorescence intensity in the cells was evaluated by real-time flow cytometry within 6 h. Free Fe^{2+} determination in yeast suspensions without a stressor (dashed lines) and with stressor treatment (continuous lines). A) H_2O_2 12 mM, B) menadione 80 μM, C) ethanol 10% v/v, D) Free Fe^{2+} determination at 6 h of treatment with ethanol (10%). Results represent the fluorescence intensity of yeast cells. Values are the mean of three independent experiments with 20,000 cells counted by flow cytometry per each point. SEM values are indicated as bars (n = 3), one-way ANOVA with Bonferroni's post-hoc test was used to compare mutants to controls. Significant differences ($p<0.05$) are indicated with (*) for (A–C). Tukey's post-hoc test was used for (D), and significant differences ($p<0.05$) with respect to the WT control are indicated with different letters for the treatments; lowercase and uppercase letters indicate without and with ethanol treatment, respectively.
doi:10.1371/journal.pone.0111585.g003

with increased concentrations of Fe^{2+}. *ssq1*Δ and *isa1*Δ mutants showed the highest ROS generation; in contrast, *grx5*Δ mutants showed a moderate increment in ROS compared to the WT strain, but this increment was lower than that observed in *ssq1*Δ and *isa1*Δ mutants. For *atx1*Δ, *mrs4*Δ, and *aft1*Δ iron-homeostasis deficient mutants, both the DHE and DHR123 probes showed that the ROS content was similar to those observed in the WT and *grx5*Δ strains (Fig. 5a–b). These results indicated that at Fe^{2+}concentrations below 10 μM, $O_2^{\bullet-}$ was the main species produced, while at concentrations of Fe^{2+} between10–20 μM, an increment of H_2O_2 was also observed (Fig. 5a–b). In addition, determination of ROS generation in YPD-grown cultures showed that the ROS increment was significantly decreased in all mutants by addition of the metal chelator phenanthroline, although this effect was not statistically significant in the WT cells (Fig. 5c). These results confirm the notion that free iron is responsible for an important proportion of the ROS generated in both *ISC* and defective iron-transport mutants.

The role of free iron in ROS generation in the presence of ethanol in *ISC* mutants was further confirmed by determination of cell survival in cultures treated with a toxic concentration of ethanol (10%) and the addition of an iron chelator (10 μM phenanthroline). The *ISC* mutants showed decreased survival following ethanol treatment, and *ssq1*Δ and *isa1*Δ mutants were most sensitive; when a Fe^{2+} chelator was added to the cultures, survival was significantly restored in all strains (Fig. 5d). These results are in concordance with an increased free iron content and exacerbation of ROS generation observed in *ISC* mutants. Likewise, phenanthroline also exerted a significant protective effect against toxic ethanol concentrations in the iron homeostasis defective mutants *atx1*Δ, *mrs4*Δ, and *aft1*Δ. These results indicate that the toxic effects produced by ethanol and other oxidant agents were associated with intracellular Fe^{2+} release in a dose-dependent manner, and that this phenomenon is exacerbated by dysfunction of the ISC system.

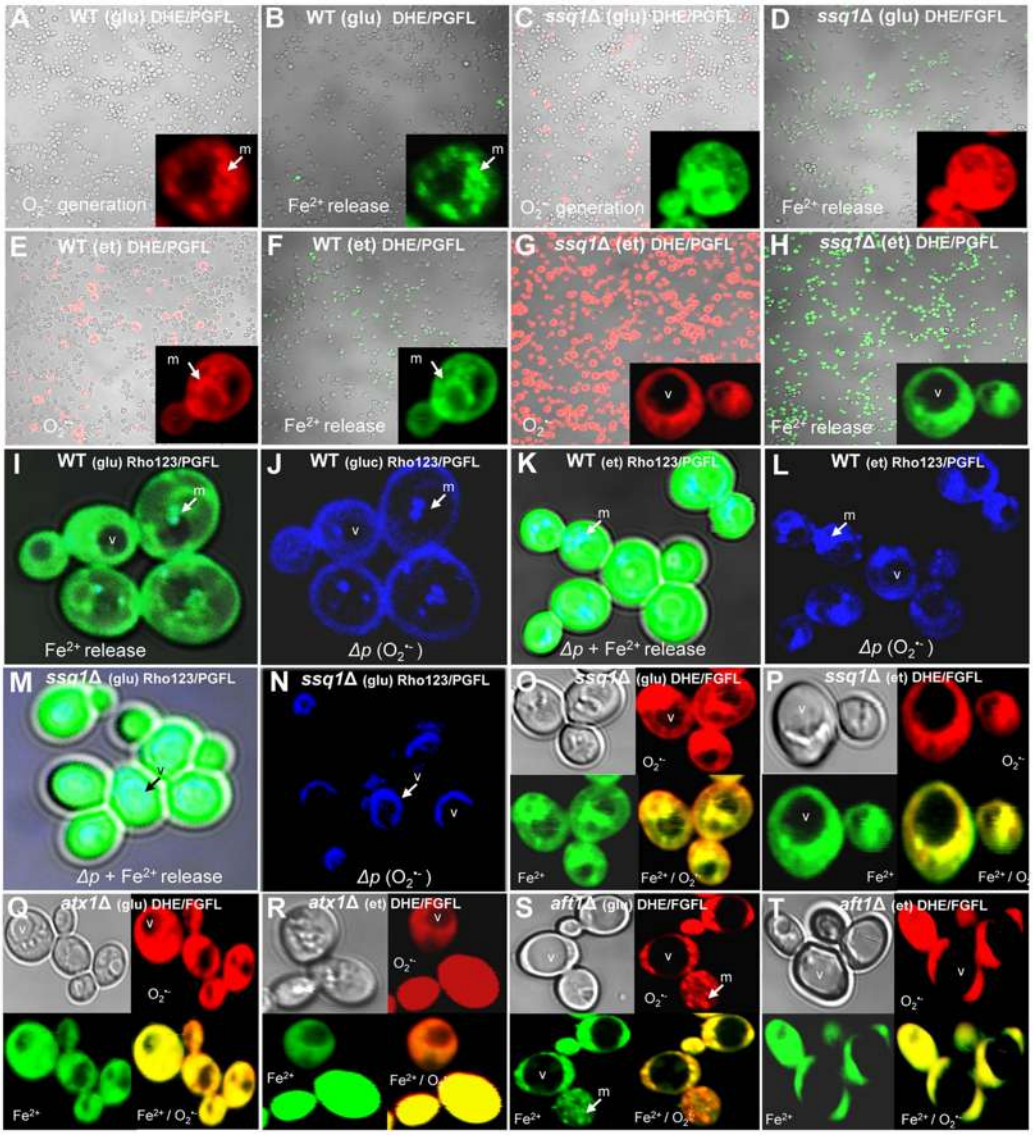

Figure 4. Confocal microscopy images of S. cerevisiae cultures treated with oxidant agents to detect localization of ROS and free Fe^{2+} in intracellular compartments. Yeast YPD-grown cultures were loaded with the fluorescent probe DHE or PGFL and treated with and without ethanol (10%), incubated for 30 min at 30°C and co-loaded with Rho123 as a mitochondrial co-localization marker, and observed using a confocal microscope (Olympus FV1000). (A–D) WT and *ssq1*Δ mutant grown on glucose (2%) and with ethanol (10%) (E–H), using DHE probe for superoxide determination or PGFL probe for free Fe^{2+} determination, as indicated. Cells are shown in boxes, and mitochondria and vacuoles are indicated with (m) and (v). (I–L) Images of WT yeast growth in glucose or treated with ethanol 10% and stained with PGFL and Rhodamine 123 probes, as indicated. (M–P) Images of *ssq1*Δ mutants treated with glucose or ethanol (10%), using PGFL and Rhodamine 123 probes, as indicated. (Q–T) Images of $O_2^{\bullet-}$ and free Fe^{2+} co-localization in *atx1*Δ and *aft1*Δ mutants grown on glucose or treated with ethanol (10%), and staining with PGFL or DHE probes, as indicated. Superoxide generation areas are shown as fluorescent granules within the cells (see inset of A, J–L), free Fe^{2+} is shown as green cells and green granules within the cells (see inset of B and I), merged images are shown as yellow cells and granules within cells (O–T), and mitochondrial structures are shown as cyan granules within the cells, using the Rho123 probe (I–L). Images of the yeast cells were taken using 10× magnification, 40× magnification, and 65× magnification of yeast cells.
doi:10.1371/journal.pone.0111585.g004

Cellular free iron release is correlated with a decrement in Fe-S proteins content

The above results led us to hypothesize that the increment in free iron levels induced by oxidative stress and ethanol and exacerbated by ISC system dysfunction arise partially from iron sources such as proteins containing Fe–S centers, including complexes II and III of the ETC. Raman spectroscopy analysis has been used as an analytical tool for determination of Fe–S

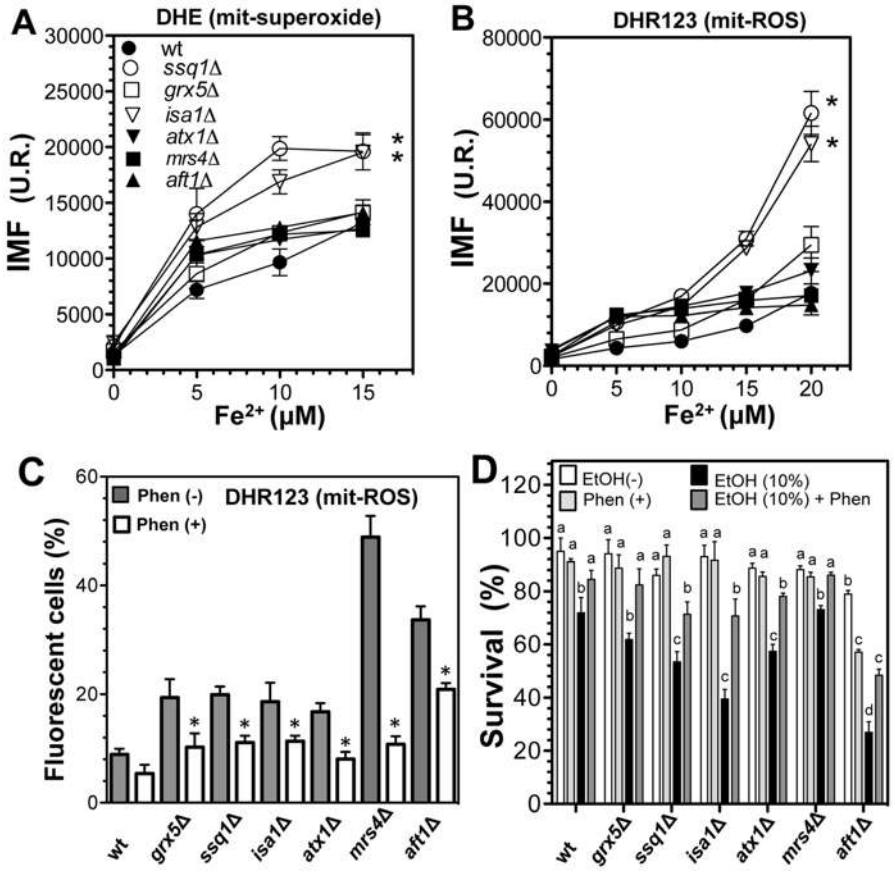

Figure 5. Effect of Fe^{2+} treatment on *S. cerevisiae ISC* mutants. YPD-grown yeast cultures were harvested and suspended in YPD at 1×10^7 cell/mL, loaded with ROS-sensitive probes, and subjected to Fe^{2+} dose-response assays. Fluorescence intensity was determined by flow cytometry using DHE probe (A), and DHR123 (B). Yeast suspensions were treated with Fe^{2+} [$FeSO_4(NH_4)$] (10 μM) with and without the metal chelator 1,10-phenanthroline (1 mM), and the percentage of fluorescent cells was determined by flow cytometry (C). Values are the mean of three independent experiments with 20,000 cells counted by flow cytometry for each point. (D) Yeast survival using ethanol as a ROS-inducer. Yeast suspensions were treated with and without ethanol (10%) and with 1,10-phenanthroline (20 mM), and the percentage of surviving cells was determined using Trypan Blue staining; yeast counting was performed using a Neubauer chamber [20]. SEM values are indicated as bars (n = 3), one-way ANOVA with Bonferroni's post-hoc test was used to compare mutants with the control WT strain (A–C), significant differences ($p<0.05$) are indicated by (*); or Tukey's post-hoc for (D), significant differences ($p<0.05$) with respect to the WT control are indicated with different lowercase letters.
doi:10.1371/journal.pone.0111585.g005

species and contents; therefore, this technique was utilized to determine the Fe–S content in mitochondria isolated from *ISC* mutants or the iron-transport defective mutants *atx1*Δ and *mrs4*Δ grown in YPD. Signal intensities in the interval 200–700 cm^{-1} at 632.8 nm in the Raman spectra are in agreement with signals corresponding to photonic emission, characteristics of previously described [2Fe–2S] and [4Fe–4S] centers [26,33]. In our system, mitochondria from *S. cerevisiae* clearly showed Raman signals in stretching regions of peaks at 345–365, 390–440, 460–480, 490–500, 510–520, and 640–660 cm^{-1} (Fig. 6a). The intensity of Raman signals of the Fe–S centers were clearly diminished in mitochondria from *ssq1*Δ and *isa1*Δ mutants compared to WT mitochondria, whereas in *grx5*Δ mutants, the signal peaks showed increased intensities. Interestingly, the iron deficient *atx1*Δ and *mrs4*Δ mutants showed peaks intensities higher than those of the WT. These results indicate that the amount of mitochondrial Fe–S center signals were diminished in mitochondria from *ssq1*Δ and *isa1*Δ mutants, but were overproduced in *grx5*Δ, *atx1*Δ, and *mrs4*Δ mutants.

To investigate the role of Fe-S proteins in Fe^{2+} release under oxidative stress, we conducted a functional analysis of the 4Fe–4S protein *cis*-aconitase, which has been described as ROS-sensitive and as an iron donor for the Fenton reaction. With respect to [2Fe–2S] clusters, we assayed the activity of ETC complex III which is rich in that center and is known to be a main source of $O_2^{\bullet-}$ generation in mitochondria [34]. *Cis*-aconitase activity was almost totally abolished in the *isa1*Δ mutants compared to the WT strain (Fig. 6b), confirming that in the ISC assembly system, the Isa1 protein is essential for assembly of the [4Fe–4S] cluster into aconitase enzyme. Moreover, aconitase activity was partially inhibited in the remaining *ISC* mutants, whereas in *mrs4*Δ and *atx1*Δ mutants, a decrease in aconitase activity was also observed but to lesser extent that in *ISC* mutants.

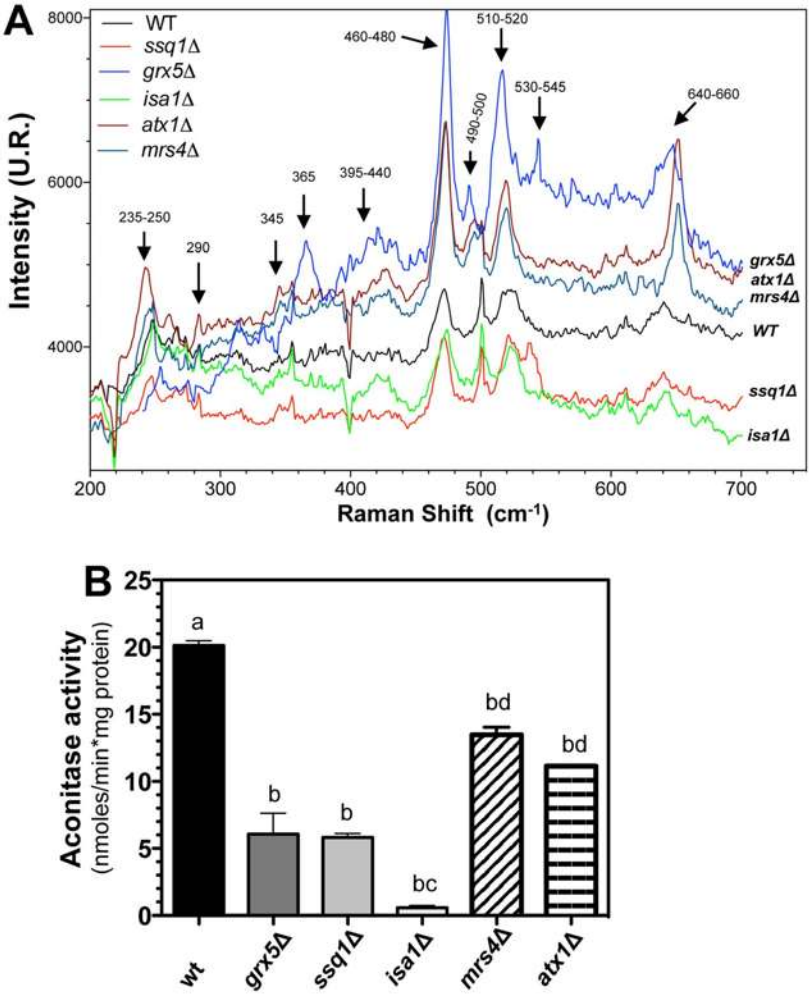

Figure 6. Analysis of mitochondrial Fe–S-containing proteins in *S. cerevisiae ISC* mutants. Cell extracts of yeast cultures grown in YPD to the late exponential growth phase were used to isolate mitochondria, as described in the Materials and Methods section. A) Raman scattering spectra of the mitochondria isolated from *S. cerevisiae ISC* mutants. Raman spectra were recorded at a laser excitation of 632.8 nm with 30 mW. Each spectrum is the average of scans recorded over 60 sec, using photon counting at 0.5 cm^{-1} increment spectral resolution. Bands corresponding to the [2Fe–2S] and [4Fe–4S] clusters are indicated with arrows [26]. B) Enzymatic activity of *cis*-aconitase was determined in mitochondrial suspensions as described in the Materials and Methods. Values are the mean of three independent experiments. SE values are indicated as bars (n = 3), one-way ANOVA with Tukey's post-hoc test was used to compare yeast strains, and significant differences ($p<0.05$) are indicated with different lowercase letters.

doi:10.1371/journal.pone.0111585.g006

However, respiratory complex assembly studies have indicated that the [2Fe–2S]-Rieske protein of complex III is essential for the correct formation of ETC supercomplexes, constituted of complex III (ubiquinol-cytochrome *c* reductase or bc_1 complex) and complex IV (cytochrome *c* oxidase) [4,35].Therefore, we analyzed the assembly of ETC supercomplexes using BN-PAGE gels [27–30].

Interestingly, the results of the BN-PAGE gels indicated that assembly of the III_2IV_2 and III_2IV_1 supercomplexes is dependent on the functionality of the ISC system. The band corresponding to the III_2IV_2 supercomplex was almost absent in mitochondria from *ssq1*Δ and *isa1*Δ mutants, but the band corresponding to the III_2IV_1 supercomplex was detected at low levels in all *ISC* mutants (Fig. 7a). Remarkably, in the densitometric analysis of the gels, the intensity of the bands corresponding to the III_2IV_2 supercomplex was significantly affected in *ssq1*Δ and *isa1*Δ mutants; the III_2IV_1 supercomplex was also diminished in *ssq1*Δ, *isa1*Δ, *grx5*Δ, and *mrs4*Δ mutants, whereas in *atx1*Δ mutant, a response similar to the WT was observed (Fig. 7b). In addition, densitometry data indicated that the content of dimeric complex V (i.e. the F_1F_0 ATPase) and its monomer were significantly increased in *grx5*Δ mutants, whereas the dimer of complex IV and II remained unaffected in *ISC* mutants but not in the iron-transporter deficient strains. Immunoblotting assays using anti-Rip1 antibody (Rieske protein) confirmed the supercomplexes formation and Raman spectrometry findings. In western blot analysis of mitochondrial

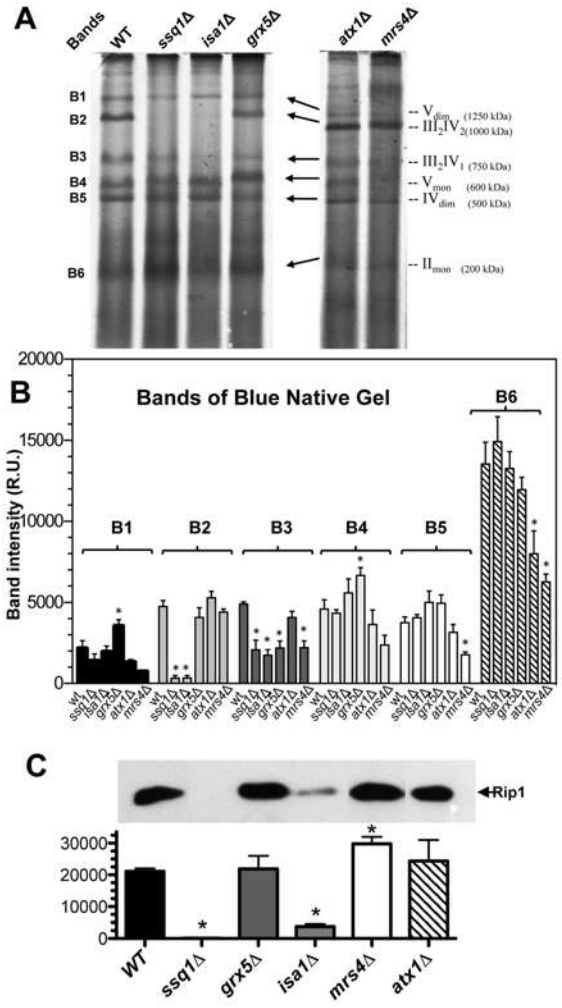

Figure 7. Analyses of supercomplex formation in the mitochondrial ETC of *S. cerevisiae ISC* mutants. To analyze ETC supercomplex formation, mitochondrial suspensions isolated from yeast grown on glucose at the late exponential growth phase were solubilized and the proteins separated using blue native polyacrylamide gel electrophoresis (BN-PAGE) as described in the Materials and Methods [27–29]. The ETC mitochondrial supercomplexes and their molecular mass in kilodaltons are indicated to the right of the gel (A) as described elsewhere [27,28,30]. B) Analysis of band intensities of the supercomplexes observed in (A). C) Immunoblotting of mitochondrial extracts using anti-Rip1 antibody as the first antibody [4] and monoclonal anti-mouse IgG HRP conjugate as the second antibody; the densitometry analysis plot is shown below. Data correspond to three independent assays determining the band intensity by densitometry analysis using Image J software. Values are the mean of three independent mitochondrial isolations. SE values are indicated as bars (n = 3), one-way ANOVA with Bonferroni's post-hoc test was used to compare yeast strains, and significant differences ($p<0.05$) with respect to the WT control are indicated by (*).
doi:10.1371/journal.pone.0111585.g007

protein extracts from the *S. cerevisiae* strains, the protein signal corresponding to Rip1p was absent from mitochondria from *ssq1*Δ mutant, and significantly diminished in the *isa1*Δ mutant, but in *grx5*Δ, *mrs4*Δ, and *atx1*Δ mutants similar levels to the WT was observed, while *mrs4*Δ mutant showed a stronger signal (Fig. 7c).

Mitochondrial ETC functionality is affected by *ISC* mutations

Raman spectroscopy observations of mitochondria isolated from *S. cerevisiae* under iron sufficiency indicated that the [Fe–S] cluster content was diminished in *ssq1*Δ and *isa1*Δ mutants, and native gels showed a clear alteration in the amount of the III_2IV_2 and III_2IV_1 supercomplexes. We therefore evaluated the *in situ* mitochondrial oxygen consumption rates (OCR) to determinate the functionality of the ETC in *ISC* mutants. In this case, *atx1*Δ and *mrs4*Δ mutants were included as controls, because *aft1*Δ cells showed decreased mitochondrial content and severely impaired function following isolation (data not shown). Respiration was completely abolished in both the coupled and uncoupled states in *ssq1*Δ and *isa1*Δ mutants, whereas in *grx5*Δ, *atx1*Δ, and *mrs4*Δ mutants, the OCR was partially decreased in comparison with the WT strain (Fig. 8a–b). Remarkably, ethanol treatment caused oxygen release in the assay chamber (i.e. negative values for OCR, Fig. 8d–f) instead of oxygen consumption in *ISC* mutants, except for *grx5*Δ and *atx1*Δ. This is suggestive of ROS production, since superoxide dismutase catalyzes the conversion of $O_2^{\bullet-}$ to O_2 and H_2O_2, while catalase converts the latter species into H_2O and O_2. In *S. cerevisiae* mitochondria, complex III is the only site of ROS generation in the ETC, since it lacks a rotenone-sensitive complex I, the other site of ROS production in the ETC of superior eukaryotes [35]. We exposed the cells to antimycin A, an inhibitor of complex III, to further explore the possible role of complex III in ROS generation. In the absence of ethanol, a small amount of O_2 generation was detected in all *ISC* mutants except in *grx5*Δ, whereas in the presence of ethanol, higher rates of O_2 generation were detected in these mutants, and O_2 consumption was fully inhibited in *grx5*Δ cells (Fig. 8f). Conversely, antimycin A-insensitive oxygen consumption was observed in WT, *grx5*Δ, and *atx1*Δ cells in the absence of ethanol, and only in WT and *atx1*Δ cells in the presence of ethanol. In contrast to the behavior of *ISC* mutants, *mrs4*Δ mutant, which shows affected iron homeostasis, displayed an OCR similar to that of the WT strain in the presence of glucose in the coupled state (Fig. 8a). To further corroborate the degree of mitochondrial dysfunction in the various strains, we evaluated mitochondrial membrane potential (Δp). In concordance with their inability to respire, *ssq1*Δ and *isa1*Δ mutants did not exhibit Δp (Fig. 9a). Furthermore, OCR correlated with the magnitude of Δp in WT, *grx5*Δ, *atx1*Δ, and *mrs4*Δ cells, since membrane potential was 2–4-fold higher in WT than in *grx5*Δ or *atx1*Δ and *mrs4*Δ mutants. The OCR in a coupled state followed a similar pattern (Fig. 8a and 9a), which in turn may be related to the decreased complex II signal observed for these mutants (Fig. 7a and 7b).

To determine which segment of the ETC was responsible for the effects described above, partial ETC reactions were analyzed. Succinate-DCIP oxidoreductase activity (representative of complex II activity) was observed to be abolished in *ssq1*Δ and *isa1*Δ mutants, and to be severely affected but not abolished in control mutants *atx1*Δ and *mrs4*Δ, which displayed behavior similar to *grx5*Δ mutants, that showed 30–40% of the WT activity (Fig. 9b).

The same trend was observed in both antimycin A-sensitive succinate-cytochrome *c* oxidoreductase (representative of the activity of complex III, using the endogenous ubiquinol-6 pool as a substrate) [24] and cytochrome *c* oxidase (representative of complex IV) activities; their activities in complexes III and IV were almost entirely abolished in *ssq1*Δ and *isa1*Δ mutants, whereas in

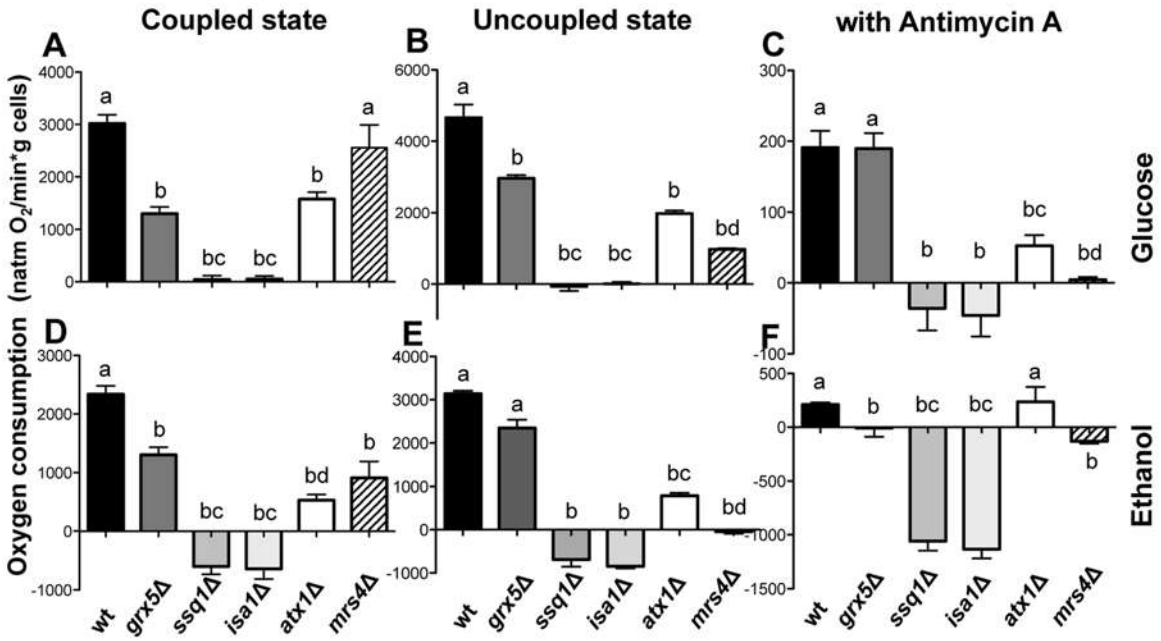

Figure 8. Respiration test of cell suspensions from *S. cerevisiae ISC* mutants. Mitochondrial functionality was evaluated in yeast suspensions obtained from cultures grown in liquid YPD medium, cells were harvested in the late exponential growth phase and re-suspended in MES-TEA buffer with glucose or with ethanol and incubated at 30°C with light shaking. Cells were used for oxygen consumption rate (OCR) measurements with a Clark-type oxygen electrode coupled to a biological oxygen monitor as described in the Materials and Methods. A–C) Basal OCR with glucose as substrate, D–F) with ethanol treatment. A and D) OCR under coupled state conditions, B and E) OCR under uncoupled state conditions using CCCP for uncoupling, C and F) OCR under complex III blocking conditions using antimycin A as an inhibitor. Values are the mean of three independent experiments. SE values are indicated as bars (n = 3), one-way ANOVA with Tukey's post-hoc test was used to compare yeast strains, significant differences ($p<0.05$) are indicated with different lowercase letters.
doi:10.1371/journal.pone.0111585.g008

*grx5*Δ, *atx1*Δ, and *mrs4*Δ strains, a remnant activity of ~20–40% with respect to WT mitochondria was detected (Fig. 9c and 9f).

Antimycin A-sensitive succinate-cytochrome *c* oxidoreductase activity is dependent on electron transfer between complex II and complex III. Thus, to eliminate the possibility that impaired succinate-cytochrome *c* oxidoreductase activity was the result of impaired complex II activity, and not of direct damage of complex III, the activity of complex III was tested by reducing the mitochondrial quinone pool with glycerol via the concerted action of porin-associated glycerol kinase and mitochondrial glycerol-3-phosphate dehydrogenase [36,37]. No differences in this activity with respect to mitochondria from WT cells were observed in *grx5*Δ, *isa1*Δ, or *atx1*Δmutant, while mitochondria from *ssq1*Δ and *mrs4*Δ mutants exhibited a 3-fold diminution (Fig. 9d). Another respiratory enzyme that utilizes cytochrome *c* as its electron acceptor is L-lactate-cytochrome *c* oxidoreductase or cytochrome b_2 [38]. This activity was similar in all the mutants tested; however, it was three-fold lower in the mutants than in the WT strain (Fig. 9e).

Discussion

The toxic effects of ethanol on mitochondrial function have been attributed to a variety of factors, ranging from alteration of ETC complex activities [39], loss of heme groups from cytochromes [40], oxidative degradation and depletion of mtDNA [41], diminished number of active ribosomes [34], decreased glutathione pools and lipid peroxidation [42]. Although many of these events are related to increased ROS generation, none of these reports have addressed the possibility that disturbances in mitochondrial free iron from Fe–S clusters may be related to ethanol toxicity. Nevertheless, earlier reports have identified a link between ROS overproduction and iron overload in the toxic effects of ethanol, since iron chelation attenuates some of the disturbances in the antioxidant defenses caused by ethanol consumption [43,44]. We have recently observed in yeast cells that ROS generation during ethanol stress was exacerbated by mutations in *ISC*, which participate in the various steps in Fe–S biogenesis [20]. In the present study, we hypothesized that the increased free iron content was correlated with the dysfunctional mitochondrial Fe–S assembly system, which affects iron homeostasis after treatment with ethanol or ROS generators. The results obtained in the present study indicate that a dysfunctional ISC assembly system increases susceptibility to ethanol and ROS generators, such as H_2O_2 and menadione (Fig. 1), probably via both increased mitochondrial ROS levels and disruption of ETC functionality. These effects seem to be linked to an increment in the free iron pool, since iron chelation had a protective effect in ISC mutants exposed to ROS inducers. This suggests a close relationship between levels of free iron and ROS generation, where the Fe–S assembly system plays a relevant role in iron homeostasis and its dysfunction may partially contribute to excessive iron release to the cell.

The sensitivity of the mutants to ROS generators and ethanol, as well as their levels of ROS production and free iron release (Fig. 1–3), appear to be highly dependent on the functionality of

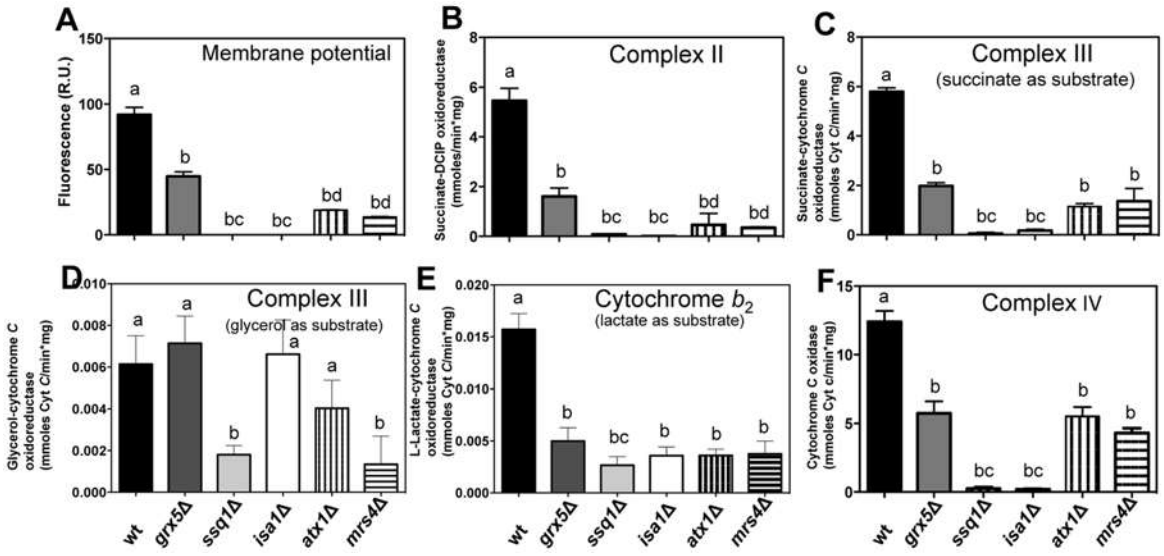

Figure 9. Analyses of the functionality of mitochondrial respiratory chain complexes in *S. cerevisiae ISC* mutants. Mitochondrial functionality was evaluated in mitochondrial suspensions obtained from cultures grown in liquid YPD medium, cells were harvested in the late exponential growth phase, mitochondria were isolated and re-suspended in the appropriate buffer, and mitochondrial activities were measured as described in the Materials and Methods. A) membrane potential, B) activity of succinate-DCIP oxidoreductase, C) activity of succinate-cytochrome *c* oxidoreductase, D) activity of glycerol-cytochrome *c* oxidoreductase, E) activity of L-lactate-cytochrome *c* oxidoreductase, and F) activity of cytochrome *c* oxidase. Values are the mean of three independent experiments. SE values are indicated as bars (n = 3), one-way ANOVA with Tukey's post-hoc test was used to compare yeast strains, and significant differences ($p<0.05$) are indicated with different lowercase letters.
doi:10.1371/journal.pone.0111585.g009

the ETC (Figs. 8–9), since strains that showed better respiratory rates, higher activity of ETC complexes and higher mitochondrial transmembrane potentials (i.e. WT and *grx5*Δ cells), also exhibited lower sensitivity to ethanol and ROS generators, presented lower levels of free Fe^{2+}, and showed decreased levels of ROS production than mutants with null membrane potential and fully impaired ETCs (i.e. *ssq1*Δ and *isa1*Δ). These results also indicate that a dysfunctional ISC assembly system produces an increased sensitivity to ROS generators. Concordantly, ethanol and other ROS inducers also produce a ROS imbalance in *ISC* mutants in a concentration-dependent manner [20].

The findings obtained using the fluorescent ROS probes DHE and DHR123 (Fig. 2) suggest that ROS are mainly generated and probably accumulated in mitochondria after treatment with toxic concentrations of ROS inducers; an additive effect on ROS generation was observed in *ISC* mutants. In addition, the results obtained for *atx1*Δ, *mrs4*Δ, and *aft1*Δ mutants confirmed that altered iron homeostasis caused an increased generation of ROS (such as superoxide and hydrogen peroxide), which was exacerbated when ethanol, H_2O_2, or menadione were used as inducers, suggesting the participation of free iron in the ROS sensitivity (Fig. 2).

Biogenesis of Fe–S centers in *S. cerevisiae* occurs mainly in mitochondria, and the assembly mechanism of these centers depends on the functionality of *ISC* gene products. Iron is an essential component of this process, and its cellular content is dependent on transport systems, chelating proteins and storage. It is well known that iron can be released from Fe–S proteins by $O_2^{\bullet-}$ or H_2O_2 [1,5,12,29], which in turn can lead to the generation of the strongly oxidant $OH^{\bullet}$ radical via Fenton's chemistry.

The findings for Fe^{2+} release in *ssq1*Δ and *isa1*Δ mutants suggest that accumulation of preassembled Fe–S clusters, due to insertion failure caused by disruption of *ISC* or the absence of the target apoproteins (i.e., mitochondrial Fe–S-containing proteins), leads to an increment in the free Fe^{2+} pool, provoking an oxidative stress event (Fig. 3). This may lead to denaturing/dissociation of already assembled Fe–S hemoproteins as an iron source; the prosthetic groups of these proteins could also be one of the iron sources that cause the iron imbalance, leading to a vicious circle of ROS generation (Fig. 10). This is concordant with the impairment of cytochrome b_2, a heme enzyme, observed in all mutants tested. Additionally, it has been reported that in yeast mitochondrial superoxide dismutase (SOD2) can be metallated with iron instead of manganese when iron homeostasis is disrupted, leading to enzyme inactivation. Thus, SOD2 inactivation derived from the intramitochondrial free iron increment may be an additional factor involved in superoxide accumulation, since this mis-metallation is more apparent in Grx5p and Ssq1p mutants, and affects downstream steps in iron-sulfur biogenesis [45,46].

The fact that excess iron in *ssq1*Δ and *isa1*Δ mutants causes an additive increase in ROS generation (Fig. 3) is in agreement with the increment in O_2 generation observed in these mutants in the presence of glucose plus 10% ethanol (Fig. 8f). Because the release of Fe^{2+} was enhanced in these mutants, $OH^{\bullet}$ radicals may have also been formed due to the Haber-Weiss cycle. This event would lead to a worsening of the redox state with catastrophic consequences for the cell, due to the high reactivity of $OH^{\bullet}$ with virtually any class of biomolecule. In summary, we suggest that the iron-mediated mechanism of ROS inducer toxicity in *ssq1*Δ and *isa1*Δ mutants may be also be the result of impaired electron transfer at complexes II and IV (Fig. 9 b and 9f), which in turn leads to a reduction in electron transporters in complex III, as

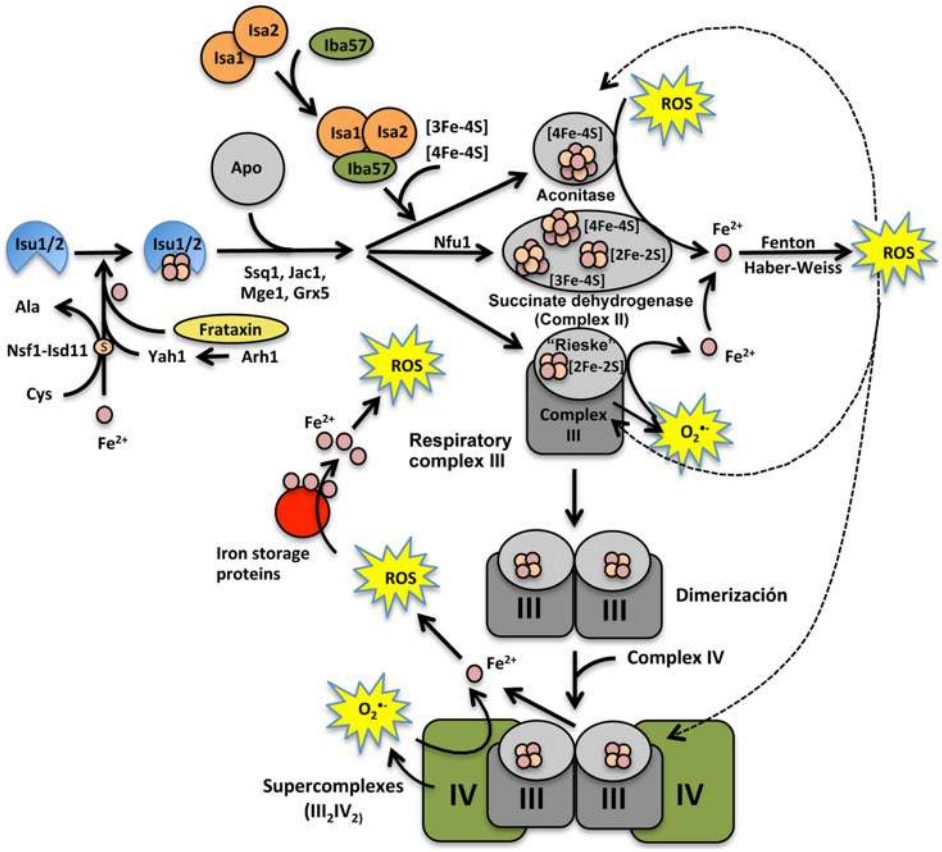

Figure 10. Model proposed for the mechanism of mitochondrial generation of ROS dependent on free Fe^{2+} release from Fe–S-containing proteins in *S. cerevisiae*. The [2Fe–2S] commonly carried by the multi-protein complex (Ssq1-Jac1-Mge1-Grx5) can also be assembled into recipient apoproteins, such as the Rieske protein of cytochrome *bc1* from respiratory complex III. The Isa1 and Iba57 proteins may function as iron reservoirs, from which the metal can subsequently be transferred to [Fe–S] centers or heme prosthetic groups from cytochrome bc_1. When superoxide ($O_2^{\bullet-}$) is generated by electron leaking in the ETC, and other ROS are produced by oxidative metabolism or by oxidant agents, the [4Fe–4S], [3Fe–4S], or [2Fe–2S] clusters contained in the ETC complexes are disrupted. This event provokes a generalized uncoupling/denaturation of Fe–S proteins, causing a release and thus an increment in the iron labile pool (Fe^{2+}), which increases mitochondrial ROS levels via the Fenton and Haber–Weiss reactions. If the ISC assembly system is dysfunctional, supercomplex (III_2IV_2) formation is affected, as is [Fe–S] recycling, provoking ETC dysfunction. Hence, the levels of ROS generation increase in an additive manner by a vicious circle of disruption of iron-containing or iron storage proteins, causing an imbalanced ROS content (increment of species such as H_2O_2 and superoxide species), that provokes mitochondrial dysfunction and may ultimately lead to apoptotic events.
doi:10.1371/journal.pone.0111585.g010

reflected by the effect of antimycin A in the Fig. 8f, and further generation of ROS. The increment in ROS may enable the release of more iron from storage systems, and probably from the prosthetic groups of Fe–S or heme proteins, contributing in this way to a feedback mechanism for ROS generation via the increment in the free iron pool (Fig. 10). Moreover, this may be related to an apoptotic phenotype in *ssq1*Δ and *isa1*Δ mutants, observed in the presence of toxic quantities of the ROS inducer, ethanol [20]. These suggestions are supported by the fact that *grx5*Δ, in which lower levels of Fe^{2+} were released in the presence of ethanol, still displayed OCR and partial activity of all ETC complexes, as well as null oxygen release even in the presence of antimycin A (Figs. 8 and 9). The effects of Grx5p deletion suggest that the main function of this protein is the transitory storage of Fe–S clusters during ISC assembly, which is reflected by the lower iron release and resultant lower ROS generation observed in the *grx5*Δ mutant.

Importantly, *isa1*Δ and ssq*1*Δ mutants showed similar phenotypes for ROS susceptibility, ROS generation, Fe^{2+} release, OCR, and ETC complexes activities. We speculate that the free iron released may originate from Fe–S-containing proteins such as ETC complex II, because the *isa1*Δ and *ssq1*Δ mutants were the major producers of ROS, and both completely lack complex II activity (Fig. 9b), suggesting that Fe–S-dependent recipient proteins are involved. These facts also suggest that the Isa1 protein could be involved in *de novo* Fe–S assembly or recycling of Fe-containing proteins from complex II, because Isa1p/Isa2p have also been described as iron reservoirs [12]. However, it is possible that the iron release mainly proceeds from iron storage sources, such as vacuoles or iron-chelation proteins, such as frataxin, which make iron already present within mitochondria available for Fe–S

cluster synthesis when iron concentrations are low or the Fe–S content is diminished [16].

With the objective to elucidating this last hypothesis, concerning the roles of Isa1 in Fe–S assembly and iron recycling, three types of possible recipient proteins were evaluated: (1) the [4Fe–4S] cluster from *cis*-aconitase, which has been described as highly sensitive to ROS and which is considered to be an iron donor for the Fenton reaction; (2) the Rieske protein from ETC complex III, which is rich in [2Fe–2S] clusters, and which is recognized as the main source of superoxide generation in mitochondria [47], (3) along with succinate dehydrogenase from complex II, which contains [2Fe–2S], [3Fe–4S], and [4Fe–4S] clusters [48]. As shown in Fig. 6b, *cis*-aconitase was not affected in *atx1*Δ or *mrs4*Δ mutant, but it was affected in *ISC* mutants (*ssq1*Δ and *grx5*Δ), and it was almost totally abolished in the *isa1*Δ strain. Concordant with our results, a reduction in aconitase protein expression and enzymatic activity has been described in *mrs4*Δ iron-transport mutant, along with iron dependence for *de novo* Fe–S cluster formation, dependent on the Mrs3/Mrs4 iron-transporters or frataxin involved in iron homeostasis (its diverse functions include Fe–S clusters synthesis, heme biosynthesis, aconitase repair, respiratory regulation, iron detoxification, iron storage, and oxidative stress protection) [15–17]. These findings confirm that in [4Fe–4S] clusters, assembly into target proteins such as *cis*-aconitase is dependent on the Isa1 protein, as described previously [12]. Interestingly, *grx5*Δ mutant showed a diminution in complex II activity, suggesting that assembly of the Fe–S clusters of complex II may also be assisted by the Grx5 protein. Abolishment of succinate dehydrogenase activity (null activity of complex II) in the *isa1*Δ strain strongly suggests its involvement in assembly of Fe–S clusters in the Sdh protein of complex II (Fig. 9b). Interestingly, our Raman spectrophotometry results were in agreement with these observations, indicating that the [2Fe–2S] and [4Fe–4S] cluster content in isolated mitochondria was severely diminished in *isa1*Δ and *ssq1*Δ mutants, compared with the WT. Meanwhile, in the conditional iron-transport mutants *atx1*Δ and *mrs4*Δ, and in *grx5*Δ strain mutants, an increased content of Fe–S clusters was observed (Fig. 6a). Iron-deficiency has been described to provoke a decrease in the iron uptake in *atx1*Δ mutants [31], a condition that causes an increment in iron uptake, as in *mrs4*Δ mutants [17]. This iron-limiting condition induces upregulation of iron-dependent genes controlled by the transcriptional regulator Aft1 [49], and in some genes involved in the ISC system [50]; these observations are concordant with the increased [2Fe–2S] and [4Fe–4S] clusters, corresponding to signals in the Raman spectra of mitochondria from *atx1*Δ, *mrs4*Δ, and *grx5*Δ mutants.

The assembly of ETC supercomplexes formed by cytochrome bc_1 complex and cytochrome *c* oxidase (complexes III and IV of the ETC) is dependent on the integration of Rieske protein into the bc_1 complex [4,35,51]. In this context, we examined formation of ETC supercomplexes III/IV in *S. cerevisiae ISC* mutants using native-blue gels [27–30]. We found that supercomplex III_2/IV_2 was virtually undetectable in mitochondria isolated from *ssq1*Δ and *isa1*Δ mutants, but supercomplex III_2/IV_1 was diminished in both *ISC* mutants, as well as in *grx5*Δ mutants (Fig. 7). In agreement, with these findings, immunoblotting using an anti-Rip1 antibody showed that the ISC system is involved in the assembly of the Rieske subunit of complex III, and that Ssq1p is essential, but Isa1p and Grx5p are not. Moreover, in *grx5*Δ, *atx1*Δ, and *mrs4*Δ mutants, the Rieske protein was up-regulated (Fig. 7c). This result is coincident with the increase in Fe–S cluster signals observed in the Raman spectra (Fig. 6). These findings suggest that the ISC system plays an important role in the assembly of supercomplexes III/IV of the ETC, probably in a Rieske-dependent manner. Alternatively, these findings suggest that these proteins are related to heme biogenesis or assembly in ETC cytochrome-containing proteins such as complex IV or cytochrome b_5, by modulating the bioavailability/recycling of iron. However, further studies are required to corroborate these hypotheses in detail.

We expected that disruption of ISC biogenesis would only impair complexes containing Fe–S clusters. This expectation was concordant with the observed abolishment of complex II activity in *ssq1*Δ and *isa1*Δ mutants, as this complex contains [2Fe–2S], [3Fe–4S], and [4Fe–4S] clusters in the catalytic dimer of the enzyme that play a central role in catalysis, as they receive electrons from $FADH_2$ and transfer them to the membrane domain where quinone reduction occurs [24]. Interestingly, the activities of complexes II and III in *grx5*Δ mutants, although decreased, were not totally abolished, as in the other *ISC* mutants; indeed, the activity of complex III with glycerol was similar to that of the WT strain (Fig. 9d). This result seems to contradict the essential role of Grx5p in the activity of complex II, reported by Rodríguez-Manzaneque et al. (2002) [9]. However, this discrepancy may be attributed to the different technique used to measure complex II activity in that study, which involved following the formation of formazan resulting from the reduction of a tetrazolium salt by complex II [52], formazan can also be formed by the reduction of tetrazolium salts by ROS [53]. We avoided this issue by monitoring reduction of DCIP. It has been proposed that Grx5p participates in ISC cluster biogenesis by assisting in the transference of Fe–S clusters from the scaffold to target proteins [54] and/or by repairing mixed disulfides between glutathione and ISC assembly factors [55], in addition, it may constitute transitory Fe–S cluster storage [56], although its exact role remains to be elucidated. Thus, it appears that the function of Grx5p in the assembly of Fe–S clusters from complexes II and III may partially be replaced by other glutaredoxins.

Collectively, these results indicate that the respiratory incompetence of *ssq1*Δ and *isa1*Δ mutants was mainly due to defective oxidation of substrates in complex II and impaired delivery of electrons to complex III, and to oxygen in complex IV.

Although they lack Fe–S clusters, both complex IV and cytochrome b_2 (i.e. both heme-containing proteins) were also affected in all *ISC* mutants, except *grx5*Δ (Fig. 9). This was not at all surprising, since in yeast decreased heme biosynthesis and cytochrome deficiency are general phenotypic features of cells with an impaired mitochondrial ISC system [6]. *ISA1* and *SSQ1* yeast mutants contain decreased amounts of both hemes c+c_1 and b and residual activity of cytochrome *c* oxidase [57]. Concerning the null complex IV activity of *ssq1* and *isa1*Δ mitochondria, a similar phenotype was reported by Gelling et al. (2008) [10]. The impaired complex IV activity observed in these mutants may also be explained by the inability of this enzyme to form supercomplexes with complex III, as it has been demonstrated that when complex III has an incorrect conformation, the activity of complex IV may be strongly affected [4,35,51]. This is in full agreement with the impaired formation of supercomplexes III_2IV_2 and III_2IV_1 in *ISC* mutants (Fig. 7).

Mitochondrial respiration was absent in *ssq1*Δ and *isa1*Δ mutants in all respiratory states. This effect seems to be mainly attributable to defective electron transfer to O_2 at complex IV, since this activity was fully inhibited in these cells (Fig. 8). Another factor contributing to the respiratory incompetence of these mutants is their inability to oxidize substrates at complex II, as demonstrated by their observed null succinate-DCIP oxidoreductase and succinate-cytochrome *c* oxidoreductase activities. The impairment in the latter activity was not attributed to defective

electron transfer at complex III, since we detected cytochrome *c* reduction in *isa1*Δ in the presence of glycerol at the same level as in WT, but at significantly diminished levels in *ssq1*Δ mutants (Fig. 8). This is concordant with the fact that Isa1p has not been described as participating in the assembly of 2Fe–2S centers, which is the type of ISC present in the Rieske subunit of complex III [5]. However, Raman spectra indicated that a decrease in Fe–S protein content in mitochondria occurs in *ssq1*Δ and *isa1*Δ mutants, also associated with loss or diminution of the Rieske protein in complex III, although the involvement of mitochondrial proteins containing heme groups cannot be neglected. The last observation is in accordance with formation of supercomplexes in the ETC that depend on Fe–S proteins, as seen in the mitochondrial extract from *ssq1*Δ and *isa1*Δ mutants in native gels and western blots, suggesting that, in addition to Fe–S cluster assembly, these proteins could also be involved in heme assembly in mitochondrial respiratory complexes.

Regarding the role of the functionality of ETC in ethanol tolerance, it must be considered that in yeast, mitochondria participate in the maintenance of the redox balance during metabolism of sugars by oxidizing the NADH generated during both glycolysis and ethanol oxidation by the cytosolic and mitochondrial isoforms of alcohol dehydrogenase [58]. This process is very important to avoid deleterious production of mitochondrial ROS, since high $NADH/NAD^+$ ratios favor higher rates of ROS production in the ETC [59]. In yeast, the NADH dehydrogenases Nde1, Nde2, and Ndi1 shuttle electrons from NADH to the quinone pool [60], and the ubiquinol generated is oxidized by the quinol-oxidase site of complex III. Although *ssq1*Δ and *isa1*Δ mutants exhibited partial or full complex III activity (Fig. 8), it is possible that the null activities of complexes II and IV indirectly interfere with NADH oxidation and ethanol metabolism. This prevents the re-oxidation of electron acceptors in complex III, which in turn may lead to an increase in the generation of semiquinone radicals, favoring the generation of $O_2^{\bullet-}$. In accordance with this notion, it has been demonstrated that the inhibition of complex II or complex IV may enhance mitochondrial ROS generation [61,62]. This point is further supported by the fact that the addition of antimycin A leads to ROS generation (Fig. 8c and 8f). This also indicates that ubiquinol is being oxidized at the quinol oxidase (Qo) site of complex III for bifurcated reduction of cytochrome *b* and posterior $O_2^{\bullet-}$ formation by inhibition of re-oxidation of cytochrome b_{562} in the quinone reductase site (Q_i) induced by antimycin A [24]. Otherwise, the generation of O_2 by antimycin A would not be possible. Furthermore, the exacerbation of O_2 release by antimycin A with ethanol treatment (Fig. 8) is suggestive of further impairment of the Q cycle in complex III, corroborating the hypothesis that the toxicity of ROS inducers is mediated by altered electron transfer in the ETC, leading to enhanced ROS generation. It must be stressed again that O_2 generation is an indicator of ROS production because O_2 is a product of the degradation of $O_2^{\bullet-}$ and H_2O_2, catalyzed by superoxide dismutase and catalase, respectively. Importantly, we also found that these mutants have increased catalase activity [20], which may be an adaptive response to enhanced ROS generation due to impaired ETC function.

In summary, exacerbation of ROS generation in *S. cerevisiae* caused by treatment with stressors such as ethanol, H_2O_2, and menadione, occurs via Fe^{2+} release, which is favored by an iron-dependent ROS generation cycle. Microscopic analysis of the WT strain showed that free Fe^{2+} release and ROS co-localized mainly in mitochondria, and were exacerbated by ethanol treatment (a ROS inducer), whereas in *ssq1*Δ mutants, both free Fe^{2+} and ROS were observed in all cells. This pattern was also observed in *atx1*Δ and *mrs4*Δ mutants, which are hyper-iron accumulators in an iron-rich media. Interestingly, a phenotype of bloated vacuole structures was observed in *ISC* mutants, as in iron-accumulator mutants (*atx1*Δ and *mrs4*Δ), suggesting dysfunctional iron homeostasis associated with mitochondria and vacuole organelles. Raman spectroscopy and supercomplex formation of mitochondria isolated from *ISC* mutants indicated that disruption of Ssq1 and Isa1 proteins provoked a decrease in [2Fe–2S] and [4Fe–4S] cluster content that was reflected in loss of the Rieske protein from complex III and disrupt supercomplex formation between complexes III and IV, leading to dysfunction of the ETC and probably to mitochondrial apoptotic events.

Our findings indicate that free Fe^{2+} release and ROS generation are interdependent and are associated with mitochondrial iron homeostasis, via Fe–S-containing proteins, and with storage/detoxification systems, such as frataxin, which are important iron sources. The bloated vacuoles observed in *ISC* mutants following treatment with ROS inducers, as well as in iron-accumulator mutants (*atx1*Δ and *mrs4*Δ) suggest that an iron imbalance occurred was important in the loss of iron homeostasis, that in turn contributed to ROS generation, and to impaired Fe–S cluster biogenesis of proteins from the ETC. The oxidative stress generated and the effects on the Fe–S-containing proteins led to mitochondrial dysfunction.

Supporting Information

Figure S1 Studies of growth in plates of the *S. cerevisiae ISC* mutants. A–D) Dilutions of yeast suspensions were cultured on YPD agar plates with or without ROS-inducers at the indicated concentrations at 30°C for 48 h. Yeast cultures grown on YPD medium plates with: A) different concentrations of the iron chelator 1,10-phenanthroline (10 μM and 20 μM). B) low-iron content using the iron chelator 1,10-phenanthroline (20 μM) and different concentrations of ferrous iron (5–20 μM). C) ROS-inducers at indicated concentrations of H_2O_2 (4 mM), menadione (80 μM), and ethanol (8%). D) low-iron content using 1,10-phenanthroline (20 μM) plus ferrous iron (20 μM) with the concentrations indicated of ROS-inducers H_2O_2 (4 mM), menadione (80 μM), and ethanol (8%). E) low-iron content using 1,10-phenanthroline (20 μM) plus ferrous iron (500 μM) with the concentrations indicated of ROS-inducers H_2O_2 (4 mM), menadione (80 μM), and ethanol (8%).
(TIF)

Acknowledgments

We thanks to Drs. G. Del Rio and S. Funes from Instituto de Fisiologia Celular/UNAM by yeast strains donation. To Conte L. and Zara V. by Anti-Rip1 antibody donation.

Author Contributions

Conceived and designed the experiments: RVPG CCR JCG. Performed the experiments: RVPG MG LAS ALDP. Analyzed the data: RVPG VMC CCR JLR SJS FR JSRZ JCG. Contributed reagents/materials/analysis tools: JLR SJS FR ASM JSRZ. Wrote the paper: CCR JCG.

References

1. Schilke B, Voisine C, Beinert H, Craig E (1999) Evidence for a conserved system for iron metabolism in the mitochondria of *Saccharomyces cerevisiae*. Proc Natl Acad Sci USA 96: 10206–10211.
2. Hoff KG, Silberg JJ, Vickery LE (2000) Interaction of the iron-sulfur cluster assembly protein IscU with the Hsc66/Hsc20 molecular chaperone system of *Escherichia coli*. Proc Natl Acad Sci USA 97: 7790–7795.
3. Dutkiewicz R, Schilke B, Knieszner H, Walter W, Craig EA, et al. (2003) Ssq1, a mitochondrial Hsp70 involved in iron-sulfur (Fe/S) center biogenesis. Similarities to and differences from its bacterial counterpart. J Biol Chem 278: 29719–29727.
4. Conte L, Zara V (2011) The Rieske Iron-Sulfur Protein: Import and Assembly into the Cytochrome bc(1) Complex of Yeast Mitochondria. Bioinorg Chem 363941.
5. Lill R, Hoffmann B, Molik S, Pierik AJ, Rietzschel N, et al. (2012) The role of mitochondria in cellular iron-sulfur protein biogenesis and iron metabolism. Biochim Biophys Acta 1823:1491–1508.
6. Lill R, Muhlenhoff U (2006) Iron-sulfur protein biogenesis in eukaryotes: components and mechanisms. Annu Rev Cell Dev Biol 22: 457–486.
7. Lill R (2009). Function and biogenesis of iron-sulphur proteins. Nature 460:831–838.
8. Schilke B, Williams B, Knieszner H, Pukszta S, D'Silva P, et al. (2006) Evolution of mitochondrial chaperones utilized in Fe-S cluster biogenesis. Curr Biol 16:1660–1665.
9. Rodríguez-Manzaneque MT, Tamarit J, Bellí G, Ros J, Herrero E (2002) Grx5 is a mitochondrial glutaredoxin required for the activity of iron/sulfur enzymes. Mol Biol Cell 13:1109–1121.
10. Gelling C, Dawes IW, Richhardt N, Lill R, Mühlenhoff U (2008) Mitochondrial Iba57p is required for Fe/S cluster formation on aconitase and activation of radical SAM enzymes. Mol Cell Biol 28:1851–1861.
11. Sheftel AD, Wilbrecht C, Stehling O, Niggemeyer B, Elsässer HP, et al. (2012) The human mitochondrial ISCA1, ISCA2, and IBA57 proteins are required for [4Fe-4S] protein maturation. Mol Biol Cel 23:1157–1166.
12. Mühlenhoff U, Richter N, Pines O, Pierik AJ, Lill R (2011) Specialized function of yeast Isa1 and Isa2 proteins in the maturation of mitochondrial [4Fe-4S] proteins. J Biol Chem 286:41205–41216.
13. Turrens JF (2003) Mitochondrial formation of reactive oxygen species. J Physiol 15:335–344.
14. Hoffmann B, Uzarska MA, Berndt C, Godoy JR, Haunhorst P, et al. (2011) The multidomain thioredoxin-monothiol glutaredoxins represent a distinct functional group. Antioxidants & redox signaling 15:19–30.
15. Foury F, Roganti T (2002) Deletion of the mitochondrial carrier genes MRS3 and MRS4 suppresses mitochondrial iron accumulation in a yeast frataxin-deficient strain. J Biol Chem 277: 24475–24483.
16. Zhang Y, Lyver ER, Knight SA, Pain D, Lesuisse E, et al. (2006) Mrs3p, Mrs4p, and frataxin provide iron for Fe-S cluster synthesis in mitochondria. J Biol Chem 281: 22493–22502.
17. Xu N, Cheng X, Yu Q, Zhang B, Ding X, et al. (2012) Identification and functional characterization of mitochondrial carrier Mrs4 in *Candida albicans*. FEMS Yeast Res 12: 844–858.
18. Rouault TA, Tong WH (2008) Iron–sulfur cluster biogenesis and human disease. Trends Genet 24: 398–407.
19. De Freitas J, Wintz H, Kim JH, Poynton H, Fox T, et al. (2003). Yeast, a model organism for iron and copper metabolism studies. Biometals 16:185–197.
20. Pérez-Gallardo RV, Sánchez-Briones L, Díaz-Pérez AL, Gutiérrez S, Rodríguez-Zavala JS, et al. (2013) Reactive oxygen species production induced by ethanol in *Saccharomyces cerevisiae* increases because of a dysfunctional mitochondrial iron-sulfur cluster assembly system. FEMS Yeast Res 13:804–819.
21. Petrat F, Rauen U, de Groot H (1999) Determination of the chelatable iron pool of isolated rat hepatocytes by digital fluorescence microscopy using the fluorescent probe, phen green SK. Hepatology 29:1171–1179.
22. Cortes-Rojo C, Calderón-Cortés E, Clemente-Guerrero M, Estrada-Villagómez M, Manzo-Avalos S, et al. (2009) Elucidation of the effects of lipoperoxidation on the mitochondrial electron transport chain using yeast mitochondria with manipulated fatty acid content. J Bioener Biomem 41:15–28.
23. Brand MD, Nicholls DG (2011) Assessing mitochondrial dysfunction in cells. Biochem J 435:297–312.
24. Muller F, Crofts AR, Kramer DM (2002) Multiple Q-cycle bypass reactions at the Qo site of the cytochrome bc1 complex. Biochemistry 41:7866–7874.
25. Henson CP, Cleland WW (1967) Purification and kinetic studies of beef liver cytoplasmic aconitase. J Biol Chem 242:3833–3838.
26. Zhang B, Crack JC, Subramanian S, Green J, Thomson AJ, et al. (2012) Reversible cycling between cysteine persulfide-ligated [2Fe-2S] and cysteine-ligated [4Fe-4S] clusters in the FNR regulatory protein. Proc. Natl. Acad. Sci. USA 109:15734–15739.
27. Schägger H (2006) Tricine-SDS-PAGE. Nature protocols 1:16–22.
28. Schagger H, Pfeiffer K (2000) Supercomplexes in the respiratory chains of yeast and mammalian mitochondria. EMBO J 19:1777–1783.
29. Musatov A, Robinson NC (2012) Susceptibility of mitochondrial electron-transport complexes to oxidative damage: focus on cytochrome c oxidase. Free Radical Research 46:1313–1326.
30. Stames EM, O'Toole JF (2013) Mitochondrial aminopeptidase deletion increases chronological lifespan and oxidative stress resistance while decreasing respiratory metabolism in *Saccharomyces cerevisiae*. PLOS ONE 10:e77234.
31. Lin SJ, Pufahl RA, Dancis A, O'Halloran TV, Culotta VC (1997) A role for the *Saccharomyces cerevisiae* ATX1 gene in copper trafficking and iron transport. J Biol Chem 272:9215–9220.
32. Blaiseau PL, Lesuisse E, Camadro JM (2001) Aft2p, a novel iron-regulated transcription activator that modulates, with Aft1p, intracellular iron use and resistance to oxidative stress in yeast. J. Biol. Chem 276:34221–34226.
33. Nelson M, Jin H, Turne IM, Grove G, Scarrow RC, et al. (1991) A novel iron-sulfur center in nitrite hydrolase from *Brevibacterium sp*. J. Am. Chem. Soc 113:7072–7073.
34. Chen Q, Vazquez EJ, Moghaddas S, Hoppel CL, Lesnefsky EJ (2003) Production of reactive oxygen species by mitochondria: central role of complex III. J Biol Chem 278:36027–36031.
35. Diaz F, Enríquez JA, Moraes CT (2012) Cells lacking Rieske iron-sulfur protein have a reactive oxygen species-associated decrease in respiratory complexes I and IV. Mol Cell Biol 32:415–429.
36. Adams V, Griffin L, Towbin J, Gelb B, Worley K, et al. (1991) Porin interaction with hexokinase and glycerol kinase: metabolic microcompartmentation at the outer mitochondrial membrane. Biochem Med Metab Biol 45:271–291.
37. Påhlman IL, Larsson C, Averét N, Bunoust O, Boubekeur S, et al. (2002) Kinetic regulation of the mitochondrial glycerol-3-phosphate dehydrogenase by the external NADH dehydrogenase in *Saccharomyces cerevisiae*. J Biol Chem 277:27991–27995.
38. Guiard B (1985) Structure, expression and regulation of a nuclear gene encoding a mitochondrial protein: the yeast L(+)-lactate cytochrome *c* oxidoreductase (cytochrome *b2*). EMBO J 4:3265–3272.
39. Venkatraman A, Landar A, Davis AJ, Chamlee L, Sanderson T, et al. (2004) Modification of the mitochondrial proteome in response to the stress of ethanol-dependent hepatotoxicity. J Biol Chem 279:22092–22101.
40. Thayer WS, Rubin E (1981) Molecular alterations in the respiratory chain of rat liver after chronic ethanol consumption. J Biol Chem 256:6090–6097.
41. Mansouri A, Demeilliers C, Amsellem S, Pessayre D, Fromenty B (2001) Acute ethanol administration oxidatively damages and depletes mitochondrial dna in mouse liver, brain, heart, and skeletal muscles: protective effects of antioxidants. J Pharmacol Exp Ther 298:737–743.
42. Hirano T, Kaplowitz N, Tsukamoto H, Kamimura S, Fernandez-Checa JC (1992) Hepatic mitochondrial glutathione depletion and progression of experimental alcoholic liver disease in rats. Hepatology 16:1423–1427.
43. Nordmann R, Ribière C, Rouach H (1987) Involvement of iron and iron-catalyzed free radical production in ethanol metabolism and toxicity. Enzyme, 37:57–69.
44. Stål P, Hultcrantz R (1993) Iron increases ethanol toxicity in rat liver. J Hepatol 17:108–115.
45. Yang M, Cobine PA, Molik S, Naranuntarat A, Lill R, et al. (2006) The effects of mitochondrial iron homeostasis on cofactor specificity of superoxide dismutase 2. EMBO J 25: 1775–1783.
46. Naranuntarat A, Jensen LT, Pazicni S, Penner-Hahn JE, Culotta VC (2009) The interaction of mitochondrial iron with manganese superoxide dismutase. J Biol Chem 284: 22633–22640.
47. Sun J, Trumpower BL (2003) Superoxide anion generation by the cytochrome bc1 complex. Arch Biochem Biophys 419:198–206.
48. Lemire BD, Oyedotun KS (2002) The *Saccharomyces cerevisiae* mitochondrial succinate:ubiquinone oxidoreductase. Biochim. Biophys. Acta 1553: 102–116.
49. Ueta R, Fujiwara N, Iwai K, Yamaguchi-Iwai Y (2012) Iron-induced dissociation of the Aft1p transcriptional regulator from target gene promoters is an initial event in iron-dependent gene suppression. Mol Cell Biol 32:4998–5008.
50. Courel M, Lallet S, Camadro J-MM, Blaiseau P-LL (2005) Direct activation of genes involved in intracellular iron use by the yeast iron-responsive transcription factor Aft2 without its paralog Aft1. Molec Cell Biol 25: 6760–6771.
51. Cui TZ, Smith PM, Fox JL, Khalimonchuk O, Winge DR (2012) Late-stage maturation of the Rieske Fe/S protein: Mzm1 stabilizes Rip1 but does not facilitate its translocation by the AAA ATPase Bcs1. Mol Cell Biol 32:4400–4409.
52. Munujos P, Coll-Cantí J, González-Sastre F, Gella FJ (1993) Assay of succinate dehydrogenase activity by a colorimetric-continuous method using iodonitrotetrazolium chloride as electron acceptor. Anal Biochem 212:506–509.
53. Esfandiari N, Sharma RK, Saleh RA, Thomas AJ Jr, Agarwal A (2003) Utility of the nitroblue tetrazolium reduction test for assessment of reactive oxygen species production by seminal leukocytes and spermatozoa. J Androl 24:862–870.
54. Lill R, Muhlenhoff U (2008) Maturation of iron-sulfur proteins in eukaryotes: mechanisms, connected processes, and diseases. Annu Rev Biochem 77:669–700.
55. Herrero E, de la Torre-Ruiz MA (2007) Monothiol glutaredoxins: a common domain for multiple functions. Cell Mol Life Sci 64:1518–1530.
56. Rouhier N, Couturier J, Johnson MK, Jacquot JP (2009) Glutaredoxins: roles in iron homeostasis. Trends in Biochem. Sci 35:43–51.

57. Lange H, Mühlenhoff U, Denzel M, Kispal G, Lill R (2004) The heme synthesis defect of mutants impaired in mitochondrial iron-sulfur protein biogenesis is caused by reversible inhibition of ferrochelatase. J Biol Chem 279:29101–29108.
58. Bakker BM, Bro C, Kötter P, Luttik MA, van Dijken JP, et al. (2000) The mitochondrial alcohol dehydrogenase Adh3p is involved in a redox shuttle in *Saccharomyces cerevisiae*. J Bacteriol 182:4730–4737.
59. Murphy MP (2009) How mitochondria produce reactive oxygen species. Biochem J 417:1–13.
60. Melo AM, Bandeiras TM, Teixeira M (2004) New insights into type II NAD(P)H:quinone oxidoreductases. Microbiol Mol Biol Rev 68:603–616.
61. Ferguson M, Mockett RJ, Shen Y, Orr WC, Sohal RS (2005) Age-associated decline in mitochondrial respiration and electron transport in *Drosophila melanogaster*. Biochem J 390:501–511.
62. Dröse S (2013) Differential effects of complex II on mitochondrial ROS production and their relation to cardioprotective pre- and postconditioning. Biochim Biophys Acta 1827:578–587.

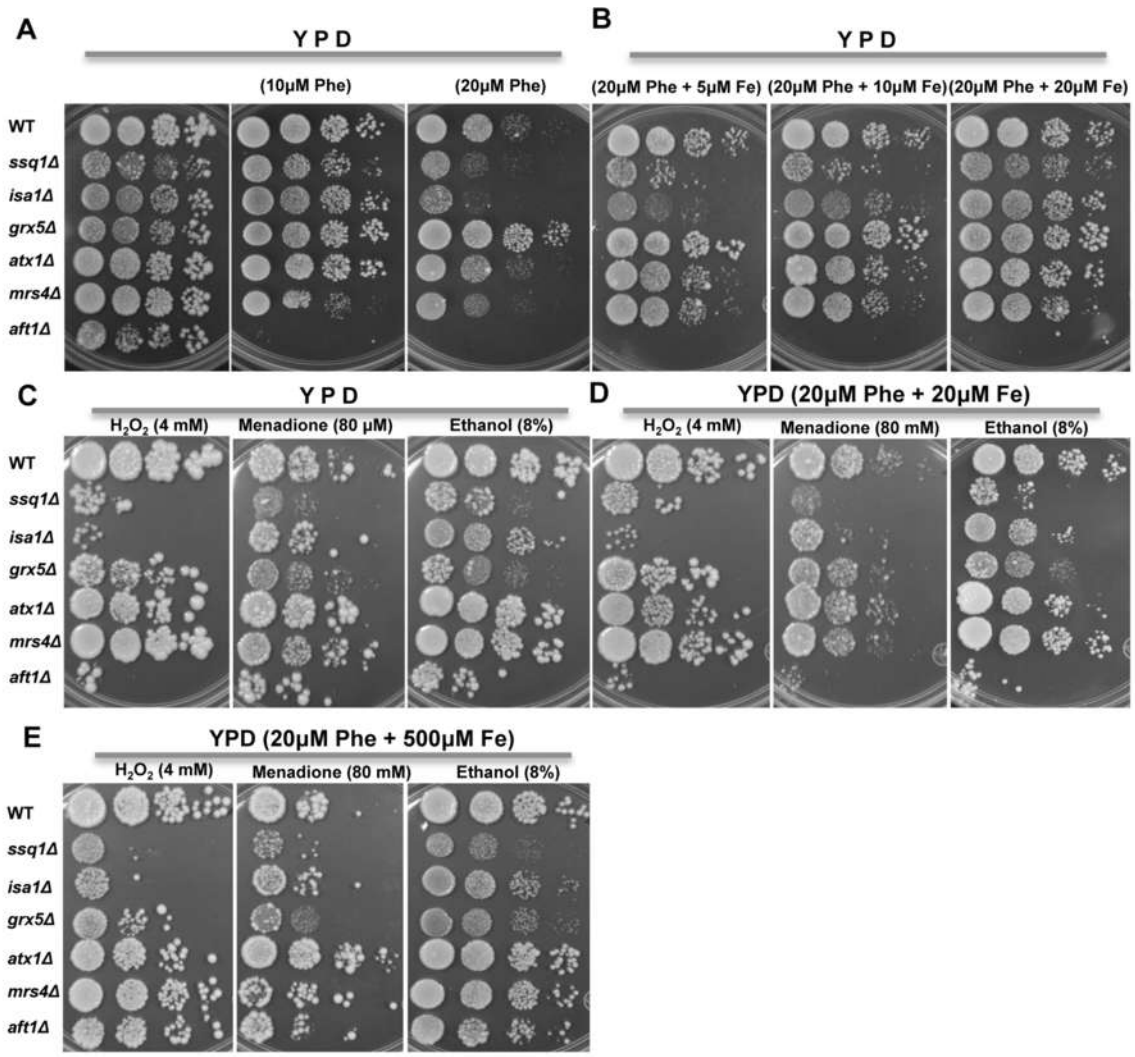

Figure S1. Studies of growth in plates of the *S. cerevisiae ISC* mutants. A–D) Dilutions of yeast suspensions were cultured on YPD agar plates with or without ROS-inducers at the indicated concentrations at 30°C for 48 h. Yeast cultures grown on YPD medium plates with: A) different concentrations of the iron chelator 1,10-phenanthroline (10 μM and 20 μM). B) low-iron content using the iron chelator 1,10-phenanthroline (20 μM) and different concentrations of ferrous iron (5–20 μM). C) ROS-inducers at indicated concentrations of H_2O_2 (4 mM), menadione (80 μM), and ethanol (8%). D) low-iron content using 1,10-phenanthroline (20 μM) plus ferrous iron (20 μM) with the concentrations indicated of ROS-inducers H_2O_2 (4 mM), menadione (80 μM), and ethanol (8%). E) low-iron content using 1,10-phenanthroline (20 μM) plus ferrous iron (500 μM) with the concentrations indicated of ROS-inducers H_2O_2 (4 mM), menadione (80 μM), and ethanol (8%).

6. CAPÍTULO II. Iba57p participa en la maduración de una proteína Rieske del grupo [2Fe-2S] y en la formación de supercomplejos III/IV de la cadena de transporte de electrones *Saccharomyces cerevisiae*.

Mitochondrion 44 (2019) 75–84

Contents lists available at ScienceDirect

Mitochondrion

journal homepage: www.elsevier.com/locate/mito

Iba57p participates in maturation of a [2Fe–2S]-cluster Rieske protein and in formation of supercomplexes III/IV of *Saccharomyces cerevisiae* electron transport chain

Luis A. Sánchez[a,1], Mauricio Gómez-Gallardo[a,1], Alma L. Díaz-Pérez[a], Christian Cortés-Rojo[b], Jesús Campos-García[a,*]

[a] Lab. de Biotecnología Microbiana, Instituto de Investigaciones Químico Biológicas, Universidad Michoacana de San Nicolás de Hidalgo, Morelia, Michoacán, Mexico
[b] Lab. de Bioquímica, Instituto de Investigaciones Químico Biológicas, Universidad Michoacana de San Nicolás de Hidalgo, Morelia, Michoacán, Mexico

ARTICLE INFO

Keywords:
Saccharomyces cerevisiae
Mitochondria
Iron–sulfur cluster
Rieske protein
Supercomplexes
Iron homeostasis
Reactive oxygen species

ABSTRACT

The [Fe-S] late-acting subsystem comprised of Isa1p/Isa2p, Grx5p, and Iba57p proteins (Fe–S-IBG subsystem) is involved in [4Fe-4S]-cluster protein assembly. The effect of deleting *IBA57* in *Saccharomyces cerevisiae* on mitochondrial respiratory complex integration and functionality associated with Rieske protein maturation was evaluated. The *iba57*Δ mutant showed decreased expression and maturation of the Rieske protein. The loss of Rieske protein caused by *IBA57* deletion affected the structure of supercomplexes III_2IV_2 and III_2IV_1 and their integration into the mitochondria, causing dysfunction in the electron transport chain. These effects were correlated with decreased cytochrome functionality and content in the *iba57*Δ mutant. These findings suggest that Iba57p participates in maturation of the [2Fe–2S]-cluster into the Rieske protein and that Rieske protein plays important roles in the conformation and functionality of mitochondrial supercomplex III/IV in the electron transport chain.

1. Introduction

The enzymatic complexes forming the electron transport chain (ETC) in the mitochondria of both mammals and yeast are organized as supramolecular structures and are known as supercomplexes. In yeast, supercomplexes are formed by interactions between the bc_1 complex (complex III) and cytochrome *c* oxidase complex (complex IV) in a stoichiometric ratio of two is to one (III_2/IV_1) or two is to two (III_2/IV_2) (Schagger and Pfeiffer, 2000). Supercomplex formation has been found to be essential for channeling of substrates, structural stabilization of individual ETC complexes, and modulation of reactive oxygen species (ROS) generation (Vartak et al., 2013). Thus, disruption of supercomplex formation may be detrimental to cell survival because of energy deficiency, enhanced oxidative stress, and/or inability to adapt to environmental changes (Gutierrez-Cirlos et al., 2002).

In yeast, supercomplex formation has been suggested to depend on the iron-sulfur protein (Rip1p) subunit of complex III (Conte et al., 2015; Cui et al., 2014; Zara et al., 2009). Rip1p (Rieske protein) is one of the three catalytic subunits of complex III and disruption of either its assembly or insertion of the Rip1p prosthetic group into the complex, a [2Fe–2S] cluster, severely alters both its structure and function (Gutierrez-Cirlos et al., 2002). The [Fe–S] clusters of the cytosolic and mitochondrial compartments are mainly synthesized by the mitochondrial iron–sulfur cluster (ISC) machinery (Braymer and Lill, 2017; Lill, 2009; Lill et al., 2012; Lill and Muhlenhoff, 2006), which is encoded in *Saccharomyces cerevisiae* by the genes *SSQ1*, *JAC1*, *NFS1*, *ISU1*, *ISU2*, *YAH1*, *YFH1*, *ISA1*, *ISA2*, *GRX5*, and *IBA57* (Lill, 2009; Schilke et al., 2006).

In contrast, the insertion and maturation of [4Fe–4S] clusters into target proteins such as aconitase, lipoic acid synthase, and homoaconitase are carried out by a specialized, late-acting Fe-S subsystem comprised of Isa1/Isa2, Iba57, and Grx5 proteins (Schilke et al., 2006), named as the Fe–S-IBG subsystem (by Isa1/2, Iba57, and Grx5 proteins). Fe–S-IBG subsystem components are not considered as essential for the maturation of mitochondrial [2Fe–2S] proteins (Muhlenhoff et al., 2011; Sheftel et al., 2012). Deletion of Isa1p, but not of Isa2p and Grx5p, is essential for [4Fe–4S] cluster assembly into target proteins. However, the essential role of Iba57p has not been demonstrated.

* Corresponding author at: Lab. de Biotecnología Microbiana, Instituto de Investigaciones Químico Biológicas, Universidad Michoacana de San Nicolás de Hidalgo, Edif. B-3, Ciudad Universitaria, 58030 Morelia, Michoacán, Mexico.
E-mail address: jcgarcia@umich.mx (J. Campos-García).
[1] Both authors contributed equally to this work and share first authorship.

https://doi.org/10.1016/j.mito.2018.01.003
Received 5 June 2017; Received in revised form 20 October 2017; Accepted 10 January 2018
Available online 16 January 2018

Previous studies indicated that the Fe–S-IBG subsystem can also act in [2Fe–2S]-cluster protein maturation (Banci et al., 2014; Beilschmidt et al., 2017; Nasta et al., 2017). Thus, altered [2Fe–2S] cluster insertion into Rieske protein and cluster dysfunction leads to full inhibition of respiration. This effect on respiration is attributed to impaired complex II-complex III activity and disruption of III_2/IV_2 supercomplexes (Conte and Zara, 2011). These findings suggest that some members of the Fe–S-IBG subsystem-assembly participate in the maturation of III/IV supercomplexes and in an optimal functionality of the ETC. Thus, we investigated the effects of *IBA57* deletion on the expression of Rieske protein in a haploid, monozygotic strain of *S. cerevisiae* to avoid heterozygous complementation. We also evaluated the effects of this deletion on integration of mitochondrial supercomplexes and on mitochondrial ETC function.

2. Materials and methods

2.1. Yeast strains, growth conditions, and survival tests

Mutant strains *grx5*Δ, *iba57*Δ, *rip1*Δ, *sdh2*Δ, and *cox11*Δ correspond to the haploid *S. cerevisiae* BY4741 wild type (Mat a, *his3*Δ, *leu2*Δ0, *met15*Δ0, *ura3*Δ0, *KanMX4*), all strains were obtained from Open Biosystems. Growth tests were carried out using yeast extract peptone dextrose (YPD) culture medium. Culture medium was inoculated with overnight-grown yeast cultures that had reached an optical density of 0.1 at 600 nm (OD_{600}) and incubated at 30 °C with low-speed shaking (50 rpm). Yeast growth (biomass) was spectrophotometrically monitored at OD_{600}.

2.2. Determination of in situ mitochondrial oxygen consumption rate

S. cerevisiae cells (25 mg wet weight) were placed in 2.5 mL of MES-TEA buffer (pH 6.0) in a sealed glass chamber with constant stirring at 25 °C. The oxygen consumption rate (OCR) was measured with a Clark-type oxygen electrode coupled to a biological oxygen monitor (YSI 5300). Basal oxygen consumption (state 4), was induced by adding 20 mM glucose as substrate, and 3 min later, 5 μM of the uncoupling agent carbonyl cyanide *m*-chlorophenyl hydrazone (CCCP) was added to stimulate maximal OCR (uncoupled (U) state). To discriminate the mitochondrial oxygen consumption from unspecific-cytosolic oxygen utilization, the mitochondrial ETC was inhibited with 1 μg antimycin A and a further addition of 0.5 mM KCN (Brand and Nicholls, 2011).

2.3. Mitochondria isolation and determination of the ETC complexes activity

Mitochondria of *S. cerevisiae* were isolated from cultures grown in liquid medium YPD at 30 °C in a shaking incubator by 12 h, using a previously described method (Perez-Gallardo et al., 2013). Detergent permeabilized mitochondria were mixed 250 μL of intact mitochondria (10 mg of protein) plus 750 μL of hypotonic buffer [(KCl 100 mM, $MgCl_2$ 10 mM, Tris-base 10 mM, pH 7.5, and Triton X-100 (0.02%))] with vigorous shaking in a vortex for 15 s. This suspension was centrifuged at 18,600 × *g* for 15 min at 4 °C. Supernatants were discarded and the mitochondrial pellets suspended in buffer composed of 50 mM KH_2PO_4, pH 7.6 and protein was quantified by the Biuret method. Suspensions of permeabilized mitochondria were used to determine the activity of the ETC complexes, as described below.

2.4. Determination of the ETC complexes activity

The activity of complex II was evaluated by measuring the succinate-DCIP oxidoreductase activity of solubilized mitochondria (Perez-Gallardo et al., 2013). For determination of complex II-III activity, the activity of antimycin A-sensitive succinate-cytochrome *c* oxidoreductase was measured using endogenous ubiquinol-6 and succinate as substrates (Perez-Gallardo et al., 2013). While that for determination of complex III activity, it was assayed under the same conditions used for the determination of complex II-III activity, except that decylubiquinol (reduced with $NaBH_4$) was added instead succinate (Cortes-Rojo et al., 2009). Finally, for determination of the complex IV activity, cytochrome *c* oxidase activity was measured as the rate of cyanide-sensitive cytochrome *c* oxidation in presence of antimycin A by adding dithionite-reduced cytochrome *c* (Perez-Gallardo et al., 2013).

2.5. Determination of cis-aconitase activity

Aconitase activity was determined by a modification of the method of Henson and Cleland (Henson and Cleland, 1967) as described elsewhere (Perez-Gallardo et al., 2013).

2.6. Mitochondrial membrane potential

Membrane potential in cells suspensions was determined using the fluorescent, cell-permeable indicator Rhodamine 123 (Rho123; Sigma). Cells suspensions (1×10^7 cells/mL) were loaded with Rho123 (5 μg/mL) and incubated at 30 °C for 30 min in the dark. Suspensions were harvested, washed once and re-suspended in PBS. Membrane potential in suspensions was determined by fluorescence generation and quantified by flow cytometry using a BD Accuri C6 Flow Cytometer (BD Biosciences), monitoring the emission fluorescence in channel FL1 (533/30 nm) (Gomez et al., 2014).

2.7. Raman spectroscopy of mitochondria

Suspensions of intact mitochondria (250 μg) from yeast cultures grown on YPD were subjected to Raman spectroscopy as described previously (Gomez et al., 2014), using a microRaman spectrometer (Dilor model LabRam) equipped with a confocal microscope with 50 × amplification, using He-Ne laser emitting at 632.8 nm and 30 mW at sample point for excitation. Mitochondrial dried-pellets were collocated in a copper plate and laser impacted into a spot of 2 μm with an integration time of 60 s; a 256 × 1024 pixel charge-coupled device (CCD) was used as a photon detector. The spectra obtained correspond to the average of spectra overlapped by 60 s of recording.

2.8. UV spectroscopy of mitochondrial cytochrome

Suspensions of intact mitochondria (2 mg/mL) from yeast cultures grown on YPD were collocated into quartz cell and absorbance spectra were recorded using a spectrophotometer (UV-2550 Shimadzu), monitoring spectrum from 400 to 650 nm. Basal spectrum was obtained using phosphates buffer adding 10 μL KCN (0.4 M) and 10 μL succinate (1 M) incubating 3 min before run the spectrum to determine cytochrome functionality. After, 10 μL antimycin A (0.09 M) was added, incubated by 3 min to total cytochrome *b* reduction. Finally, 0.1 mg dithionite was added in the cuvette and run the spectrum monitoring to determine total cytochrome presence. The spectra obtained correspond to the average of spectra overlapped at least 6 times.

2.9. DNA gene amplification

DNA amplification was carried out by standard PCR method using total or mitochondrial DNA from the *S. cerevisiae* strains, using the Platinum Pfx DNA polymerase (Invitrogen) performed according to manufacturer's instructions. The primers used for gene amplification were designed from the *S. cerevisiae* genome: *IBA57* (fw GGTACCAAA ATGTTCATCAGTAGAAG and rev GCGGCCGCTTTATGAGGCCCGTT ATT), *GRX5* (fw AAGCTTAAAATGTTTCTCCCAAAATTC and rev CTCGAGACGATCTTTGGTTTCTTCTTC), *RIP1* (fw GGATCCAAAATGTT AGGAATAAGATCATCT and rev CTCGAGACCAACAATGACCTTATC ACCATC), *COX2* (fw TCAGGATTCAGCAACACCAA and rev

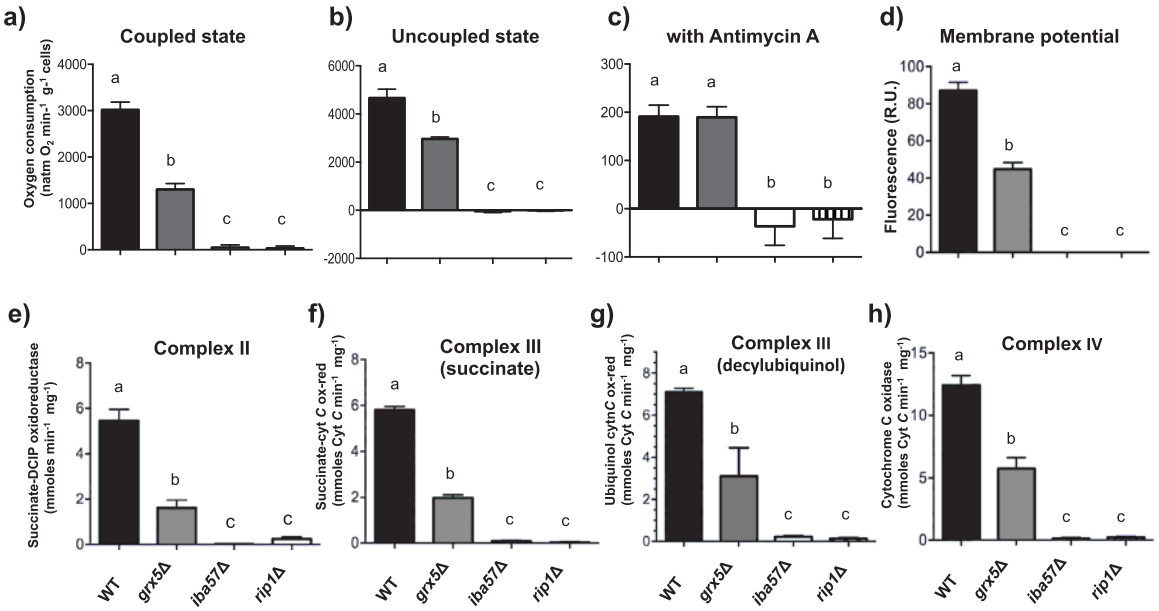

Fig. 1. Evaluation of mitochondrial ETC functionality and [Fe–S]-content in the Iba57p mutant of *Saccharomyces cerevisiae.* a–h) Mitochondria function was evaluated in mitochondria suspensions obtained as described in the Material and Methods, except for (d), in which cells suspensions were used. a–c) Basal oxygen consumption rate (OCR) with glucose as a substrate: a) OCR under coupled state conditions; b) OCR under uncoupled state conditions using CCCP for uncoupling; and c) OCR under complex III-blocking conditions using antimycin A as an inhibitor. d) Membrane potential in cell suspensions. e) Activity of succinate-DCIP oxidoreductase. f) Activity of succinate-cytochrome *c* oxidoreductase using succinate as substrate. g) Activity of ubiquinol-cytochrome *c* oxidoreductase activity using decylubiquinol as substrate. h) Activity of cytochrome *c* oxidase. Values are the mean of three independent experiments. SEs are indicated as bars ($n = 9$), one-way analysis of variance (ANOVA) with Tukey's post hoc test was used to compare yeast strains, and significant differences ($p < 0.05$) were indicated by different lowercase letters.

TCAAATTCAACAGTTTCACCACT), *COX3* (fw TTAGGTGCATGTTGACC ACC and rev CCATCAGAGATAGTGAATGCAGC).

2.10. Native gel electrophoresis and western blot

For native polyacrylamide gel electrophoresis, samples of 100 µg of mitochondrial protein isolated as described above, and solubilized using buffer A containing dodecylmaltoside (1 g/g), triton X-100 (2.4 g/g), or using digitonin (3 g/g) as described (Schagger, 2006), and separated by native polyacrylamide gel electrophoresis on 8% Bis-tris gels (BN-PAGE) (Musatov and Robinson, 2012; Schagger and Pfeiffer, 2000; Stames and O'Toole, 2013). After electrophoresis, the mitochondrial complexes visualized in the gel were excised in both horizontal or vertical manner, and incubated for 30 min in a solution containing 60 mM Tris/HCl (pH 6.8) and 0.2% SDS at room temperature. Each gel slice was placed horizontally and encased in 5% polyacrylamide stacking gel in the gel for the second dimension (SDS-PAGE), already containing the separation gel (12% polyacrylamide and 0.2% SDS). The gels were subjected to electrophoresis and in one side they were silver-stained and on the other side transferred to polyvinylidene difluoride (PVDF) membranes for Western blot procedure. Additionally, SDS-PAGE was also applied for separation in mitochondrial and cell-free extracts. For immunodetection assays, 50 µg of mitochondrial protein or cellular extracts were run in 12% SDS-PAGE gels and transferred to PVDF membranes. Membranes were blocked using dry milk in PBS-T and blotted with the *S. cerevisiae* antibodies (anti-Rip1p, anti-Cox2p or anti-Cox3p) as first antibody in blocking medium at a 1:20000 dilution for 2 h at 4 °C. After washing, the membranes were incubated with the secondary antibody, a monoclonal anti-mouse IgG HRP-conjugate (Promega), in blocking medium at a 1:10,000 dilution for 2 h at 4 °C; the membranes were washed with PBS-T and developed using Supersignal West Pico Luminol (Pierce) and exposing in light-sensitive films or luminescence determined by using a ChemiDoc MP imaging system (BioRad). Assays were conducted by at least three independent assays and representative images are shown. Bands intensities in gels or films were quantified using the Image J software.

2.11. Confocal microscopy of yeast suspensions

S. cerevisiae YPD-grown cultures were harvested and suspended in PBS at 1×10^7 cell/mL and loaded with the fluorescent probe. DNA staining in cells was visualized by fluorescence resonance energy transfer (FRET). Cells were suspended in deionized water and added 1 µL/mL of SYTO9 and propidium iodide stain mix (Live/dead FungaLight yeast viability kit for flow cytometry; Molecular Probes, Invitrogen) incubating 30 min at room temperature; after this, samples were observed by confocal microscopy at 482/502 nm and 535/617 nm, respectively. Images were acquired at 40–60 × magnifications.

3. Results

3.1. Mitochondrial ETC function is affected by IBA57 deletion

Mutants in the Fe–S-IBG subsystem components have been considered as respiratory-deficient strains, but possess normal capability to grow in fermentative conditions, suggesting that their lack of a mitochondrial DNA (mitDNA) causes the failure of respiratory complexes (petite or rho^- phenotypes) (Muhlenhoff et al., 2011). However, GRX5 mutants partially maintain their mitDNA (Rodríguez-Manzaneque et al., 2002). We observed that the *isa1*Δ mutant showed respiratory deficiency and strong/null formation of respiratory supercomplexes, while only partial effects were observed for the *grx5*Δ mutant (Gomez et al., 2014). These results suggest that some Fe–S-IBG subsystem components causing respiratory-deficiency are not a consequence of the

total lack of mitDNA; therefore, the Fe–S-IBG subsystem may affect respiratory complex conformation. Proteins other than Grx5p, such as Iba57p, may be involved in this process.

To determine to what extent *IBA57* mutation impairs the overall functionality of the ETC in *S. cerevisiae*, in situ mitochondrial oxygen consumption rates (OCRs) of the mutant were measured. Respiration was fully inhibited in both coupled and uncoupled states in the mitochondria of *iba57*Δ and *rip1*Δ mutants, whereas in the *grx5*Δ mutant, only a partial decrease in OCR was observed compared to in the WT strain (Fig. 1a–b). Notably, antimycin A treatment caused oxygen release rather than oxygen consumption in the assay chamber in the *iba57*Δ and *rip1*Δ mutants compared to the WT and *grx5*Δ mutant (Fig. 1c). Additionally, in accordance with its inability to respire, the *iba57*Δ and *rip1*Δ mutants did not exhibit membrane potential (*Δp*) (Fig. 1d). The partial reduction in OCR in the uncoupled state observed in *grx5*Δ cells supported the partial dissipation of membrane potential detected in this mutant.

Partial reactions of the ETC were analyzed to determine whether the deletion of Iba57 protein, which is part of the Fe–S-IBG subsystem dedicated to the maturation of [4Fe–4S] clusters, also affects the activity of mitochondrial complexes lacking this type of Fe–S center (i.e., III and IV). As expected, the activity of complex II, a protein complex containing a [4Fe–4S] center, was fully inhibited in *iba57*Δ and *rip1*Δ mutants; in contrast, the *grx5*Δ mutant displayed ~30–40% of activity compared to WT cells (Fig. 1e). A similar trend was observed for complexes III and IV (Fig. 1f–h).

Antimycin A-sensitive succinate–cytochrome *c* oxidoreductase activity (i.e. complex II-complex III activity) is dependent on electron transfer between complex II and complex III. Thus, to eliminate the possibility that impaired succinate–cytochrome *c* oxidoreductase activity resulted from impaired complex II activity and not from direct damage to complex III, we tested the activity of complex III by measuring the oxidation of decylubiquinol (Fig. 1g). The activity of complex III was fully abolished in *iba57*Δ and *rip1*Δ mutants, while mitochondria from *grx5*Δ exhibited activity of ~40% compared to that from the WT strain (Fig. 1g). These results indicate that deletion of *IBA57* causes the dysfunction of the ETC, and this deletion is likely associated with the disintegration of ETC surpercomplexes.

3.2. [Fe–S] cluster-containing proteins are affected by IBA57 deletion

Determination of the enzymatic activity of *cis*-aconitase has been used to monitor the assembly of [4Fe–4S] centers into target proteins (Gardner, 1997; Muhlenhoff et al., 2011). Accordingly, we determined the aconitase activity in mitochondria of the *iba57*Δ mutant. As expected, aconitase activity was nearly completely abolished in the *iba57*Δ mutant, while decreased activity was observed in the *grx5*Δ mutant (described as no essential protein for aconitase assembly) (Fig. 2a). Additionally, we tested aconitase activity in the *rip1*Δ mutant (used here as a strain lacking complex III activity because of deletion of the Rieske subunit), and found that its activity was decreased to approximately 50% compared to the WT strain. These results indicate that in the *iba57*Δ mutant, the insertion of [4Fe–4S] clusters into aconitase target proteins was prevented, confirming that the Fe–S-IBG subsystem participates in assembly of apoproteins [4Fe–4S]-dependent. This was further confirmed using Raman spectroscopy analysis in mitochondria isolated from the *iba57*Δ mutant, as in the *rip1*Δ mutant. Signal intensities at 460–545 cm^{-1} and 640–660 cm^{-1} in the 632.8 nm Raman spectra corresponding to photonic emission characteristics of the [Fe–S] centers were markedly diminished (Fig. 2b). The Raman signal peaks were clearly observed with high intensity in the mitochondria from the WT and *grx5*Δ mutant. Decreased [Fe–S] content observed in the *iba57*Δ mutant further confirmed that Iba57p is involved in the biosynthesis and assembly of [Fe–S] clusters into mitochondrial target proteins. Thus, *IBA57* deletion may be associated with the dysfunction of ETC supercomplexes, and this deletion likely affects the insertion or maturation process of the [Fe–S] center-containing proteins. In addition, the [Fe–S] centers analyzed by Raman spectrometry in the *rip1*Δ mutant indicate that the Rieske protein is related to respiratory supercomplexes maturation/assembly.

3.3. ETC supercomplexes maturation are affected by IBA57 deletion

To determine whether the deletion of Iba57p directly or indirectly disturbs the formation of III/IV supercomplexes by preventing the maturation of [Fe–S] clusters containing-proteins in mitochondrial complexes, we tested the effects of Iba57p on supercomplex maturation and the influence of Rieske protein. We analyzed ETC supercomplex assembly by blue native polyacrylamide gel electrophoresis (BN-PAGE) with two types of mitochondrial protein-solubilizing treatments: digitonin (light condition) and dodecylmaltoside (stronger condition). In addition, we conducted immunodetection with the anti-Rip1 antibody for Rieske-containing supercomplex identification in mitochondrial supercomplexes.

Mitochondrial extracts from WT cells evaluated by BN-PAGE (first dimension) showed five well-defined protein bands, B1–B5 (Fig. 3a–b). When the contents of the WT gel lane were resolved in a second dimension by SDS-PAGE, and immunodetected, the B2 and B3 bands reacted with the anti-Rip1p antibody (Fig. 3c–d). In addition, the BN-PAGE gels immunodetected with anti-Rip1p antibody showed strong signals in the B1, B2, and B3 bands, as well as in the B3, B4, and B5 bands when the anti-Cox3p antibody was used (Fig. 3e–g). These results confirm that bands B2 and B3 corresponded to the III_2IV_2 and III_2IV_1 supercomplexes, respectively (Fig. 3g). Determination of band intensity of the supercomplexes in the BN-PAGE gels showed that in mitochondria from the negative control strain *rip1*Δ, bands B1, B2, and B3 were significantly decreased (Fig. 3a–b). Remarkably, a similar banding pattern was observed for the *iba57*Δ and *grx5*Δ mutants compared to that for WT yeast or for the two control mutant strains, such as the *cox11*Δ and *sdh2*Δ. *cox11*Δ (which lacks cytochrome *c* oxidase subunit 11 of complex IV) and *sdh2*Δ (which lacks succinate dehydrogenase that forms complex II) are mutations that do not affect Rip1p expression.

On 2-D SDS-PAGE gels, the lane corresponding to the *iba57*Δ mutant from the BN-PAGE gel like the B3 band, indicated a decrease in protein content compared to in the WT strain (Fig. 3h and Supplementary Fig. S1a–b).

Immunoblotting of bands B2 and B3 cut horizontally from the BN-PAGE gels showed that Rip1 protein integration into supercomplexes III_2IV_2 and III_2IV_1 was absent in *iba57*Δ and *rip1*Δ mutants, but not in *cox11*Δ, *sdh2*Δ, and the WT strain (Fig. 4a). For the *grx5*Δ mutant, Rip1p was absent in the B2 band, but was observed in the B3 band in a similar proportion as in the WT. Interestingly, in both the *cox11*Δ and *sdh2*Δ mutants, the Rip1p blotting signal was stronger for both, B2 and B3 bands (Fig. 4a). When BN-PAGE gels were run using dodecylmaltoside-treated samples (stronger solubilizing conditions), the B3 band corresponding to the III_2IV_1 supercomplex was clearly absent from the *iba57*Δ and *rip1*Δ mutants, light in *grx5*Δ, but not affected in the *sdh2*Δ mutant (see Supplementary Fig. S1c). These results indicate that iba57p deletion abolished III_2IV_2 and III_2IV_1 supercomplex formation.

3.4. ETC-supercomplex maturation is mediated by Rieske protein integrity

The [Fe–S] centers Raman signals and bands corresponding to the respiratory supercomplexes decreased in the *iba57*Δ and *rip1*Δ mutants, suggesting that Iba57p is involved in Rieske protein maturation and, in turn, Rieske protein is related to respiratory supercomplex formation as previously suggested (Conte et al., 2015; Conte and Zara, 2011). Thus, we determined the levels of Rip1p in mitochondrial extracts of the *iba57*Δ and *rip1*Δ mutants.

As expected, Rip1p expression was not observed in the mitochondria of the *rip1*Δ mutant (Fig. 4b). However, expression of Rip1p in the mitochondria of the *iba57*Δ and *grx5*Δ mutants was decreased

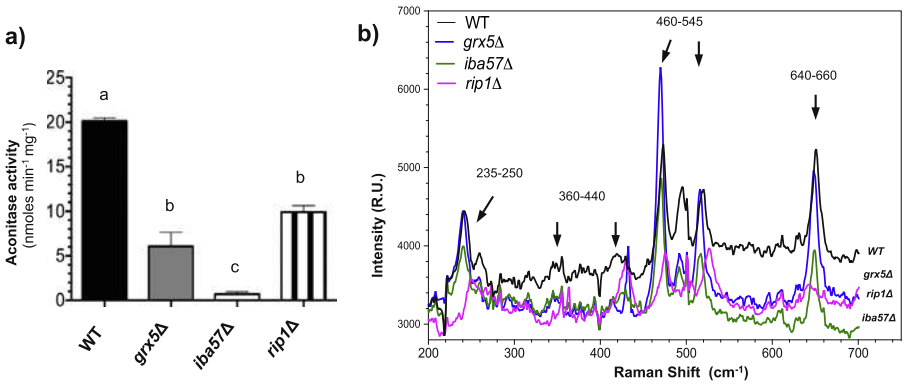

Fig. 2. Evaluation of [Fe–S]-containing proteins in *Saccharomyces cerevisiae.* a) Enzymatic activity of *cis*-aconitase was determined in mitochondrial suspensions as described in the Materials and Methods. Values are the mean of three independent experiments. SE values are indicated as bars ($n = 3$), one-way analysis of variance (ANOVA) with Tukey's post hoc test was used to compare yeast strains, and significant differences ($p < 0.05$) are indicated by lowercase letters. b) Analysis of mitochondrial Fe–S-containing proteins in *S. cerevisiae* by Raman spectroscopy. Mitochondrial suspensions were used for Raman spectra determination, recorded at a laser excitation of 632.8 nm at 30 mW. Each spectrum is the average of scans recorded over 60 s, using photon counting at 0.5 cm^{-1} increment spectral resolution. Bands corresponding to the [2Fe–2S], [3Fe–4S], and [4Fe–4S] clusters are indicated with arrows (Zhang et al., 2012).

significantly compared to in WT. In the *sdh2*Δ mutant, Rip1p expression was similar to that in the WT strain. The Cox2 and Cox3 proteins (which form the core of cytochrome *c* oxidase complex and are encoded by mitDNA) were blotted on the same membrane. The results showed that Cox2 protein was expressed at low levels in the *iba57*Δ and *rip1*Δ mutants, but Cox3 protein was unaffected (Fig. 4b). Densitometry analysis of protein expression, normalized to Cox3p expression, showed that in the *iba57*Δ and *rip1*Δ mutants, Rip1p and Cox2p expression was decreased significantly (Fig. 4c). These results indicate that Iba57p deletion affected Rip1p maturation into the mitochondrial complexes, affecting the integrity of Rieske protein associated with supercomplex maturation.

Additionally, to evaluate cytochrome integrity in the mitochondrial supercomplexes, cytochrome functionality and presence was monitored in the *iba57*Δ and *rip1*Δ mutants. Cytochrome content monitoring by spectra profiles in the WT strain clearly revealed cytochromes $c + c_1$ (signal at 550 nm), cytochromes *b* (signal at 560 nm), and cytochromes *a* (signal at 610 nm) (Fig. 5a). Interestingly, cytochromes $c + c_1$ and cytochromes *b* were also observed in the *iba57*Δ, *grx5*Δ, *rip1*Δ, and *cox11*Δ mutants, although with lower signals compared to in the WT strain, but did were not observed in the rho^- strain. While that cytochrome functionality determined by their capability of electrons transport was observed in the WT strain, although slight signal also as in the *iba57*Δ, *grx5*Δ, and *cox11*Δ mutants, but not in the *rip1*Δ mutant and rho^- strain (Fig. 5b). These results indicated that in the *iba57*Δ mutant, Cox2p, Cox3p, and cytochromes *c* and *b* were expressed and functional, indicating that the *iba57*Δ mutant contains mitDNA, further confirming that the iba57p affects complex III of the ETC.

The expression data for Cox2 and Cox3 proteins encoded by mitDNA were further confirmed by DNA gene amplification via PCR for mitochondria from the mutants. *COX2* and *COX3* (mitochondrial encoded genes) amplification was observed in WT strain, also as in *iba57*Δ, *rip1*Δ, and *grx5*Δ mutants; as expected, expression in a constructed petite mutant was not detected (Fig. 6). Unexpectedly, however, in the *grx5*Δ mutant, the *COX2* and *COX3* DNA fragments were different sizes. Confocal microscopy analysis also indicated the presence of DNA-containing mitochondrial structures in the *iba57*Δ mutant, but not in the petite yeast (Fig. 7).

4. Discussion

Isa1p is required for the maturation of [4Fe–4S] clusters (Muhlenhoff et al., 2011; Sheftel et al., 2012), which precludes its participation in both, the maturation of the [2Fe-2S] cluster contained in the Rip1 subunit of complex III and in the biogenesis or functioning of the complex IV (because this complex lacks of an [Fe–S] cluster). Thus, our previous findings regarding impaired supercomplex formation and decreased activities of both complexes III and IV in the *isa1*Δ mutant was unexpected, as we predicted that only decreased complex II activity would occur without interfering in supercomplex formation, as this complex does not take part in this process or possess a [4Fe-4S] cluster (Gomez et al., 2014). Thus, we tested the effects of mutation in *IBA57*, whose product forms the Fe–S-IBG subsystem on supercomplex formation, ETC function, emphasizing the probable participation of Rip1p in this process given that its participation in supercomplex integration has been widely recognized (Conte et al., 2015; Cui et al., 2014; Zara et al., 2009).

Respiratory supercomplexes are now considered the functional units mediating optimal electron transfer from reducing equivalents (i.e. NADH or $FADH_2$) to molecular oxygen by channeling substrates and decreasing ROS generation (Vartak et al., 2013). Therefore, impaired respiration and mitochondrial depolarization in the *iba*57Δ mutant (Fig. 1), and the inability of the mutant to form III/IV supercomplexes (Fig. 3) are in agreement with this hypothesis. Moreover, the role of Rip1p in the integrity of the supercomplexes is reinforced by the observation of full impairment of respiration and membrane potential observed in the *rip1*Δ mutant (Fig. 1). The increased release of oxygen in the *iba57*Δ and *rip1*Δ mutants in response to antimycin A suggest that increased superoxide generation occurred at the level of complex III (see Fig. 1 in Gomez-Gallardo et al., in press). It has been reported that the failure to insert the [2Fe–2S] cluster of Rip1p alters the environment of quinone redox sites of complex III (Gutierrez-Cirlos et al., 2002). These alterations may lead to enhanced ROS generation because of augmented electron leakage at these redox sites. In agreement with this prediction, the *rip1*Δ mutant exhibited a phenotype similar to that of the *iba57*Δ mutant (see Fig. 1 in Gomez-Gallardo et al., in press). This suggests that Rip1p deletion alters electron transfer between the redox sites of the complex III, likely because of the lack of [2Fe–2S] cluster insertion, which occurs in the *rip1*Δ mutant.

The role of the Fe–S-IBG subsystem in the formation of supercomplexes through a mechanism dependent on Rip1p was supported by the negligible expression of Rip1p in cellular extracts of the *iba57*Δ and *grx5*Δ mutants (Fig. 3). These results suggest that the Fe–S-IBG system affects the expression of Rip1p, the catalytic subunit [2Fe–2S] cluster

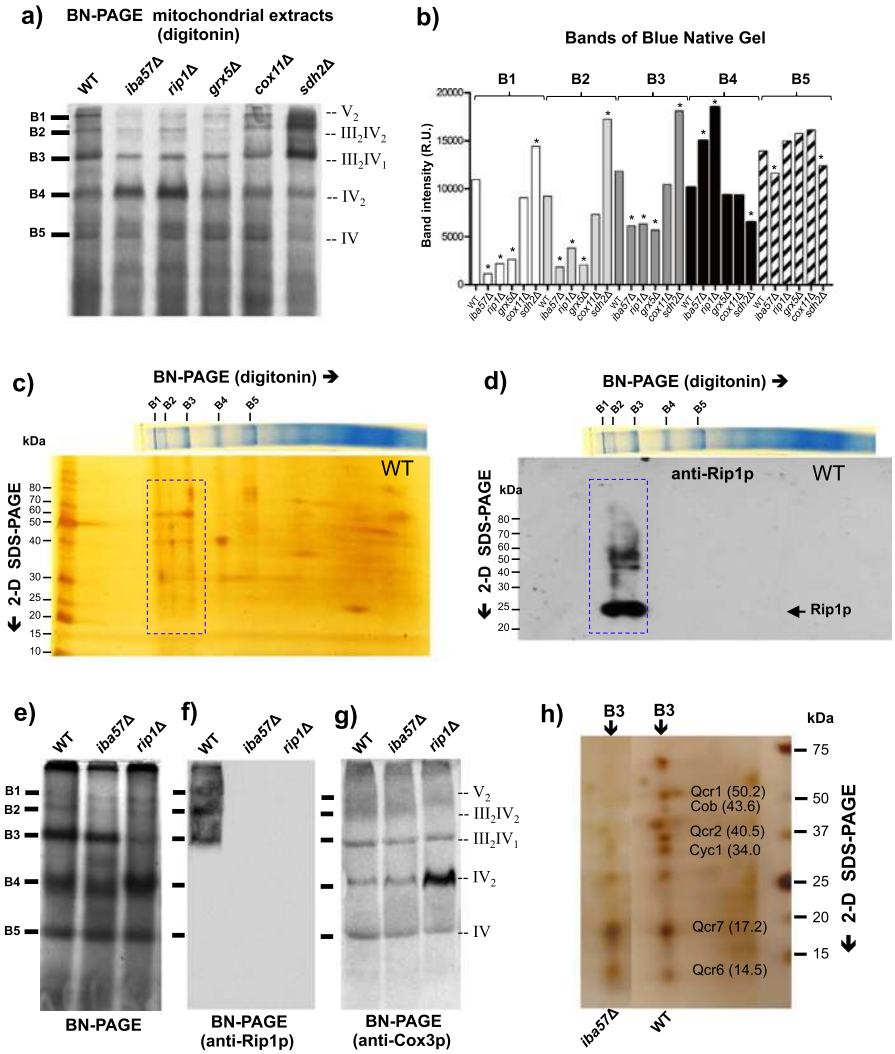

Fig. 3. Evaluation of ETC mitochondrial supercomplexes formation in the Iba57p mutant of *Saccharomyces cerevisiae*. Mitochondrial suspensions were solubilized with digitonin and the proteins were separated using blue native polyacrylamide gel electrophoresis (BN-PAGE), as described in the Materials and Methods. The ETC mitochondrial supercomplexes are indicated to the right of the gels, based on the results shown. a) BN-PAGE of mitochondrial suspensions solubilized with digitonin; B1–B5, major protein bands corresponding to mitochondrial supercomplexes. b) Densitometry analysis plot of the bands corresponding to supercomplex bands observed in panel (a) using Image J software. Values are the mean and SE values are indicated as bars (n = 3), one-way analysis of variance (ANOVA) with Tukey's post hoc test was used to compare yeast strains, and significant differences ($p < 0.05$) are indicated with asterisks. c) Second dimension (SDS-PAGE) of gel slice from BN-PAGE corresponding to the WT strain, silver-stained, SDS-PAGE BenchMark Protein Ladder (Invitrogen) is showed. d) Western blot of 2-D SDS-PAGE gel (c) using anti-Rip1 antibody and monoclonal anti-mouse IgG horseradish peroxidase (HRP) conjugate as the second antibody. e–g) Lines from BN-PAGE gel (e) were transferred to PVDF membranes and detected by western blotting using anti-Rip1 antibody (f) and anti-Cox3p antibody (g). h) 2-D SDS-PAGE gel of the B3 band from BN-PAGE gel. Proteins are indicated. Molecular mass marker in kilodaltons is shown to the right of the gel.

containing of cytochrome *c*, via cluster integration. This could be inferred as it has been demonstrated that failure in the insertion of the [2Fe–2S] cluster into Rip1p leads to augmented susceptibility to proteolysis (Gutierrez-Cirlos et al., 2002). Another line of evidence further supporting a role for the Fe–S-IBG subsystem in the formation of supercomplexes and likely in the maturation of the [2Fe–2S] cluster of Rip1p was the decreased levels of supercomplexes III_2IV_2 and III_2IV_1, observed in the *iba57*Δ mutant of the Fe–S-IBG subsystem, whose banding pattern was very similar to that observed for the *rip1*Δ mutant. Moreover, the role the Fe–S-IBG subsystem became more evident when supercomplex bands were run in a second dimension, which revealed the absence of Rip1p in the remaining supercomplex bands of *iba57*Δ and when supercomplex analysis was conducted under conditions more severe mitochondrial proteins solubilization (see Supplementary Fig. S1c). These results further suggest that Rip1p integrity plays important roles in supercomplex conformation and that its maturation depends on Iba57p from the Fe–S-IBG subsystem. In agreement with this idea, Rip1p expression was unaffected in the *sdh2*Δ mutant (which lacks succinate dehydrogenase to form complex II) and *cox11*Δ mutant (which lacks cytochrome *c* oxidase subunit 11 of complex IV) (Fig. 3).

The activity of the complex II-complex III segment of the ETC was fully inhibited in the *iba57*Δ mutant and *rip1*Δ control strain (Fig. 1).

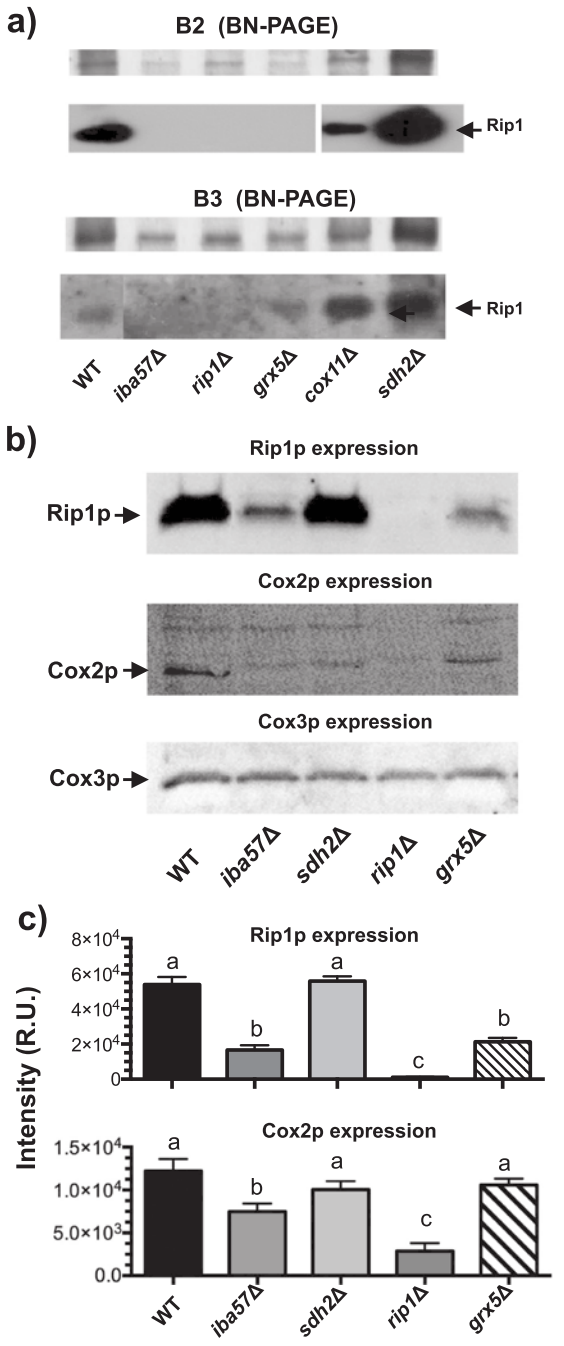

Fig. 4. Immunodetection of Rieske protein in the Iba57p mutant of *Saccharomyces cerevisiae*. a) Immunoblotting of lines B2 and B3 cut from mitochondrial extracts separated by BN-PAGE gels. b) Mitochondrial extracts separated by SDS-PAGE gels, after western blot using anti-Rip1p, anti-Cox2p, and anti-Cox3p antibodies as the primary antibody and monoclonal anti-mouse IgG horseradish peroxidase (HRP) conjugate as the secondary antibody. c) Densitometry analysis of (b) normalizing with Cox3p expression, data correspond to three independent assays determining the band intensity by densitometry analysis using Image J software. Values are the mean and SE values are indicated as bars (n = 3), one-way analysis of variance (ANOVA) with Tukey's post hoc test was used to compare yeast strains, and significant differences ($p < 0.05$) are indicated by lowercase

Although this observation may be the result of impaired complex II activity (i.e., a complex containing [4Fe–4S] clusters) arising from the use of succinate as a substrate, we observed the same result using decylubiquinol, a direct substrate for complex III. Therefore, dysfunction of complex III in the *iba57*Δ mutant may be associated with impaired Rieske subunit assembly as shown in Fig. 3. Impaired complex III activity may have resulted from oxidative damage due to uncontrolled ROS production as observed in these mutants (see Figs. 1–2 in Gomez-Gallardo et al., in press). However, based on the results of aconitase activity, this is not the main reason, as aconitase, a protein whose activity is a marker of oxidative stress (Gardner, 1997; Muhlenhoff et al., 2011), was moderately impaired in the *rip1*Δ mutant, which exhibited neither Rip1p expression nor complex III activity. This indicates that enhanced oxidative stress is not sufficient for inducing complete impairment of complex III activity.

Complex IV activity was also fully inhibited in the *iba57*Δ mutant and decreased in the *grx5*Δ mutant, which lack an [Fe–S] cluster. This may be explained by their inability or instability to form ETC supercomplexes; when complex III has an incorrect conformation, it is susceptible to protein degradation, which may strongly affect the activity of complex IV. This suggestion agrees with the observation that when complex III has an incorrect conformation, which may be associated with the absence of Rip1p, the activity of complex IV is strongly affected (Schilke et al., 2006). Therefore, the assembly of ETC supercomplexes formed by complexes III and IV is favored by integration of Rip1p into complex III (Conte et al., 2015; Conte and Zara, 2011; Cui et al., 2012; Diaz et al., 2012). In the absence of the [2Fe–2S] cluster, Rip1p is susceptible to protease degradation, although apo-Rip1 (without a Fe–S cluster) has been detected to be inserted into complex III, resulting in a nonfunctional complex (Smith et al., 2012).

Mutants in the ISC assembly system, as in the Fe–S-IBG subsystem, are unable to conduct mitochondrial respiration and are considered as $rho^{0/-}$ mutants. This suggests that the effects on supercomplexes in the *iba57*Δ mutant occurred because of the absence or down-regulation of expression of mitDNA. However, we identified in mitochondrion extracts of the *iba57*Δ mutant, the expression of Cox2 and Cox3 proteins (proteins that form the core of cytochrome *c* oxidase complex) and in isolated mitochondria the presence of cytochrome *c* and *b*, although slight signals observed, both in its functional status and presence were found (Fig. 5). Additionally, DNA staining in the mitochondria and DNA amplification of *COX2* and *COX3* in the *iba57*Δ mutant (Figs. 6–7) indicated that the *iba57*Δ mutant possesses mitDNA; thus, its inability to respire and decrease supercomplex maturation or cytochrome content is not completely attributed to its rho^- phenotype, although the less defined mitochondrial structures suggest decreased mitDNA content. ETC dysfunction has been associated to events of regulation of expression, large deletions, or less mitDNA content (rho^-). In this sense, mitDNA integrity depends on ATP synthase assembly, whose dysfunction due to either nuclear or mitochondrial mutations lead to rapid mitDNA loss, generating rho^- phenotypes; additionally, mitDNA rearrangements associated to introns may occur (Lipinski et al., 2010) or dysfunction in respiration depending on complex III of the ETC increases the levels of ROS, contributing to mitDNA loss (Gomes et al., 2013).

The Isa1/Isa2 and Iba57 proteins have been extensively described to participate in the assembly of [4Fe–4S]-type centers from specific apoproteins (Brancaccio et al., 2014; Muhlenhoff et al., 2011; Sheftel et al., 2012). The present study revealed that Iba57p may also be involved in the maturation of the Rieske subunit of ETC complex III and is probably associated with transference or recycling of its [2Fe–2S] cluster (see Fig. 3 in Gomez-Gallardo et al., in press). Although our results may appear to be in conflict with the idea of a central role for Isa1/Isa2 and Iba57 in the assembly of [4Fe–4S] clusters, this system may have a dual function in directly transferring [2Fe–2S] centers to Rip1 apoprotein or participate in the maturation of [4Fe–4S] by a fusion of two [2Fe–2S] centers, as proposed previously (Banci et al., 2014). In their working

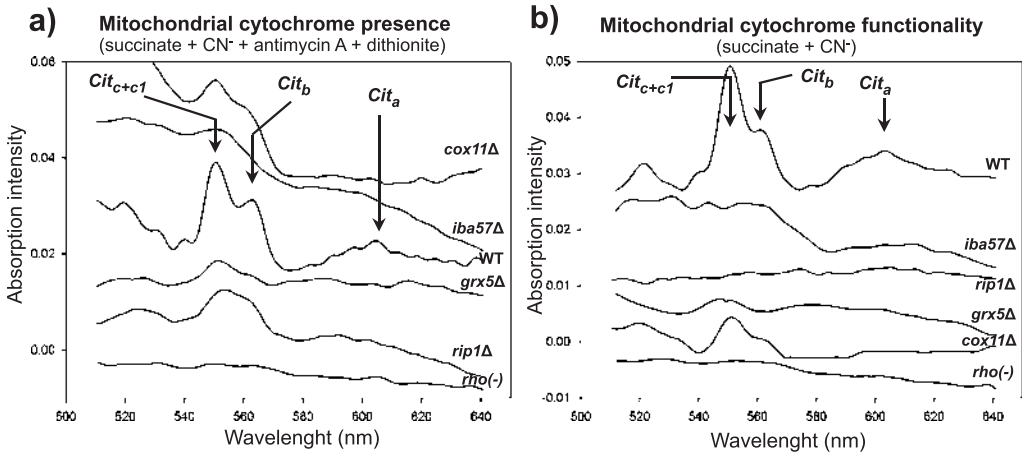

Fig. 5. Analysis of mitochondrial cytochromes in *S. cerevisiae* by UV spectroscopy. Mitochondrial suspensions were used for UV spectra determination, recording spectrum from 400 to 650 nm. a) Basal spectrum of mitochondrial suspensions using succinate as substrate, cyanide and antimycin A as inhibitors, and dithionite as cytochrome-reducing agent (to determine cytochrome presence). b) Using succinate as substrate and cyanide as inhibitor (to determine cytochrome functionality). The spectra obtained correspond to the average of spectra overlapped at least 6 times. Bands corresponding to the cytochromes are indicated with arrows.

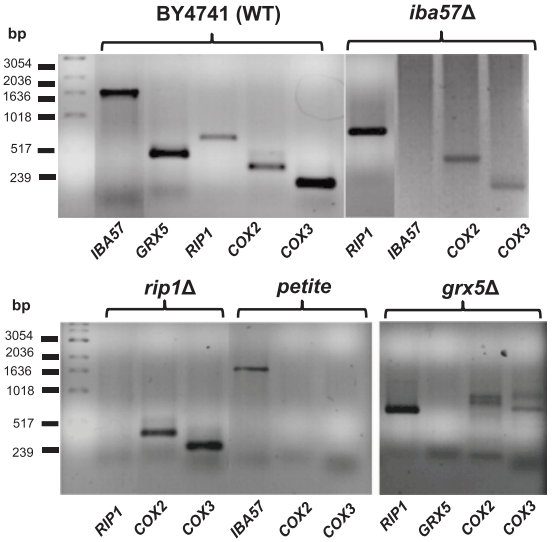

Fig. 6. Gene amplification of nuclear and mitochondrial genes in *Saccharomyces cerevisiae* strains. PCR products obtained from total DNA amplification using oligonucleotides specific for each gene as described in the Materials and Methods section. Representative agarose gels stained with ethidium bromide are presented. Petite rho^0 strain was obtained from BY4741 wild-type yeast by ethidium bromide reagent treatment. Expected sizes of DNA fragments were as follows: *IBA57* (1508 bp), RIP1(654 bp), *GRX5* (460 bp), *COX2* (357 bp), and (*COX3* (239 bp).

model, they found that the ISCA1/ISCA2 heterodimer in humans (Isa1/2p homologs of yeast) can bind either [2Fe–2S] or [4Fe–4S] clusters, with the human GRX5 (Grx5p homolog) also binding $[2Fe–2S]^{2+}$ clusters (Ajit Bolar et al., 2013; Al-Hassnan et al., 2015; Beilschmidt et al., 2017). In this mechanism, two GRX5-$[2Fe–2S]^{2+}$ complexes may generate a $[4Fe–4S]^{2+}$ cluster that can be donated to a heterodimeric ISCA1/ISCA2 complex, suggesting that the protein formed acts as an "assembler" of [4Fe–4S] clusters and is the functional unit in mitochondria that receives [2Fe–2S] clusters from human GRX5 and assembles [4Fe–4S] clusters before their transfer to the final target apoproteins. Recently, the existence of heterocomplexes [2Fe–2S]-BOLA1-GRX5 and [2Fe–2S]-BOLA3-GRX5 was also confirmed (Nasta et al., 2017). In addition, examination of the levels of several Fe/S proteins by RNAi in human HeLa cells showed that for mitochondrial aconitase, succinate dehydrogenase, several proteins of complex I, and Rieske protein, but not ferrochelatese (a [2Fe–2S]-dependent protein) and heme content, their expression decreased under deficiency of ISCA1, ISCA2, and IBA57; additionally, alterations in the mitochondrial morphology and loss of cristae membranes were observed (Sheftel et al., 2012). The authors suggested that these effects were a consequence of pleiotropic effects on other members of the ETC. However, our results support a role for Iba57p in inserting [2Fe–2S] in the Rieske subunit, likely via the Isa1/Isa2 proteins, which agrees with the ability of ISCA1/2 to bind this type of Fe–S cluster, as suggested previously (Banci et al., 2014; Beilschmidt et al., 2017; Braymer and Lill, 2017; Nasta et al., 2017).

Other approaches supporting this hypothesis are related to the bacterial fumarate and nitrate reduction regulator, which functions as a switch between aerobic and anaerobic metabolism, where its Fe–S cluster transforms from the active $[4Fe–4S]^{2+}$ form in oxygen-limiting conditions to a $[2Fe–2S]^{2+}$ form during oxygen or superoxide exposure, with $[3Fe–4S]^{1+}$ as an intermediary form, suggesting that the Fe–S cluster is involved in the molecular mechanism of O_2 sensing by fumarate and nitrate reduction regulator (Crack et al., 2007; Jervis et al., 2009; Zhang et al., 2012). Similarly, some $[2Fe–2S]^{2+}$ clusters are remodeled during O_2-induced degradation of the $[4Fe–4S]^{2+}$ clusters in biotin synthase. This suggests the occurrence of $[4Fe–4S]^{2+} \leftrightarrow [2Fe–2S]^{2+}$ cluster interconversion and raises the possibility that this process is used in vivo to regulate enzyme activity in response to oxidative stress (Zhang et al., 2012). Thus, the Isa1/Isa2/Iba57/Grx5 subsystem may participate in the sorting of both [4Fe–4S] and [2Fe–2S] clusters, where oxygen tension and/or excessive ROS generation may be the factors or "switch" controlling which type of [Fe–S] cluster is inserted into the apoproteins. This may be physiologically important for yeast because of their anaerobic metabolism, although a hypothetical signal that allows this system to "switch" between the delivery of [2Fe–2S] or [4Fe–4S] centers requires further investigation. In agreement with the versatility of the Fe–S-IBG subsystem in the metabolism of a variety of [Fe–S] species, we observed large decreases in the levels of [Fe–S] clusters and cytochromes analyzed by Raman and UV spectrometry in isolated mitochondria from the

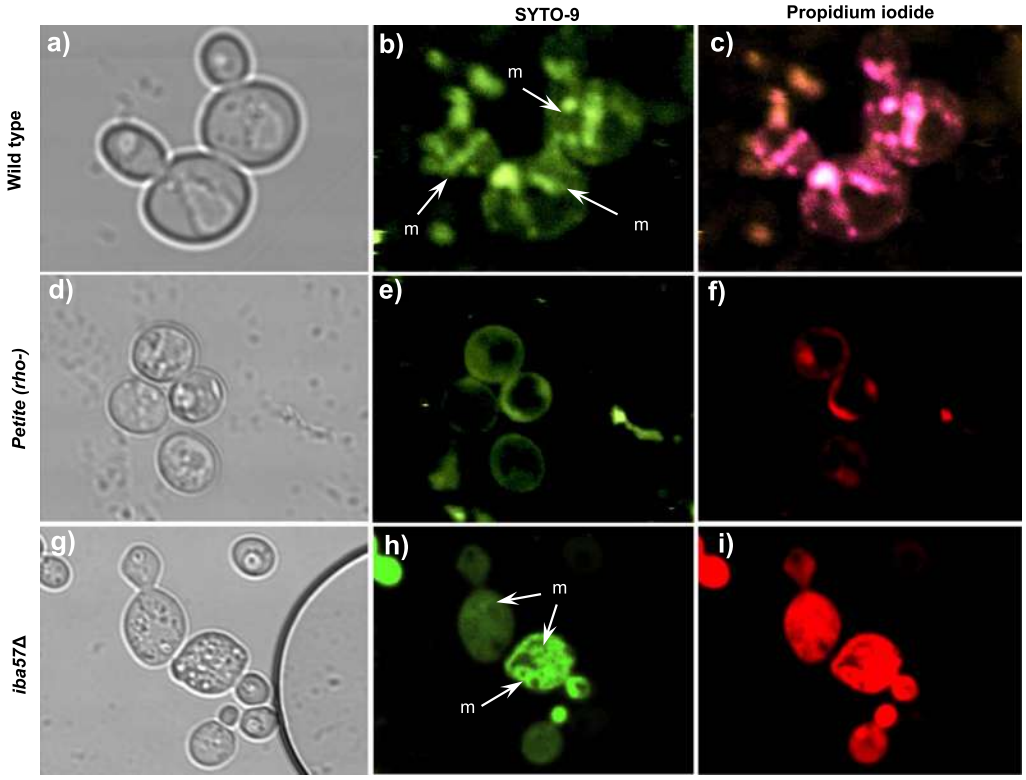

Fig. 7. Microscopy images of *Saccharomyces cerevisiae* cells and mitochondrial structures. YPD-grown yeast cultures were visualized by fluorescence resonance energy transfer (FRET) using SYTO9 and propidium iodide stain mix (Live/dead FungaLight yeast viability kit); samples were observed at 482/502 and 535/617 nm, respectively, using a confocal microscope (Olympus FV1000). a–c) Wild type BY4741 (WT) yeast; d–f) petite (rho$^-$) BY4741 strain; g–i) *iba57*Δ mutant. Cells are shown in which mitochondria is indicated by (m). Images of the cells were taken at 40–60 × magnification.

*iba57*Δ mutant, as well as in the positive control strain *rip1*Δ.

In *S. cerevisiae*, supercomplex III_2/IV_2 was significantly affected in mitochondria isolated from *iba57*Δ and *rip1*Δ mutants; interestingly, the activity of complexes II and III in the *grx5*Δ mutant, although reduced, was not completely inhibited as in other mutants. These results confirm that the Iba57 protein plays an important role in the maturation or insertion of the Rieske subunit on the supercomplex III/IV of the ETC in a process influenced by the integrity of the Rieske protein. Thus, the mitochondrial energy metabolism of yeast is strongly dependent on the correct assembly of Rieske protein in complex III and, in turn, on the possibility that the Fe–S-IBG assembly subsystem is involved directly or indirectly in the maturation of the [2Fe–2S] cluster into the Rieske subunit of complex III.

Supplementary data to this article can be found online at https://doi.org/10.1016/j.mito.2018.01.003.

Acknowledgments

This research was funded by CONACYT (106567), FOMIX-C01-117130, and C.I.C. 2.14/UMSNH grants and Fundación Marcos Moshisky-2014. LAS and MG received a scholarship by CONACYT. We thanks to Drs. G. Del Río and S. Funes from Instituto de Fisiología Celular/UNAM by yeast strains donation. To González-Halphen D. by anti-Cox2p and anti-Cox3p antibodies supply and to Conte L. and Zara V. by anti-Rip1 antibody donation.

References

Ajit Bolar, N., Vanlander, A.V., Wilbrecht, C., Van der Aa, N., Smet, J., De Paepe, B., Vandeweyer, G., Kooy, F., Eyskens, F., De Latter, E., Delanghe, G., Govaert, P., Leroy, J.G., Loeys, B., Lill, R., Van Laer, L., Van Coster, R., 2013. Mutation of the iron-sulfur cluster assembly gene *IBA57* causes severe myopathy and encephalopathy. Hum. Mol. Genet. 22, 2590–2602.

Al-Hassnan, Z.N., Al-Dosary, M., Alfadhel, M., Faqeih, E.A., Alsagob, M., Kenana, R., Almass, R., Al-Harazi, O.S., Al-Hindi, H., Malibari, O.I., Almutari, F.B., Tulbah, S., Alhadeq, F., Al-Sheddi, T., Alamro, R., AlAsmari, A., Almuntashri, M., Alshaalan, H., Al-Mohanna, F.A., Colak, D., Kaya, N., 2015. *ISCA2* mutation causes infantile neurodegenerative mitochondrial disorder. J. Med. Genet. 52, 186–194.

Banci, L., Brancaccio, D., Ciofi-Baffoni, S., Del Conte, R., Gadepalli, R., Mikolajczyk, M., Neri, S., Piccioli, M., Winkelmann, J., 2014. [2Fe-2S] cluster transfer in iron-sulfur protein biogenesis. Proc. Natl. Acad. Sci. U. S. A. 111, 6203–6208.

Beilschmidt, L.K., Ollagnier de Choudens, S., Fournier, M., Sanakis, I., Hograindleur, M.-A., Clémancey, M., Blondin, G., Schmucker, S., Eisenmann, A., Weiss, A., Koebel, P., Messaddeq, N., Puccio, H., Martelli, A., 2017. *ISCA1* is essential for mitochondrial Fe4S4 biogenesis in vivo. Nat. Commun. 8, 15124.

Brancaccio, D., Gallo, A., Mikolajczyk, M., Zovo, K., Palumaa, P., Novellino, E., Piccioli, M., Ciofi-Baffoni, S., Banci, L., 2014. Formation of [4Fe-4S] clusters in the mitochondrial iron-sulfur cluster assembly machinery. J. Am. Chem. Soc. 136, 16240–16250.

Brand, M.D., Nicholls, D.G., 2011. Assessing mitochondrial dysfunction in cells. The Biochem. J. 435, 297–312.

Braymer, J.J., Lill, R., 2017. Iron-sulfur cluster biogenesis and trafficking in mitochondria. J. Biol. Chem. 292, 12754–12763.

Cortes-Rojo, C., Calderon-Cortes, E., Clemente-Guerrero, M., Estrada-Villagomez, M., Manzo-Avalos, S., Mejia-Zepeda, R., Boldogh, I., Saavedra-Molina, A., 2009. Elucidation of the effects of lipoperoxidation on the mitochondrial electron transport chain using yeast mitochondria with manipulated fatty acid content. J. Bioenerg. Biomembr. 41, 15–28.

Conte, L., Zara, V., 2011. The Rieske iron-sulfur protein: import and assembly into the cytochrome bc(1) complex of yeast mitochondria. Bioinorg. Chem. Appl. 2011, 363941.

Conte, A., Papa, B., Ferramosca, A., Zara, V., 2015. The dimerization of the yeast cytochrome bc1 complex is an early event and is independent of Rip1. Biochim. Biophys. Acta 1853, 987–995.
Crack, J.C., Green, J., Cheesman, M.R., Le Brun, N.E., Thomson, A.J., 2007. Superoxide-mediated amplification of the oxygen-induced switch from [4Fe-4S] to [2Fe-2S] clusters in the transcriptional regulator FNR. Proc. Natl. Acad. Sci. U. S. A. 104, 2092–2097.
Cui, T.Z., Smith, P.M., Fox, J.L., Khalimonchuk, O., Winge, D.R., 2012. Late-stage maturation of the Rieske Fe/S protein: Mzm1 stabilizes Rip1 but does not facilitate its translocation by the AAA ATPase Bcs1. Mol. Cell. Biol. 32, 4400–4409.
Cui, T.Z., Conte, A., Fox, J.L., Zara, V., Winge, D.R., 2014. Modulation of the respiratory supercomplexes in yeast: enhanced formation of cytochrome oxidase increases the stability and abundance of respiratory supercomplexes. J. Biol. Chem. 289, 6133–6141.
Diaz, F., Enriquez, J.A., Moraes, C.T., 2012. Cells lacking Rieske iron-sulfur protein have a reactive oxygen species-associated decrease in respiratory complexes I and IV. Mol. Cell. Biol. 32, 415–429.
Gardner, P.R., 1997. Superoxide-driven aconitase FE-S center cycling. Biosci. Rep. 17, 33–42.
Gomes, F., Tahara, E.B., Busso, C., Kowaltowski, A.J., Barros, M.H., 2013. nde1 deletion improves mitochondrial DNA maintenance in *Saccharomyces cerevisiae* coenzyme Q mutants. The Biochem. J. 449, 595–603.
Gomez, M., Perez-Gallardo, R.V., Sanchez, L.A., Diaz-Perez, A.L., Cortes-Rojo, C., Meza Carmen, V., Saavedra-Molina, A., Lara-Romero, J., Jimenez-Sandoval, S., Rodriguez, F., Rodriguez-Zavala, J.S., Campos-Garcia, J., 2014. Malfunctioning of the iron-sulfur cluster assembly machinery in *Saccharomyces cerevisiae* produces oxidative stress via an iron-dependent mechanism, causing dysfunction in respiratory complexes. PLoS One 9, e111585.
Gutierrez-Cirlos, E.B., Merbitz-Zahradnik, T., Trumpower, B.L., 2002. Failure to insert the iron-sulfur cluster into the Rieske iron-sulfur protein impairs both center N and center P of the cytochrome bc1 complex. J. Biol. Chem. 277, 50703–50709.
Henson, C.P., Cleland, W.W., 1967. Purification and kinetic studies of beef liver cytoplasmic aconitase. J. Biol. Chem. 242, 3833–3838.
Jervis, A.J., Crack, J.C., White, G., Artymiuk, P.J., Cheesman, M.R., Thomson, A.J., Le Brun, N.E., Green, J., 2009. The O2 sensitivity of the transcription factor FNR is controlled by Ser24 modulating the kinetics of [4Fe-4S] to [2Fe-2S] conversion. Proc. Natl. Acad. Sci. U. S. A. 106, 4659–4664.
Lill, R., 2009. Function and biogenesis of iron-sulphur proteins. Nature 460, 831–838.
Lill, R., Muhlenhoff, U., 2006. Iron-sulfur protein biogenesis in eukaryotes: components and mechanisms. Annu. Rev. Cell Dev. Biol. 22, 457–486.
Lill, R., Hoffmann, B., Molik, S., Pierik, A.J., Rietzschel, N., Stehling, O., Uzarska, M.A., Webert, H., Wilbrecht, C., Muhlenhoff, U., 2012. The role of mitochondria in cellular iron-sulfur protein biogenesis and iron metabolism. Biochim. Biophys. Acta 1823, 1491–1508.
Lipinski, K.A., Kaniak-Golik, A., Golik, P., 2010. Maintenance and expression of the *S. cerevisiae* mitochondrial genome—from genetics to evolution and systems biology. Biochimica et Biophysica Acta (BBA) - Bioenergetics 1797, 1086–1098.
Muhlenhoff, U., Richter, N., Pines, O., Pierik, A.J., Lill, R., 2011. Specialized function of yeast Isa1 and Isa2 proteins in the maturation of mitochondrial [4Fe-4S] proteins. J. Biol. Chem. 286, 41205–41216.
Musatov, A., Robinson, N.C., 2012. Susceptibility of mitochondrial electron-transport complexes to oxidative damage. Focus on cytochrome c oxidase. Free Radic. Res. 46, 1313–1326.
Nasta, V., Giachetti, A., Ciofi-Baffoni, S., Banci, L., 2017. Structural insights into the molecular function of human [2Fe-2S] BOLA1-GRX5 and [2Fe-2S] BOLA3-GRX5 complexes. Biochim. Biophys. Acta Gen. Subj. 1861, 2119–2131.
Perez-Gallardo, R.V., Briones, L.S., Diaz-Perez, A.L., Gutierrez, S., Rodriguez-Zavala, J.S., Campos-Garcia, J., 2013. Reactive oxygen species production induced by ethanol in *Saccharomyces cerevisiae* increases because of a dysfunctional mitochondrial iron-sulfur cluster assembly system. FEMS Yeast Res. 13, 804–819.
Rodríguez-Manzaneque, M.T., Tamarit, J., Bellí, G., Ros, J., Herrero, E., 2002. Grx5 is a mitochondrial glutaredoxin required for the activity of iron/sulfur enzymes. Mol. Biol. Cell 13, 1109–1121.
Schagger, H., 2006. Tricine-SDS-PAGE. Nat. Protoc. 1, 16–22.
Schagger, H., Pfeiffer, K., 2000. Supercomplexes in the respiratory chains of yeast and mammalian mitochondria. EMBO J. 19, 1777–1783.
Schilke, B., Williams, B., Knieszner, H., Pukszta, S., D'Silva, P., Craig, E.A., Marszalek, J., 2006. Evolution of mitochondrial chaperones utilized in Fe-S cluster biogenesis. Current Biol. 16, 1660–1665.
Sheftel, A.D., Wilbrecht, C., Stehling, O., Niggemeyer, B., Elsasser, H.P., Muhlenhoff, U., Lill, R., 2012. The human mitochondrial *ISCA1*, *ISCA2*, and *IBA57* proteins are required for [4Fe-4S] protein maturation. Mol. Biol. Cell 23, 1157–1166.
Smith, P.M., Fox, J.L., Winge, D.R., 2012. Biogenesis of the cytochrome bc(1) complex and role of assembly factors. Biochim. Biophys. Acta 1817, 276–286.
Stames, E.M., O'Toole, J.F., 2013. Mitochondrial aminopeptidase deletion increases chronological lifespan and oxidative stress resistance while decreasing respiratory metabolism in *S. cerevisiae*. PLoS One 8, e77234.
Vartak, R., Porras, C.A., Bai, Y., 2013. Respiratory supercomplexes: structure, function and assembly. Protein and Cell 4, 582–590.
Zara, V., Conte, L., Trumpower, B.L., 2009. Evidence that the assembly of the yeast cytochrome bc1 complex involves the formation of a large core structure in the inner mitochondrial membrane. FEBS J. 276, 1900–1914.
Zhang, B., Crack, J.C., Subramanian, S., Green, J., Thomson, A.J., Le Brun, N.E., Johnson, M.K., 2012. Reversible cycling between cysteine persulfide-ligated [2Fe-2S] and cysteine-ligated [4Fe-4S] clusters in the FNR regulatory protein. Proc. Natl. Acad. Sci. U. S. A. 109, 15734–15739.

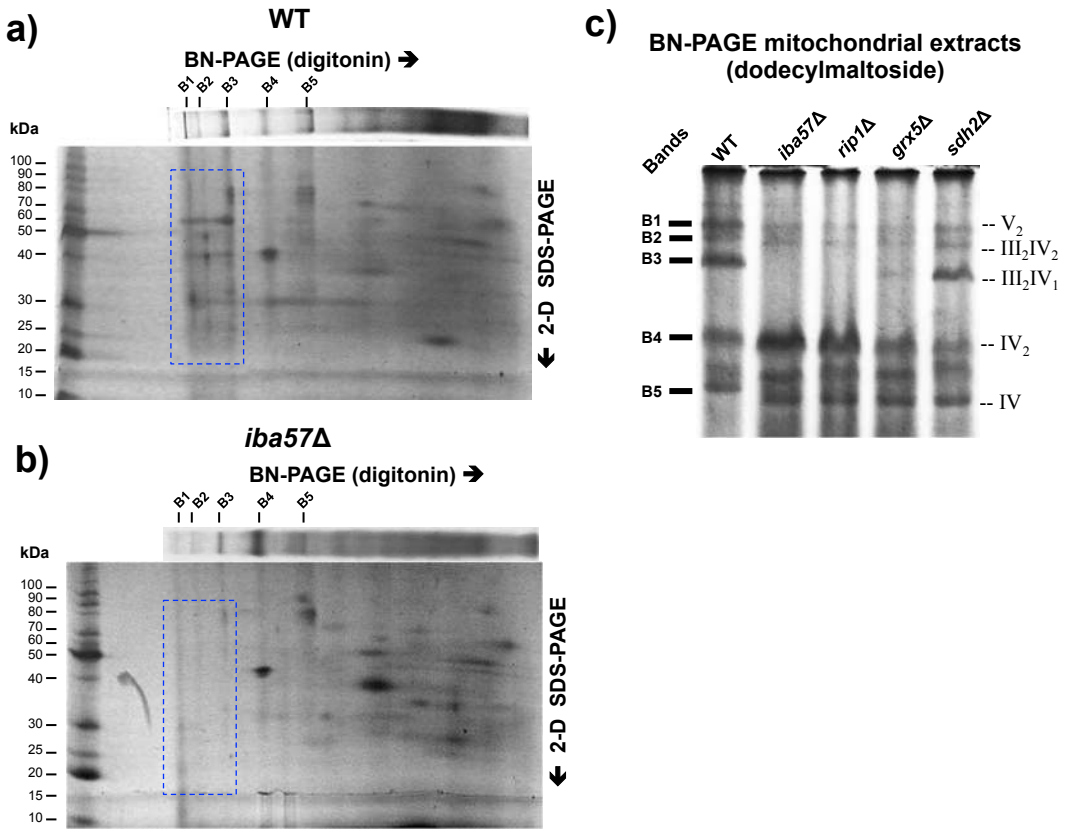

Figure S1. **Evaluation of ETC mitochondrial supercomplexes formation in the Iba57p mutant of *Saccharomyces cerevisiae*.** Mitochondrial suspensions were solubilized with digitonin and the proteins were separated using blue native polyacrylamide gel electrophoresis (BN-PAGE), after gel lanes were resolved in a second dimension by SDS-PAGE as described in the Material and Methods. BN-PAGE line resolved in SDS-PAGE gel corresponding to the WT strain (**a**) and to the *iba57*Δ mutant (**b**). B1–B5, major protein bands corresponding to mitochondrial supercomplexes are shown. BenchMark Protein Ladder (Invitrogen) is showed in silver-stained, SDS-PAGE gels. **c**) BN-PAGE gel of mitochondrial extract solubilized using dodecylmaltoside (1 g/g) and triton X-100 (2.4 g/g) as described in Materials and Methods section. Bands corresponding to mitochondrial supercomplexes are shown.

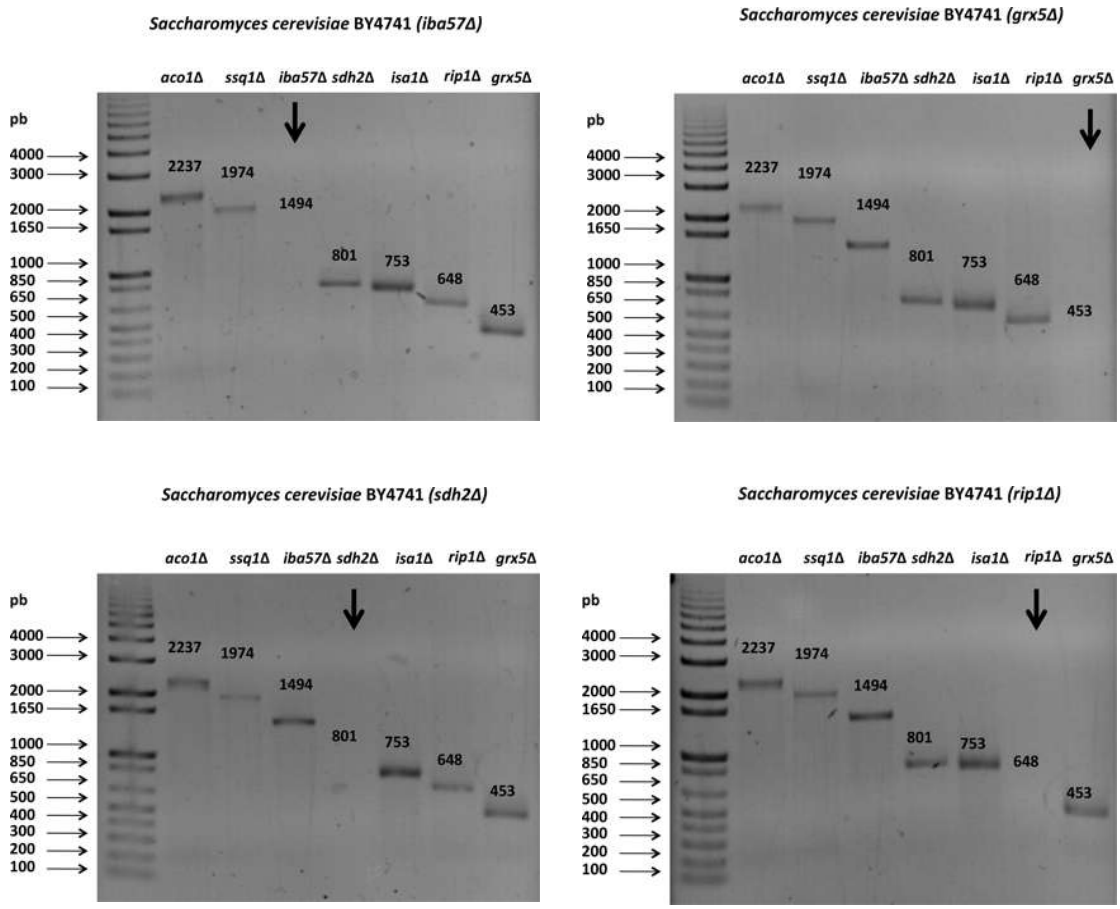

Figure S2. Characterization by PCR of the *Saccharomyces cerevisiae* BY4741 mutants used in this study. Total DNA of each strain was used for PCR amplification using specific oligonucleotides. Arrows in the gels show the lack of DNA fragment amplification, indicating the deletion in the corresponding gene.

7. CAPÍTULO III. El papel de iba57p en la liberación de Fe^{2+} y la generación de O_2^- en *Saccharomyces cerevisiae*

Data in Brief 18 (2018) 198–202

Contents lists available at ScienceDirect

Data in Brief

journal homepage: www.elsevier.com/locate/dib

Data Article

Data on the role of iba57p in free Fe^{2+} release and $O_2^{\bullet-}$ generation in *Saccharomyces cerevisiae*

Mauricio Gomez-Gallardo [a,1], Luis A. Sánchez [a,1], Alma L. Díaz-Pérez [a], Christian Cortés-Rojo [b], Jesús Campos-García [a,*]

[a] *Lab. de Biotecnología Microbiana, Instituto de Investigaciones Químico Biológicas, Universidad Michoacana de San Nicolás de Hidalgo, Morelia, Mich., Mexico*
[b] *Lab. de Bioquímica, Instituto de Investigaciones Químico Biológicas, Universidad Michoacana de San Nicolás de Hidalgo, Morelia, Mich., Mexico*

ARTICLE INFO

Article history:
Received 12 January 2018
Received in revised form
3 March 2018
Accepted 5 March 2018
Available online 11 March 2018

ABSTRACT

The related study has confirmed that in *Saccharomyces cerevisiae*, iba57 protein participates in maturation of the [2Fe–2S] cluster into the Rieske protein, which plays important roles in the conformation and functionality of mitochondrial supercomplexes III/IV in the electron transport chain (Sánchez et al., 2018) [1]. We determined in *S. cerevisiae* the effects of mutation in the *IBA57* gene on reactive oxygen species (ROS) and iron homeostasis. Flow cytometry and confocal microscopy analyses showed an increased generation of ROS, correlated with free Fe^{2+} release in the *IBA57* mutant yeast. Data obtained support that a dysfunction in the Rieske protein has close relationship between ROS generation and free Fe^{2+} content, and which is possible that free Fe^{2+} release mainly proceeds from [Fe–S] cluster-containing proteins.

DOI of original article: https://doi.org/10.1016/j.mito.2018.01.003
* Correspondence to: Lab. de Biotecnología Microbiana, Instituto de Investigaciones Químico Biológicas, Universidad Michoacana de San Nicolás de Hidalgo, Edif. B-3, Ciudad Universitaria, 58030 Morelia, Michoacán, Mexico.
E-mail address: jcgarcia@umich.mx (J. Campos-García).
[1] Both authors contributed equally to this work and share first authorship.

https://doi.org/10.1016/j.dib.2018.03.023

Specifications Table

Subject area	*Biology*
More specific subject area	*Cell biology*
Type of data	*Graphs, figures*
How data was acquired	*ROS and Fe^{2+} determination by flow cytometry using a BD Accuri C6 Flow Cytometer (BD Biosciences) and observation by using a confocal microscope (Olympus FV1000).*
Data format	*Analyzed and images*
Experimental factors	*ROS and Fe^{2+} determination in S. cerevisiae cells using fluorescent probes.*
Experimental features	*Real-time quantification of ROS and Fe^{2+} in S. cerevisiae cells suspensions were determined by flow cytometry and cellular structures were co-localized by confocal microscopy.*
Data source location	*Instituto de Investigaciones Químico Biológicas, Universidad Michoacana de San Nicolás de Hidalgo, Morelia, Michoacán, México.*
Data accessibility	*Data are provided with this article.*

Value of the data

- There is an established relation between *IBA57* mutation and the Rieske protein maturation in *S. cerevisiae*, which affects the electron transport chain functionality.
- *IBA57* mutation in *S. cerevisiae* is correlated with ROS generation and loss of iron homeostasis.
- This dataset provides new insights into the mechanism of ROS generation in *S. cerevisiae*, dependent of the ETC functionality.

1. Data

Treatments with 80 μM menadione in the *Saccharomyces cerevisiae iba57Δ* mutant caused significant impairment in its growth rate (Fig. 1a–b). The levels of free Fe^{2+} even without oxidant were significantly incremented in a time-dependent fashion in cell suspensions of the *iba57Δ* mutant yeast (Fig. 1c). The *iba57Δ* mutant displayed a significant increment of superoxide radical ($O_2^{\bullet-}$) generation with a dose-dependent of Fe^{2+}, determined by flow cytometry (Fig. 1d).

The western blot assays showed that the Rieske protein (Rip1p) was absent in the *rip1Δ* mutant, and decreased expression level was found in the *iba57Δ* mutant (Fig. 1e). When extracts from cultures grown on YPD plus high Fe^{2+} concentration (20 μM) or menadione as ROS-inducer were used, the Rip1p expression increased significantly in the WT, but not in the *iba57Δ* mutant.

Microscopy analysis shows an increment in ROS generation, associated with release of free Fe^{2+} in the *iba57Δ* mutant (Fig. 2). Interestingly, the high-intensity fluorescence observed in the *iba57Δ* mutant, which exhibited a full dissipation of mitochondrial membrane potential was associated with loss of iron homeostasis in the yeast cells.

2. Materials and methods

2.1. Yeast strains and growth conditions

Mutant strains *iba57*Δ, *rip1*Δ, and *grx5*Δ correspond to the haploid *S. cerevisiae* BY4741 (Mat a, *his3*Δ, *leu2*Δ0, *met15*Δ0, *ura3*Δ0) and its *KanMX4* interruption gene (Open Biosystems). Growth tests were carried out as described [1].

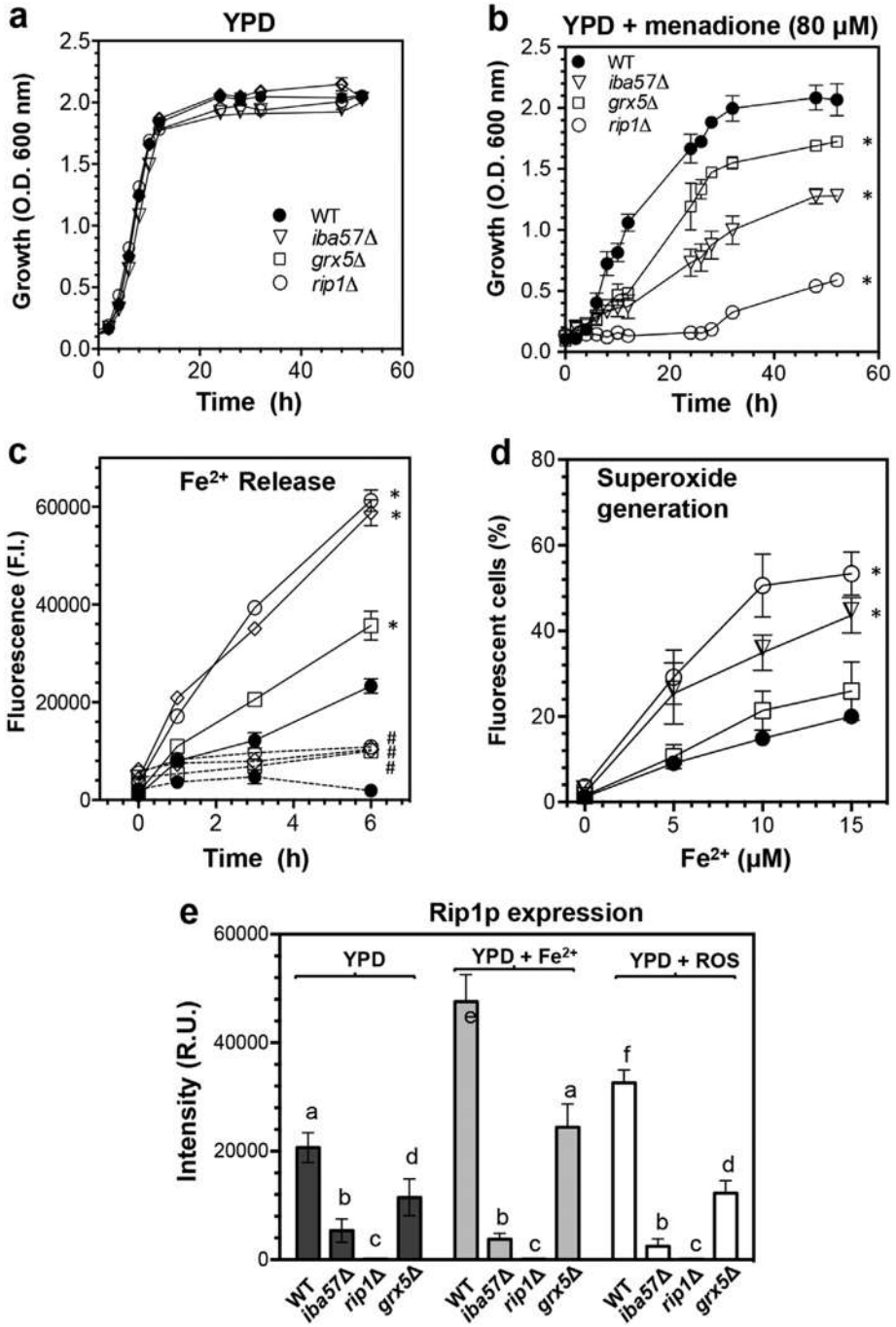

Fig. 1. Effect of the *IBA57* deletion over the growth of *Saccharomyces cerevisiae*, iron release, superoxide generation and Rip1 protein expression. a–b) Growth kinetics of *S. cerevisiae* strains grown without and in the presence of menadione 80 μM as ROS-inducer. **c**) Kinetics of Fe^{2+} release. Treatments without menadione (dashed lines) and with 80 μM menadione (continuous lines). d) $O_2^{\bullet-}$ generation in yeast suspensions treated with different concentrations of Fe^{2+} [$FeSO_4(NH_4)$]. a–d) Values are the mean of three independent experiments. **e**) Densitometry analysis of cellular extracts free-cells immunoblotted for Rip1p expression; yeast extract of cultures grown on: YPD (glucose), YPD with Fe^{2+} [$FeSO_4(NH_4)$] 20 μM, and YPD with menadione 80 μM. Means and SE are indicated as bars ($n = 3$). ANOVA was used to compare treatments. Significant differences ($p < 0.05$) are indicated as symbols (*, #) or with different lowercase letters.

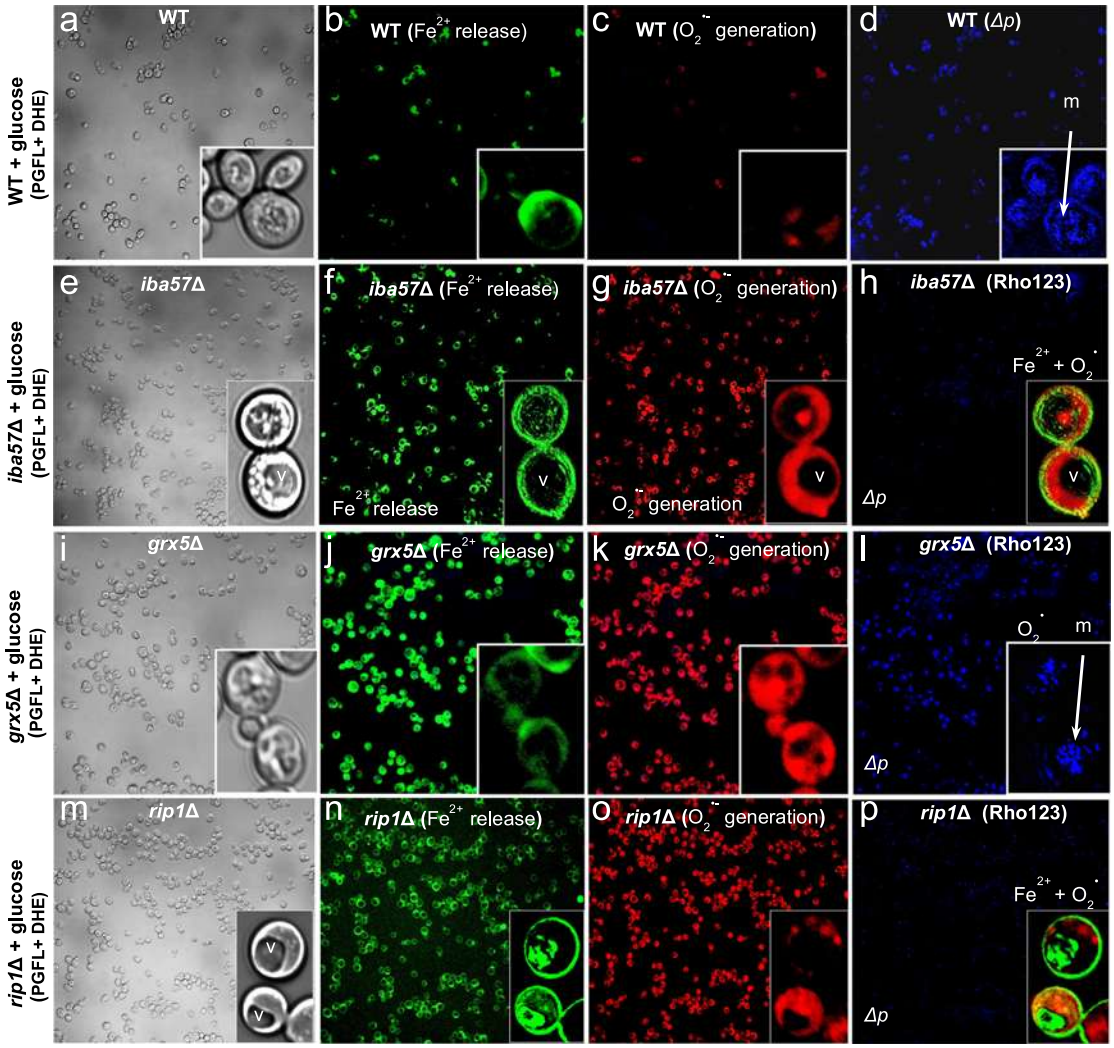

Fig. 2. Microscopy images of *Saccharomyces cerevisiae* cells for co-localization of free Fe^{2+} and superoxide in intracellular compartments. YPD-grown yeast cultures were loaded with the fluorescent probes PGFL and DHE for determination of free Fe^{2+} and $O_2^{\bullet-}$, respectively; incubated for 30 min at 30 °C and co-loaded with Rhodamine 123 for membrane potential (*Δp*) detection as a mitochondrial co-localization marker, and observed using a confocal microscope. a–d) Wild type (WT) yeast; e-h) *iba57*Δ mutant; i-l) *grx5*Δ mutant; and m-p) *rip1*Δ mutant. Cells are shown in which mitochondria and vacuoles are indicated by (m) and (v), respectively. Free Fe^{2+} accumulation is shown as green cells and green granules within the cells, $O_2^{\bullet-}$ generation areas are shown as red granules within the cells, and mitochondrial structures (*Δp*) are shown as cyan granules within the cells, using the Rho123 probe. Images of the cells were taken at 10× to 60× magnifications using a confocal microscope (Olympus FV1000).

2.2. Real-time quantification of ROS and Fe^{2+} content in S. cerevisiae cultures

Intracellular ROS and Fe^{2+} in cell suspensions were determined using cell-permeant fluorescent probes quantified by flow cytometry [1–3]. For superoxide ($O_2^{\bullet-}$) determination, yeast were incubated with 5 μg/mL dihydroethidium (DHE, Molecular Probes, Invitrogen); while as for free Fe^{2+} was used the indicator for heavy metals Phen green FL 5 μg/mL (PGFL; Molecular Probes, Invitrogen) in presence of 1 mM of the chelator 1,10-Phenanthroline (Sigma). DHE- and PGFL-fluorescence was quantified by flow cytometry monitoring the emission fluorescence at 587/40 nm and 533/30 nm, respectively; using a BD AccuriC6 Flow Cytometer (BD Biosciences).

2.3. Determination of Rip1p expression by Western blot in S. cerevisiae

Mitochondrial protein extracts 50 μg were separated by electrophoresis on SDS-PAGE gels, membranes for Western blot procedure were treated as described [1–3]. Bands intensity in films were quantified using the Image J software and data graphed as Rip1p expression intensity.

2.4. Confocal microscopy of yeast suspensions

S. cerevisiae YPD-grown cultures were loaded with the fluorescent probes DHE or PGFL and Rhodamine 123 as detailed [1–3], treated with menadione (80 μM) and mitochondrial co-localization was analyzed using a confocal microscope (Olympus FV1000). The emission signal of fluorescence was monitored at 560–580 nm for DHE, 405–505 nm for PGFL, and 533–563 nm for Rhodamine 123.

Acknowledgements

This research was funded by CONACYT (106567) and C.I.C.2.14/UMSNH grants. MG and LAS received a scholarship by CONACYT.

Transparency document. Supplementary material

Transparency document associated with this article can be found in the online version at https://doi.org/10.1016/j.dib.2018.03.023.

References

[1] L.A. Sanchez, M. Gomez-Gallardo, A.L. Diaz-Perez, C. Cortes-Rojo, J. Campos-Garcia, Iba57p participates in maturation of a [2Fe–2S]-cluster Rieske protein and in formation of supercomplexes III/IV of *Saccharomyces cerevisiae* electron transport chain, Mitochondrion (17) (2018) 30136–30138. http://dx.doi.org/10.1016/j.mito.2018.01.003.

[2] M. Gomez, R.V. Perez-Gallardo, L.A. Sanchez, A.L. Diaz-Perez, C. Cortes-Rojo, V. Meza Carmen, A. Saavedra-Molina, J. Lara-Romero, S. Jimenez-Sandoval, F. Rodriguez, J.S. Rodriguez-Zavala, J. Campos-Garcia, Malfunctioning of the iron-sulfur cluster assembly machinery in *Saccharomyces cerevisiae* produces oxidative stress via an iron-dependent mechanism, causing dysfunction in respiratory complexes, PLoS One 9 (2014) e111585.

[3] R.V. Perez-Gallardo, L.S. Briones, A.L. Diaz-Perez, S. Gutierrez, J.S. Rodriguez-Zavala, J. Campos-Garcia, Reactive oxygen species production induced by ethanol in *Saccharomyces cerevisiae* increases because of a dysfunctional mitochondrial iron-sulfur cluster assembly system, FEMS Yeast Res. 13 (2013) 804–819.

8. DISCUSIÓN

Las mitocondrias son orgánulos que tienen funciones en procesos fisiológicos diversos como la síntesis de ATP, la regulación del calcio citoplásmatico **[McBride y Scorrano, 2013]**, el control del estado redox celular, la generación y liberación de especies reactivas de oxígeno (ERO), la liberación de metabolitos que regulan procesos y vías críticas como el succinato y α-cetoglutarato **[Stanley et al., 2014]**, la regulación de la apoptosis **[Galluzzi et al., 2012]**, la adaptación celular a los cambios en la disponibilidad del sustrato mediante diferentes vías de señalización, y la remodelación de su estructura y dinámica **[Liesa y Shirihai, 2013]**. Estos orgánulos por tanto, son fundamentales para mantener el delicado equilibrio entre la vida y la muerte celular, y su función debe ser estrictamente regulada. Esta regulación se produce tanto a través de respuestas a largo plazo en el nivel de expresión, transcripción y traducción; como a través de respuestas postranscripcionales a corto plazo. Hallazgos recientes sugieren que un nivel adicional de regulación a corto plazo es la organización dinámica de los supercomplejos (SC) respiratorios en la membrana mitocondrial interna. Muchos de los procesos celulares más rápidos y dinámicos están mediados por modificaciones postraduccionales, así, la activación de quinasas y fosfatasas y sus efectos se producen en períodos de tiempo muy cortos, lo que permite que la célula se adapte a los desafíos emergentes. La fosforilación/desfosforilación, la acetilación/desacetilación y las alteraciones redox pueden afectar los componentes de los SC, lo que podría alterar su estabilidad y/o su función. De manera que, la red mitocondrial está controlada por un equilibrio entre la fusión y la fisión de sus componentes **[Griparic y van der Bliek, 2001; Cipolat et al., 2004]**. Así, la reorganización de las crestas mitocondriales durante la fusión y la fisión requiere que los SC se reubiquen para mantener una función adecuada, lo cual requiere de su montaje y desmontaje.

La formación, estabilización y función de los SC está críticamente influenciada por la composición lipídica de la membrana mitocondrial interna. La importancia de la interacción lípido-proteína se ha demostrado en cepas de levadura deficientes en cardiolipina y fosfolípidos, en las que la formación de los SC y su actividad, resultan ser defectuosas **[Wenz et al., 2008; Pfeiffer et al., 2003]**. Los lípidos son determinantes y esenciales de la asociación de los supercomplejos **[Lenaz y Genova, 2007]**, sin embargo, pueden modificar la naturaleza y el alcance de las asociaciones sólo en escalas de tiempo muy largas, ya que se ven afectadas por la especie del organismo y el tejido, que a su vez es determinada por la dieta y estilo de vida. Las fuerzas responsables de la asociación de supercomplejos parecen depender en gran medida del contenido y la composición de lípidos y, probablemente, de la forma de la membrana mitocondrial interna; ya que la dilución de las proteínas con un exceso de fosfolípidos puede debilitar las fuerzas que mantienen unidos a los complejos respiratorios. Entre los lípidos, la cardiolipina y la fosfatidil etanolamina son cruciales para las funciones mitocondriales; ambos son fosfolípidos que no forman bicapa, debido a sus pequeñas cabezas polares en comparación con las colas voluminosas de las no polares **[Killian y de Kruijff, 2004; Osman et al., 2011]**. El requisito absoluto de la cardiolipina para la actividad de complejos I, II y IV sugiere que este fosfolípido desempeña un papel crucial en el proceso de transferencia de electrones **[Fry y Green, 1980; Fry y Green, 1981]**, además estabiliza los supercomplejos respiratorios, así como los complejos individuales. La interacción directa (proteína-proteína) entre los complejos III y IV en levaduras requiere de una molécula de cardiolipina y una de fosfatidiletanolamina, proporcionando un enlace flexible entre las subunidades que interactúan entre estos complejos **[Claypool et al., 2008]**. Está bien documentado que la exposición de las mitocondrias a especies reactivas de oxígeno (ERO) puede afectar la actividad respiratoria a través del daño oxidativo de la cardiolipina, que es necesaria para el funcionamiento óptimo de los complejos multienzimáticos **[Paradies et al., 2000; Petrosillo et al., 2003]**, así mismo la distorsión de la bicapa lipídica inducida por la peroxidación y la alteración de los fosfolípidos afectan la disociación de los SC.

El ensamble dinámico de los complejos en la CTE permite que la célula se adapte a diferentes fuentes de carbono y condiciones fisiológicas variables, de manera que una mayor comprensión de estos procesos promete un mejor entendimiento del sistema de fosforilación oxidativa. Aunque se ha establecido que el ensamblaje de complejos respiratorios de forma individual en la membrana mitocondrial interna pueden formar diferentes asociaciones de supercomplejos, se ha encontrado que uno de los factores requeridos para este ensamblaje es la proteína Cox7a2l o factor de ensamble de supercomplejos I (SCAFI) en mamíferos, que define tres poblaciones de asociación con el complejo IV:

1) La fracción ensamblada con los complejos I y III en el respirasoma, que puede recibir electrones sólo del NADH; **2)** La fracción ensamblada sólo con el complejo III, que recibe electrones únicamente de enzimas que contienen $FADH_2$; y **3)** Una fracción que no interactúa y que puede recibir electrones de cualquier sustrato. Este factor modula la interacción entre los complejos III y IV sin afectar la estabilidad de los complejos individuales, con lo cual se valida sustancialmente el modelo de plasticidad **[Acín-Pérez y Enriquez, 2014]**.

La CTE es responsable de la oxidación de los equivalentes reductores, en forma de NADH o $FADH_2$, que se originan en diferentes vías metabólicas (glucólisis, oxidación de ácidos grasos o el ciclo de Krebs). La oxidación de NADH y $FADH_2$ está acoplada al bombeo de protones en el espacio intermembrana, y el gradiente de protones resultante es utilizado por la ATPasa para generar energía en forma de ATP. El NADH se oxida en el complejo I, mientras que el $FADH_2$ en el complejo II u otras deshidrogenasas, como ocurre en levaduras. Los electrones son transferidos a la coenzima Q (CoQ) y, posteriormente, al complejo III, el citocromo *c* y el complejo IV, que los transfiere al oxígeno como el aceptor final **[Acin-Perez y Enriquez, 2014]**. A lo largo de este proceso se ha registrado un comportamiento de "poza" de la CoQ y la formación de supercomplejos ha demostrado la existencia de dos "pozas" distintas: una dedicada a oxidar equivalentes provenientes de NADH y un segundo grupo independiente proveniente de $FADH_2$. Específicamente, los sustratos para el NADH (piruvato + malato) y $FADH_2$ (succinato) tienen un efecto aditivo sobre la actividad respiratoria cuando se agregan a las mitocondrias que contienen el supercomplejo III+IV, pero este comportamiento aditivo es deficiente o muy reducido en ausencia de dicha asociación. Este efecto aditivo permite que las mitocondrias optimicen el uso simultáneo de diferentes sustratos de carbono cuya oxidación genera proporciones variables tanto de NADH como $FADH_2$.

A lo largo de nuestra investigación para determinar la participación del sistema ISC en el daño oxidativo y la disfunción mitocondrial, se partió de antecedentes directos del mismo grupo de trabajo **[Perez-Gallardo et al., 2013]**; donde por más de 10 años se ha buscado mediante diferentes enfoques dar respuesta a esta interrogante, lo cual ha permitido conocer con mejor detalle como es regulado el Fe intracelular, su relación con el aumento del estrés oxidativo y a su ves con la funcionalidad mitocondrial (CTE). Retomando los resultados obtenidos previamente **[Pérez-Gallardo et al., 2013; Gómez et al., 2014; Gómez-Gallardo et al., 2018; Sánchez et al., 2019]** podemos observar que se ha estudiado la mayoría de las proteínas que participan en el ensamble de centros Fe-S y aquellas proteínas blanco que los contienen y participan en la CTE. El conjunto de dichas proteínas las podemos catalogar en tres niveles distintos: 1) aquellas que participan en la regulación y transporte del hierro (Aft1, Atx1, Mrs4); 2) las proteínas de andamiaje que traslocan e insertan el hierro en la correspondiente apoproteína (Isu1, Ssq1, Grx5, Isa1, Iba57); y 3) las proteínas blanco que contienen Fe/S (Aco1, Sdh2, Rip1). De manera inicial se determinó si la mutación en cada unos de los genes de interés afectaría el crecimiento y viabilidad de la levadura, para ello se realizaron curvas de crecimiento bajo condiciones normales (YPD) y de estrés oxidativo, empleando distintas concentraciones de agentes oxidantes (Etanol, H_2O_2, Menadiona) (**Pérez-Gallardo et al., 2013 Fig. 1** y **2; Gómez et al., 2014 Fig. 1**). Observando como en condiciones de medio enriquecido no hay afectaciones, pero si existe una mayor susceptibilidad, reflejado en una disminución del crecimiento en todas las cepas mutantes respecto a la WT en presencia de los agentes oxidantes; presentando un mayor efecto en las mutantes *atx1Δ* y *ssq1Δ*; es decir, en el regulador transcripcional inducido por hierro (Atx1) y la proteína de andamiaje de centros Fe/S (Ssq1). Tanto los transportadores de hierro citosólico y mitocondrial Atx1 y Mrs4 no muestran este comportamiento debido a la posible expresión de otros transportadores que pueden llegar a complementar éstas mutaciones y restituyen el crecimiento a niveles cercanos a la WT, siendo observable que la redundancia génica en los transportadores celulares permite una adecuada captación del hierro como elemento clave para el desarrollo celular **[Pufahl et al.,1997; Mühlenhoff et al., 2003; Froschauer et al., 2009]**. Las disfunciones mitocondriales, especialmente las causadas por alteraciones en el ciclo de los ácidos tricarboxílicos o la respiración, inducen la vía de señalización retrógrada mitocondrial, que produce reconfiguraciones metabólicas y transcripcionales en el metabolismo de carbohidratos y del nitrógeno, y de esta manera adapta las células con defectos mitocondriales **[Liu y Butow, 2006]**.

Posteriormente, se determinó que las mutaciones en el sistema ISC aumentan la generación de ERO citosólico y mitocondrial (**Pérez-Gallardo et al., 2013**. **Fig. 3**; **Gómez et al., 2014. Fig. 2** y **3**) debido al aumento de Fe^{2+} libre al interior de las mitocondrias respecto a la WT, cuyos efectos se elevan drásticamente en presencia de los agentes oxidantes (**Pérez-Gallardo et al., 2013. Fig. 2**; **Gómez et al., 2014. Fig. 3; Gómez-Gallardo et al., 2018 Fig. 1**). Este efecto se observa claramente en las microscopias de florescencia empleando diferentes sondas intracelulares e intramitocondriales (**Gómez et al., 2014 Fig. 4**; **Gómez-Gallardo et al., 2018 Fig. 2**); produciendo una activación en los mecanismos de defensa antioxidante; cuantificables mediante los niveles de Glutatión (GSH-GSSG) (**Pérez-Gallardo et al., 2013. Fig. 5)** y la sobreactivación de la enzima Catalasa (**Pérez-Gallardo et al., 2013. Fig. 6**). En conjunto, la disfunción del sistema ISC incrementa los niveles de Fe^{2+}, y este hierro libre que no es incorporado a las correspondientes apoproteínas reacciona con los niveles basales de ERO mediante las reacciones de Fenton y Haber-Weiss, generando un ciclo continuo de oxido-reducción que potencia la formación de ERO, el cual es exacebado cuando se adiciona alguno de los agentes oxidantes. Resaltando que las mutantes *ssq1Δ, isa1Δ, iba57Δ* y *rip1Δ* muestran un marcado incremento en todos los niveles de ERO analizados. Para determinar que dicho efecto se debía a la actividad específica del Fe^{2+}, mas allá de la generación basal de ERO ocasionada por cada mutación *perse*. Se procedió a la adición de un quelante (secuestrante) de hierro al medio de crecimiento y así limitar su biodisponibilidad (**Gómez et al., 2014. Fig. 5 C-D**). Ello nos indicó claramente como los niveles de ERO bajaron a niveles similares a la WT para todas las cepas mutantes, al limitar los niveles de Fe^{2+}. Observando una notable disminución en el porcentaje de células fluorescentes (positivas al aumento de ERO) y aumentando la sobrevivencia de la población, aún en presencia de agentes oxidantes. Corroborando así, la participación directa del hierro libre en la inducción de ERO que afectan directamente la viabilidad celular, mas allá de cada mutación dentro del sistema ISC. Hasta este punto sabemos que la levadura responde ante los efectos tóxicos del Hierro induciendo repuestas antioxidantes y contrarrestar así el daño celular. Dicho efecto se corrobora también en otros estudios, considerando que las mitocondrias son actores clave, de manera que los defectos en los sistemas ISC inducen a su vez los sistemas de captación de hierro a nivel de la membrana plasmática **[Lill et al., 2012; Lill et al., 2014]**, y si el hierro intracelular se acumula en altos niveles dentro de las mitocondrias originan daño oxidativo que agrava aun más los defectos existentes en las funciones mitocondriales **[Hadzhieva et al., 2014]**.

Para conocer si efectivamente el Fe^{2+} libre proviene de los centros Fe/S inducido por las mutaciones del sistema ISC, se cuantificaron mediante espectrometría de Raman los niveles de centros Fe/S (**Gómez et al., 2014 Fig. 6A**; **Sánchez et al., 2019 Fig. 2B**), siendo nuevamente las mutantes *ssq1Δ, isa1Δ, iba57Δ* y *rip1Δ* las que presentan un menor nivel de formación de centros Fe/S; si bien, las tres primeras forman parte del sistema ISC y se ha establecido que son esenciales en la inserción de todos los centros 4Fe-4S, nos sorprendió que la mutante en *rip1Δ* presentara niveles tan bajos al ser ya una proteína que contiene un centro 2Fe-2S. Destacando que Rip1p puede ser necesaria para regular la formación de otras proteínas blanco, o que los altos niveles de ERO afecten directamente al sistema ISC de manera general, e incluso Rip1p podría ser clave para la función de la CTE. Ante esta interrogante y para descartar una disfunción generalizada rio abajo en la CTE por las distintas mutaciones ISC, se analizó una de las proteínas mas activas que participa en el ciclo de Krebs y contiene un centro 4Fe-4S, la Aconitasa (Aco1p)(**Gómez et al., 2014 Fig. 6B**; **Sánchez et al., 2019 Fig. 2A**). Los resultados nos muestran como hay una correlación directa entre la disminución de la actividad de la Aco1p, con la respectiva falla en la formación de su centro catalítico Fe/S en las mutantes ISC (*ssq1Δ, isa1Δ, grx5Δ* e *iba57Δ*) y un efecto menos marcado en los transportadores de hierro (*atx1Δ* y *mrs4Δ*). Sin embargo, al analizar la actividad en la mutante *rip1Δ*, no se entiende porque una mutación rio abajo en la CTE llega a disminuir tanto la eficiencia de una proteína que actúa rio arriba y no participa en la formación de centros Fe/S. Ello, mas que aclararnos nos generó mas dudas. De manera que se decidió analizar el funcionamiento de toda la CTE y conocer que producía este efecto. Inicialmente se determinó el potencial de membrana mitocondrial (**Gómez et al., 2014 Fig. 9A**; **Sánchez et al., 2019 Fig. 1D**) para verificar de manera general el estado funcional de la mitocondria. Se resalta nuevamente que las mutantes ISC y los transportadores de hierro citosólico y mitocondrial presentan una disminución o muy bajo nivel de actividad, lo cual era de esperarse en dichas mutantes, sin embargo este efecto se mantenía también en la mutante *rip1Δ*, indicándonos nuevamente la importancia de esta proteína en la actividad y funcionalidad a nivel mitocondrial. Ya que la CTE funciona de manera secuencial en el transporte de los electrones,

procedimos a analizar la actividad de cada complejo respiratorio de forma individual para relacionarlo con la disfunción de cada mutante ISC y compararlo con las mutantes de la misma CTE como controles positivos para cada complejo de manera independiente. Para ello se aislaron mitocondrias mediante centrifugaciones diferenciales y se medió la actividad adicionando sustratos e inhibidores específicos (**Gómez et al., 2014 Fig. 9B-F**; **Sánchez et al., 2019 Fig. 1E-H**). Como era de esperarse las mutantes ISC mostraron una baja o nula actividad en todos los complejos analizados, indicando que la falla en el ensamble de centros Fe/S afecta la función catalítica de las proteínas blanco en la CTE. Lo importante a destacar, es que la mutante e *iba57Δ* presenta una nula actividad del complejo III, donde no se había demostrado su participación directa en el ensamble de centros 2Fe-2S (característico de Rip1p – CIII), pero si de centros 4Fe-4S. Ello se corroboró también, midiendo los niveles de consumo de oxígeno en todas las mutantes estudiadas, con la finalidad de relacionar la actividad de la CTE y la respuesta antioxidante de manera conjunta (**Gómez et al., 2014 Fig. 8**; **Sánchez et al., 2019 Fig. 1A-C**), ya que cuando existe una sobreactivación de estos sistemas de respuesta aparte del consumo normal de O_2 puede llegar a ver una ligera producción del mismo, debido a la actividad de la Superoxido Dismutasa (SOD), mostrando niveles negativos, lo que representa un aumento del estrés oxidativo en presencia de agentes oxidantes o al bloquear el flujo de electrones directamente en el Complejo III.

Se ha propuesto que la oxidación bifurcada del ubiquinol en el complejo III se produce por dos mecanismos diferentes. El primero es un mecanismo secuencial, donde un electrón se transfiere primero a la proteína Rip1p de alto potencial. Esta reacción da como resultado que el electrón restante, ahora presente como una semiquinona inestable (Q•), se transfiera al hemo b_L y luego al hemo b_H. El segundo modelo propone un modelo mas refinado en el que la oxidación de ubiquinol se produce por un mecanismo concertado en el que los dos electrones se donan simultáneamente a la proteína de Rip1P y al hemo b_L **[Trumpower, 2002]**. El citocromo b_L reduce inmediatamente el citocromo b_H, que luego reduce la ubiquinona a la semiquinona en el sitio Qi. La transferencia de electrones de los hemos b_L a b_H también da como resultado un cambio conformacional que facilita el movimiento de la proteína ISP entre los citocromos *b* y c_1 **[Covian y Trumpower, 2008]**, evitando así la formación del radical semiquinona, el cual podría ser también una fuente de ERO permitiendo una mejor transferencia de los electrones.

Si bien los resultados anteriores se enfocaron en determinar los punto clave en la disfunción del sistema ISC sobre la funcionalidad de la CTE de manera individual (CII, CIII, CIV), debemos recordar que los complejos respiratorios se encuentran formando distintas asociaciones (SC) **[Schägger y Pfeiffer, 2000; Schägger y Pfeiffer, 2001; Genova y Lenaz, 2014]**. Por lo cual continuamos con el análisis de formación de SC, mediante BN-PAGE para determinar si las mutaciones del sistema ISC también afectan el ensamble de estas superestructuras, alterando así la eficiencia de la CTE (**Gómez et al., 2014 Fig. 7**; **Sánchez et al., 2019 Fig. 3A-B**). Los resultados de las electroforesis así como la densitomería de las bandas, nos indican una fuerte disminución en la formación de SC III_2-IV_2 y III_2-IV_1 (recordemos que las levaduras carecen de complejo I en el Respirasoma) en las mutantes del sistema ISC (*ssq1Δ, isa1Δ, grx5Δ* e *iba57Δ*). Ello nos indica que la biogénesis de centros Fe/S es determinante no solo para la inserción de cofactores en las correspondientes apoproteínas, sino también para establecer las asociaciones correspondientes entre los complejos respiratorios, necesarias para llevar a cabo su función catalítica. La maduración del citocromo *b* (Cob) es el factor de nucleación en la biogénesis del complejo III en eucariontes, del mismo modo la hemilación de Cob es necesaria para la maduración posterior del subcomplejo Cob/Qcr7/Qcr8 mediante la adición de las subunidades Cor1, Cor2, Cyt1 y Qcr9 **[Crivellone et al., 1988; Zara et al., 2009]**. El ultimo paso en la maduración del complejo III incluye la adición de Rip1 (que contienen un centro 2Fe-2S) y Qcr10. Como Rip1 contiene el centro 2Fe-2S que realiza la transferencia de electrones a la subunidad Cyt1 del citocromo c_1, el intermediario tardío (sin Rip1) carece de función. La adición de Rip1 y Qcr10 permite la asociación con el complejo IV (CcO), formando el supercomplejo III_2IV_2 en levaduras **[Zara et al., 2009; Cruciat et al., 2000]**.

Se han propuesto las siguientes ventajas en la formación de estos SC multienzimáticos sobre las actividades individuales de cada complejo, entre las que destacan: la canalización del sustrato, la potenciación catalítica, el evitar la formación de intermedios reactivos y una rápida transferencia intramolecular. La canalización del sustrato permite dirigir un intermediario a una enzima específica en

lugar de permitir la competencia de otras enzimas; así, el uso de una molécula de sustrato localizado (ubiquinol y citocromo *c*) hace que una reacción sea independiente de las propiedades globales de un grupo de sustratos. De este modo, la existencia de los supercomplejos en la CTE proporciona una base estructural para la canalización del sustrato y la potenciación catalítica mediante la reducción del tiempo de difusión, de manera que la canalización del sustrato daría la mayor ventaja a la CTE en bajas concentraciones de sustrato. De forma que las interacciones de los complejos respiratorios representan un modelo en forma de red de complejos denominado "Respirasoma".

En conjunto, la serie de resultados anteriores nos reflejan claramente la importancia del sistema ISC en el ensamble y actividad de la CTE, pero aún quedaba la duda sobre la falta específica de actividad en el Complejo III de la mutante *iba57Δ*, de la cual no se ha establecido relación directa en el ensamble específico de centros 2Fe-2S característico de la proteína Rip1 del complejo III y cuyos resultados de ERO, Fe^{2+}, niveles de centros Fe/S y actividad de la CTE son muy similares o en su defecto iguales para ambas mutantes (*iba57Δ y rip1Δ*). Ello nos desconcertó, pues en la literatura no existía ningún reporte de interacción entre ambas proteínas y nuestros datos mostraban una clara relación sinérgica. Para disipar esa duda, se tomo la decisión de identificar con anticuerpos específicos la presencia de la proteína Rip1 en la serie de mutantes ISC y poder descartar de manera específica su participación o no en la biogénesis del centro Fe/S de la proteína Rip1. Los resultados fueron concluyentes y logramos demostrar que efectivamente la proteína Iba57 participa en el ensamble del centro 2Fe-2S de Rip1 (**Gómez et al., 2014 Fig. 7C**; **Gómez-Gallardo et al., 2018 Fig. 1E; Sánchez et al., 2019 Fig. 3F**). Ante este resultado tan importante, no podíamos dejar de lado la implicación que ello tenía, pues sería la evidencia clave de la participación de Iba57 en la inserción específica del centro 2Fe-2S en la proteína Rip1. Cuyo fenotipo característico es tan significativo que permite la correcta formación de los SC III_2-IV_2 y III_2-IV_1. Para corroborar este resultado y descartar que fuera un efecto por la alta generación de ERO o los altos niveles de Fe^{2+} que presentan ambas mutantes (*iba57Δ y rip1Δ*); pudiendo esto afectar las formación de SC. Se determinó la expresión de Rip1 en la batería de mutantes ISC, así como de otro par de proteínas de la CTE (Cox2, Cox3) específicas del complejo IV, ya que la formación de los SC III_2-IV_1 y III_2-IV_2 (trímero y tetrámero) se lleva a cabo de manera simultanea entre subunidades del Complejo III y IV (**Gómez et al., 2014 Fig. 7C**; **Sánchez et al., 2019 Fig. 4 y 6**). Los resultados mostraron que Cox3 se expresa de manera constitutiva sin importar la mutación del Sistema ISC o en la CTE, de manera que ésta proteína mitocondrial clave en el complejo iniciador de la formación del complejo IV, se ensambla correctamente en el trímero y el tetrámero (III_2-IV_1 y III_2-IV_2) respectivamente.

Por último y no menos importante, analizamos la presencia y funcionalidad de los grupos Hemo, los cuales al igual que los centros Fe/S, dependen del hierro para su función catalítica. Ello nos permitirá entender de mejor manera como es que se afecta la función de la CTE debido a que 4 distintos tipos de citocromos participan directamente en la transferencia de electrones en los diferentes complejos respiratorios (CII, CIII y CIV)(**Fig. 2; Sánchez et al., 2019 Fig. 5**). Las espectroscopias muestran claramente una fuerte disminución, tanto en la cantidad como la funcionalidad de los citocromos en las mutantes ISC y CTE analizadas. Concluyendo así, la importancia del sistema ISC en la correcta formación de centros Fe/S, permitiendo su adecuado ensamble en las correspondientes apoproteínas (Fe/S y grupos Hemo), que en consecuencia favorecen la formación de SC, de manera que existe un correcto control de los niveles de Fe^{2+} intramitocondriales, evitando así la generación excesiva de ERO.

Las proteínas con cofactores Hemo están involucradas en una variedad de vías metabólicas esenciales, y la deficiencia de estos es letal **[Schultz et al., 2010; Sinclair y Hamza, 2015; Yuan et al., 2013]**. Lo mismo ocurre con la mayoría de los 17 miembros conocidos del sistema ISC, ya que son esenciales para la viabilidad celular, y las mutaciones en estos genes se asocian con enfermedades recesivas y fenotipos relacionados con daños neurodegenerativos, hematológicos y metabólicos **[Beilschmidt y Puccio, 2014; Rouault, 2012; Stehling y Lill, 2013]**. Además, los defectos en los genes implicados en el transporte de hierro mitocondrial causan enfermedades recesivas con fenotipos hematológicos **[Richardson et al., 2010; Shaw et al., 2006; Wang et al., 2011]**. En *S. cerevisiae* hay una clara correlación entre los niveles de expresión de los transportadores mitocondriales (Mrs3 y Mrs4) con los niveles de hierro mitocondrial, la eficacia de la síntesis de grupos Hemo y Fe/S, y el ensamble de los suspercomplejos en la CTE **[Foury y Roganti, 2002; Muhlenhoff et al., 2003; Zhang et al., 2005; Zhang et al., 2006; Gómez et al., 2014]**. Las mitocondrias son orgánulos

clave para modular y cambiar el metabolismo optimizando el rendimiento de la célula. La reorganización de los SCs en la membrana mitocondrial interna en respuesta a diferentes estímulos, fuentes de carbono o condiciones de estrés, está revelando un mecanismo adaptativo importante y novedoso controlado por las mitocondrias.

9. CONCLUSIÓN GENERAL

Los resultados indican que el sistema **ISC** es necesario para mantener la homeostasis del **Fe**, regular la generación de **ERO**, mantener la funcionalidad de los complejos respiratorios y el ensamblaje del grupos Hemo (citocromos *a*, *b*, *c y* c_1) en la **CTE**.

10. REFERENCIAS

Acín-Pérez, R., Fernández-Silva, P., Peleato, M. L., Pérez-Martos, A., & Enriquez, J. A. (2008). Respiratory active mitochondrial supercomplexes. *Molecular cell*, *32*(4), 529-539.

Acín-Pérez, R., & Enriquez, J. A. (2014). The function of the respiratory supercomplexes: the plasticity model. *Biochimica et Biophysica Acta (BBA)-Bioenergetics*, *1837*(4), 444-450.

Althoff, T., Mills, D. J., Popot, J. L., & Kühlbrandt, W. (2011). Arrangement of electron transport chain components in bovine mitochondrial supercomplex I1III2IV1. *The EMBO journal*, *30*(22), 4652-4664.

Antonini, E. (1971). Hemoglobin and Myoglobin in their Reactions with Ligands. *Frontiers of biology*, *21*, 27-31.

Arnone, A. (1974). Mechanism of action of hemoglobin. *Annual review of medicine*, *25*(1), 123-130.

Baracca, A., Chiaradonna, F., Sgarbi, G., Solaini, G., Alberghina, L., & Lenaz, G. (2010). Mitochondrial Complex I decrease is responsible for bioenergetic dysfunction in K-ras transformed cells. *Biochimica et Biophysica Acta (BBA)-Bioenergetics*, *1797*(2), 314-323.

Barros, M. H., Nobrega, F. G., & Tzagoloff, A. (2002). Mitochondrial Ferredoxin Is Required for Heme A Synthesis inSaccharomyces cerevisiae. *Journal of Biological Chemistry*, *277*(12), 9997-10002.

Barupala, D. P., Dzul, S. P., Riggs-Gelasco, P. J., & Stemmler, T. L. (2016). Synthesis, delivery and regulation of eukaryotic heme and Fe–S cluster cofactors. *Archives of biochemistry and biophysics*, *592*, 60-75.

Beilschmidt, L. K., & Puccio, H. M. (2014). Mammalian Fe–S cluster biogenesis and its implication in disease. *Biochimie*, *100*, 48-60.

Benard, G., Bellance, N., Jose, C., & Rossignol, R. (2011). Relationships between mitochondrial dynamics and bioenergetics. In *Mitochondrial Dynamics and Neurodegeneration* (pp. 47-68). Springer, Dordrecht.

Benn, D. E., Robinson, B. G., & Clifton-Bligh, R. J. (2015). 15 YEARS OF PARAGANGLIOMA: Clinical manifestations of paraganglioma syndromes types 1–5. *Endocrine-related cancer*, *22*(4), T91-T103.

Boukhalfa, H., & Crumbliss, A. L. (2002). Chemical aspects of siderophore mediated iron transport. *Biometals*, *15*(4), 325-339.

Boumans, H., Grivell, L. A., & Berden, J. A. (1998). The respiratory chain in yeast behaves as a single functional unit. *Journal of Biological Chemistry*, *273*(9), 4872-4877.

Bratic, A., & Larsson, N. G. (2013). The role of mitochondria in aging. *The Journal of clinical investigation*, *123*(3), 951-957.

Burke, P. V., Raitt, D. C., Allen, L. A., Kellogg, E. A., & Poyton, R. O. (1997). Effects of oxygen concentration on the expression of cytochrome c and cytochrome c oxidase genes in yeast. *Journal of Biological Chemistry*, *272*(23), 14705-14712.

Cameron, J. M., Janer, A., Levandovskiy, V., MacKay, N., Rouault, T. A., Tong, W. H., ... & Robinson, B. H. (2011). Mutations in iron-sulfur cluster scaffold genes NFU1 and BOLA3 cause a fatal deficiency of multiple respiratory chain and 2-oxoacid dehydrogenase enzymes. *The American Journal of Human Genetics*, *89*(4), 486-495.

Castells-Roca, L., Mühlenhoff, U., Lill, R., Herrero, E., & Bellí, G. (2011). The oxidative stress response in yeast cells involves changes in the stability of Aft1 regulon mRNAs. *Molecular microbiology*, *81*(1), 232-248.

Chaban, Y., Boekema, E. J., & Dudkina, N. V. (2014). Structures of mitochondrial oxidative phosphorylation supercomplexes and mechanisms for their stabilisation. *Biochimica et Biophysica Acta (BBA)-Bioenergetics*, *1837*(4), 418-426.

Chance, B., & Williams, G. R. (1955a). A method for the localization of sites for oxidative phosphorylation. *Nature*, *176*(4475), 250.

Cipolat, S., de Brito, O. M., Dal Zilio, B., & Scorrano, L. (2004). OPA1 requires mitofusin 1 to promote mitochondrial fusion. *Proceedings of the National Academy of Sciences*, *101*(45), 15927-15932.

Claypool, S. M., Oktay, Y., Boontheung, P., Loo, J. A., & Koehler, C. M. (2008). Cardiolipin defines the interactome of the major ADP/ATP carrier protein of the mitochondrial inner membrane. *J Cell Biol*, *182*(5), 937-950.

Courel, M., Lallet, S., Camadro, J. M., & Blaiseau, P. L. (2005). Direct activation of genes involved in intracellular iron use by the yeast iron-responsive transcription factor Aft2 without its paralog Aft1. *Molecular and cellular biology*, *25*(15), 6760-6771.

Covian, R., & Trumpower, B. L. (2008). Regulatory interactions in the dimeric cytochrome bc1 complex: the advantages of being a twin. *Biochimica Et Biophysica Acta (BBA)-Bioenergetics*, *1777*(9), 1079-1091.

Crichton, R., Crichton, R. R., & Boelaert, J. R. (2001). *Inorganic biochemistry of iron metabolism: from molecular mechanisms to clinical consequences*. John Wiley & Sons.

Crisp, R. J., Pollington, A., Galea, C., Jaron, S., Yamaguchi-Iwai, Y., & Kaplan, J. (2003). Inhibition of heme biosynthesis prevents transcription of iron uptake genes in yeast. *Journal of Biological Chemistry*, *278*(46), 45499-45506.

Crivellone, M. D., Wu, M. A., & Tzagoloff, A. (1988). Assembly of the mitochondrial membrane system. Analysis of structural mutants of the yeast coenzyme QH2-cytochrome c reductase complex. *Journal of Biological Chemistry*, *263*(28), 14323-14333.

Cruciat, C. M., Brunner, S., Baumann, F., Neupert, W., & Stuart, R. A. (2000). The Cytochrome bc 1 and Cytochromec Oxidase Complexes Associate to Form a Single Supracomplex in Yeast Mitochondria. *Journal of Biological Chemistry*, *275*(24), 18093-18098.

Dixon, S. J., & Stockwell, B. R. (2014). The role of iron and reactive oxygen species in cell death. *Nature chemical biology*, *10*(1), 9.

Dixon, S. J., Lemberg, K. M., Lamprecht, M. R., Skouta, R., Zaitsev, E. M., Gleason, C. E., ... & Morrison III, B. (2012). Ferroptosis: an iron-dependent form of nonapoptotic cell death. *Cell*, *149*(5), 1060-1072.

Dutkiewicz, R., Schilke, B., Knieszner, H., Walter, W., Craig, E. A., & Marszalek, J. (2003). Ssq1, a mitochondrial Hsp70 involved in iron-sulfur (Fe/S) center biogenesis Similarities to and differences from its bacterial counterpart. *Journal of Biological Chemistry*, *278*(32), 29719-29727.

Echtay, K. S., Roussel, D., St-Pierre, J., Jekabsons, M. B., Cadenas, S., Stuart, J. A., ... & Clapham, J. C. (2002). Superoxide activates mitochondrial uncoupling proteins. *Nature*, *415*(6867), 96.

Eisenstein, R. S. (2000). Iron regulatory proteins and the molecular control of mammalian iron metabolism. *Annual review of nutrition*, *20*(1), 627-662.

Fenna, R., Zeng, J., & Davey, C. (1995). Structure of the green heme in myeloperoxidase. *Archives of biochemistry and biophysics*, *316*(1), 653-656.

Foury, F., & Roganti, T. (2002). Deletion of the mitochondrial carrier genes MRS3 andMRS4 suppresses mitochondrial iron accumulation in a yeast frataxin-deficient strain. *Journal of Biological Chemistry*, *277*(27), 24475-24483.

Frenzel, M., Rommelspacher, H., Sugawa, M. D., & Dencher, N. A. (2010). Ageing alters the supramolecular architecture of OxPhos complexes in rat brain cortex. *Experimental gerontology*, *45*(7-8), 563-572.

Froschauer, E. M., Schweyen, R. J., & Wiesenberger, G. (2009). The yeast mitochondrial carrier proteins Mrs3p/Mrs4p mediate iron transport across the inner mitochondrial membrane. *Biochimica et Biophysica Acta (BBA)-Biomembranes*, *1788*(5), 1044-1050.

Fry, M., & Green, D. E. (1980). Energized cation transport by complex III (ubiquinone-cytochrome C reductase). *Biochemical and biophysical research communications*, *97*(3), 852-859.

Fry, M., & Green, D. E. (1981). Cardiolipin requirement for electron transfer in complex I and III of the mitochondrial respiratory chain. *Journal of Biological Chemistry*, *256*(4), 1874-1880.

Galluzzi, L., Kepp, O., Trojel-Hansen, C., & Kroemer, G. (2012). Mitochondrial control of cellular life, stress, and death. *Circulation research*, *111*(9), 1198-1207.

Gelling, C., Dawes, I. W., Richhardt, N., Lill, R., & Mühlenhoff, U. (2008). Mitochondrial Iba57p is required for Fe/S cluster formation on aconitase and activation of radical SAM enzymes. *Molecular and cellular biology*, *28*(5), 1851-1861.

Genova, M. L., & Lenaz, G. (2014). Functional role of mitochondrial respiratory supercomplexes. *Biochimica et Biophysica Acta (BBA)-Bioenergetics*, *1837*(4), 427-443.

George, S. J., Armstrong, F. A., Hatchikian, E. C., & Thomson, A. J. (1989). Electrochemical and spectroscopic characterization of the conversion of the 7Fe into the 8Fe form of ferredoxin III from Desulfovibrio africanus. Identification of a [4Fe–4S] cluster with one non-cysteine ligand. *Biochemical Journal*, *264*(1), 275-284.

Gómez, L. A., Monette, J. S., Chavez, J. D., Maier, C. S., & Hagen, T. M. (2009). Supercomplexes of the mitochondrial electron transport chain decline in the aging rat heart. *Archives of biochemistry and biophysics*, *490*(1), 30-35.

Gómez, L. A., & Hagen, T. M. (2012). Age-related decline in mitochondrial bioenergetics: does supercomplex destabilization determine lower oxidative capacity and higher superoxide production?. In *Seminars in cell & developmental biology* (Vol. 23, No. 7, pp. 758-767). Academic Press.

Gómez, M., Pérez-Gallardo, R. V., Sánchez, L. A., Díaz-Pérez, A. L., Cortés-Rojo, C., Carmen, V. M., ... & Rodríguez-Zavala, J. S. (2014). Malfunctioning of the iron–sulfur cluster assembly machinery in Saccharomyces cerevisiae produces oxidative stress via an iron-dependent mechanism, causing dysfunction in respiratory complexes. *PloS one*, *9*(10), e111585.

Gomez-Gallardo, M., Sánchez, L. A., Díaz-Pérez, A. L., Cortés-Rojo, C., & Campos-García, J. (2018). Data on the role of iba57p in free Fe2+ release and O2·− generation in Saccharomyces cerevisiae. *Data in Brief*, *18*, 198-202.

Gray, H. B., & Winkler, J. R. (1996). Electron transfer in proteins. *Annual review of biochemistry*, *65*(1), 537-561.

Green, D. E., & Tzagoloff, A. (1966). The mitochondrial electron transfer chain. *Archives of biochemistry and biophysics*, *116*, 293-304.

Griparic, L., & van der Bliek, A. M. (2001). The many shapes of mitochondrial membranes. *Traffic*, *2*(4), 235-244.

Hackenbrock, C. R., Chazotte, B., & Gupte, S. S. (1986). The random collision model and a critical assessment of diffusion and collision in mitochondrial electron transport. *Journal of bioenergetics and biomembranes*, *18*(5), 331-368.

Hadzhieva, M., Kirches, E., & Mawrin, C. (2014). Iron metabolism and the role of iron in neurodegenerative disorders. *Neuropathology and applied neurobiology*, *40*(3), 240-257.

Hatefi, Y., Haavik, A. G., Fowler, L. R., & Griffiths, D. E. (1962). Studies on the electron transfer system XLII. Reconstitution of the electron transfer system. *Journal of Biological Chemistry*, *237*(8), 2661-2669.

Heeney, M. M., & Andrews, N. C. (2004). Iron homeostasis and inherited iron overload disorders: an overview. *Hematology/Oncology Clinics*, *18*(6), 1379-1403.

Hodge, M. R., Kim, G., Singh, K., & Cumsky, M. G. (1989). Inverse regulation of the yeast COX5 genes by oxygen and heme. *Molecular and cellular biology*, *9*(5), 1958-1964.

Hoffmann, B., Uzarska, M. A., Berndt, C., Godoy, J. R., Haunhorst, P., Lillig, C. H., ... & Mühlenhoff, U. (2011). The multidomain thioredoxin-monothiol glutaredoxins represent a distinct functional group. *Antioxidants & redox signaling*, *15*(1), 19-30.

Hu, R. G., Wang, H., Xia, Z., & Varshavsky, A. (2008). The N-end rule pathway is a sensor of heme. *Proceedings of the National Academy of Sciences*, *105*(1), 76-81.

Hu, Y., Lu, W., Chen, G., Wang, P., Chen, Z., Zhou, Y., ... & Chiao, P. J. (2012). K-ras G12V transformation leads to mitochondrial dysfunction and a metabolic switch from oxidative phosphorylation to glycolysis. *Cell research*, *22*(2), 399.

Hüttemann, M., Kadenbach, B., & Grossman, L. I. (2001). Mammalian subunit IV isoforms of cytochrome c oxidase. *Gene*, *267*(1), 111-123.

Hüttemann, M., Lee, I., Liu, J., & Grossman, L. I. (2007). Transcription of mammalian cytochrome c oxidase subunit IV-2 is controlled by a novel conserved oxygen responsive element. *The FEBS journal*, *274*(21), 5737-5748.

Janssen, S., Schäfer, G., Anemüller, S., & Moll, R. (1997). A succinate dehydrogenase with novel structure and properties from the hyperthermophilic archaeon Sulfolobus acidocaldarius: genetic and biophysical characterization. *Journal of bacteriology*, *179*(17), 5560-5569.

Johnson, D. C., Dean, D. R., Smith, A. D., & Johnson, M. K. (2005). Structure, function, and formation of biological iron-sulfur clusters. *Annu. Rev. Biochem.*, *74*, 247-281.

Johnson, M. K., & Smith, A. D. (2011). Iron–sulfur proteins. *Encyclopedia of Inorganic and Bioinorganic Chemistry*.

Khalimonchuk, O. and Rodel, G. 2005. Biogenesis of cytochrome c oxidase. Mitochondrion 5:363–388.

Kaplan, C. D., & Kaplan, J. (2009). Iron acquisition and transcriptional regulation. *Chemical reviews*, *109*(10), 4536-4552.

Keilin, D. (1925). On cytochrome, a respiratory pigment, common to animals, yeast, and higher plants. *Proceedings of the Royal Society of London. Series B, Containing Papers of a Biological Character*, *98*(690), 312-339.

Keilin, D., & Hartree, E. F. (1947). Activity of the cytochrome system in heart muscle preparations. *Biochemical Journal*, *41*(4), 500.

Killian, J. A., & de Kruijff, B. (2004). Nonbilayer lipids affect peripheral and integral membrane proteins via changes in the lateral pressure profile. *Biochimica et Biophysica Acta (BBA)-Biomembranes*, *1666*(1-2), 275-288.

Kim, H. J., Khalimonchuk, O., Smith, P. M., & Winge, D. R. (2012). Structure, function, and assembly of heme centers in mitochondrial respiratory complexes. *Biochimica et Biophysica Acta (BBA)-Molecular Cell Research*, *1823*(9), 1604-1616.

Kollberg, G., Tulinius, M., Melberg, A., Darin, N., Andersen, O., Holmgren, D., ... & Holme, E. (2009). Clinical manifestation and a new ISCU mutation in iron–sulphur cluster deficiency myopathy. *Brain*, *132*(8), 2170-2179.

Kröger, A., Klingenberg, M., & Schweidler, S. (1973a). Further evidence for the pool function of ubiquinone as derived from the inhibition of the electron transport by antimycin. *European journal of biochemistry*, *39*(2), 313-323.

Kröger, A., & Klingenberg, M. (1973b). The kinetics of the redox reactions of ubiquinone related to the electron-transport activity in the respiratory chain. *European journal of biochemistry*, *34*(2), 358-368.

Lancaster, C. R. D. (2002). Succinate: quinone oxidoreductases: an overview. *Biochim. Biophys. Acta* 1553 (2002) 1–6.

Lapuente-Brun, E., Moreno-Loshuertos, R., Acín-Pérez, R., Latorre-Pellicer, A., Colás, C., Balsa, E., ... & Navas, P. (2013). Supercomplex assembly determines electron flux in the mitochondrial electron transport chain. *Science*, *340*(6140), 1567-1570.

Lemire, B. D., & Oyedotun, K. S. (2002). The Saccharomyces cerevisiae mitochondrial succinate: ubiquinone oxidoreductase. *Biochimica et Biophysica Acta (BBA)-Bioenergetics*, *1553*(1-2), 102-116.

Lemos, R. S., Fernandes, A. S., Pereira, M. M., Gomes, C. M., & Teixeira, M. (2002). Quinol: fumarate oxidoreductases and succinate: quinone oxidoreductases: phylogenetic relationships, metal centres and membrane attachment. *Biochimica et Biophysica Acta (BBA)-Bioenergetics*, *1553*(1-2), 158-170.

Lenaz, G., & Genova, M. L. (2007). Kinetics of integrated electron transfer in the mitochondrial respiratory chain: random collisions vs. solid state electron channeling. *American Journal of Physiology-Cell Physiology*, *292*(4), C1221-C1239.

Lenaz, G., & Genova, M. L. (2010). Structure and organization of mitochondrial respiratory complexes: a new understanding of an old subject. *Antioxidants & redox signaling*, *12*(8), 961-1008.

Liesa, M., & Shirihai, O. S. (2013). Mitochondrial dynamics in the regulation of nutrient utilization and energy expenditure. *Cell metabolism*, *17*(4), 491-506.

Lill, R., & Mühlenhoff, U. (2006). Iron-sulfur protein biogenesis in eukaryotes: components and mechanisms. *Annu. Rev. Cell Dev. Biol.*, *22*, 457-486.

Lill, R. (2009). Function and biogenesis of iron–sulphur proteins. *Nature*, *460*(7257), 831.

Lill, R., Hoffmann, B., Molik, S., Pierik, A. J., Rietzschel, N., Stehling, O., ... & Mühlenhoff, U. (2012). The role of mitochondria in cellular iron–sulfur protein biogenesis and iron metabolism. *Biochimica et Biophysica Acta (BBA)-Molecular Cell Research*, *1823*(9), 1491-1508.

Lill, R., Srinivasan, V., & Mühlenhoff, U. (2014). The role of mitochondria in cytosolic-nuclear iron–sulfur protein biogenesis and in cellular iron regulation. *Current opinion in microbiology*, *22*, 111-119.

Lill, R., Dutkiewicz, R., Freibert, S. A., Heidenreich, T., Mascarenhas, J., Netz, D. J., ... & Srinivasan, V. (2015). The role of mitochondria and the CIA machinery in the maturation of cytosolic and nuclear iron–sulfur proteins. *European journal of cell biology*, *94*(7-9), 280-291.

Liu, Z., & Butow, R. A. (2006). Mitochondrial retrograde signaling. *Annu. Rev. Genet.*, *40*, 159-185.

Lyons, T. J., & Eide, D. J. (2007). Transport and storage of metal ions in biology. *Biological inorganic chemistry: Structure and reactivity*, *57*, 77.

Maklashina, E., Rajagukguk, S., McIntire, W. S., & Cecchini, G. (2010). Mutation of the heme axial ligand of Escherichia coli succinate–quinone reductase: Implications for heme ligation in mitochondrial complex II from yeast. *Biochimica et Biophysica Acta (BBA)-Bioenergetics*, *1797*(6-7), 747-754.

Marchi, S., Giorgi, C., Suski, J. M., Agnoletto, C., Bononi, A., Bonora, M., ... & Rimessi, A. (2012). Mitochondria-ros crosstalk in the control of cell death and aging. *Journal of signal transduction*, *2012*.

McBride, H., & Scorrano, L. (2013). Mitochondrial dynamics and physiology. *Biochimica et biophysica acta*, *1833*(1), 148.

McKenzie, M., Lazarou, M., Thorburn, D. R., & Ryan, M. T. (2006). Mitochondrial respiratory chain supercomplexes are destabilized in Barth Syndrome patients. *Journal of molecular biology*, *361*(3), 462-469.

Mense, S. M., & Zhang, L. (2006). Heme: a versatile signaling molecule controlling the activities of diverse regulators ranging from transcription factors to MAP kinases. *Cell research*, *16*(8), 681.

Mick, D. U., Fox, T. D., & Rehling, P. (2011). Inventory control: cytochrome c oxidase assembly regulates mitochondrial translation. *Nature reviews Molecular cell biology*, *12*(1), 14.

Mileykovskaya, E., Penczek, P. A., Fang, J., Mallampalli, V. K., Sparagna, G. C., & Dowhan, W. (2012). Arrangement of the respiratory chain complexes in Saccharomyces cerevisiae supercomplex III2IV2 revealed by single particle cryo-electron microscopy. *Journal of Biological Chemistry*, *287*(27), 23095-23103.

Moreno-Loshuertos, R., Acín-Pérez, R., Fernández-Silva, P., Movilla, N., Pérez-Martos, A., de Cordoba, S. R., ... & Enríquez, J. A. (2006). Differences in reactive oxygen species production explain the phenotypes associated with common mouse mitochondrial DNA variants. *Nature genetics*, *38*(11), 1261.

Mueller, S., & Pantopoulos, K. (2002). [32] Activation of iron regulatory protein-1 by oxidative stress. In *Methods in enzymology* (Vol. 348, pp. 324-337). Academic Press.

Mühlenhoff, U., Stadler, J. A., Richhardt, N., Seubert, A., Eickhorst, T., Schweyen, R. J., ... & Wiesenberger, G. (2003). A specific role of the yeast mitochondrial carriers MRS3/4p in mitochondrial iron acquisition under iron-limiting conditions. *Journal of Biological Chemistry*, *278*(42), 40612-40620.

Mühlenhoff, U., Molik, S., Godoy, J. R., Uzarska, M. A., Richter, N., Seubert, A., ... & Lillig, C. H. (2010). Cytosolic monothiol glutaredoxins function in intracellular iron sensing and trafficking via their bound iron-sulfur cluster. *Cell metabolism*, *12*(4), 373-385.

Mühlenhoff, U., Richter, N., Pines, O., Pierik, A. J., & Lill, R. (2011). Specialized function of yeast Isa1 and Isa2 proteins in the maturation of mitochondrial [4Fe-4S] proteins. *Journal of Biological Chemistry*, *286*(48), 41205-41216.

Mühlenhoff, U., Hoffmann, B., Richter, N., Rietzschel, N., Spantgar, F., Stehling, O., ... & Lill, R. (2015). Compartmentalization of iron between mitochondria and the cytosol and its regulation. *European journal of cell biology*, *94*(7-9), 292-308.

Muñoz, M., García-Erce, J. A., & Remacha, Á. F. (2011). Disorders of iron metabolism. Part II: iron deficiency and iron overload. *Journal of clinical pathology*, *64*(4), 287-296.

Narendra, D., Tanaka, A., Suen, D. F., & Youle, R. J. (2008). Parkin is recruited selectively to impaired mitochondria and promotes their autophagy. *The Journal of cell biology*, *183*(5), 795-803.

Netz, D. J., Mascarenhas, J., Stehling, O., Pierik, A. J., & Lill, R. (2014). Maturation of cytosolic and nuclear iron–sulfur proteins. *Trends in cell biology*, *24*(5), 303-312.

Nobrega, M. P., Nobrega, F. G., & Tzagoloff, A. (1990). COX10 codes for a protein homologous to the ORF1 product of Paracoccus denitrificans and is required for the synthesis of yeast cytochrome oxidase. *Journal of Biological Chemistry*, *265*(24), 14220-14226.

Ohshima, K., Montermini, L., Wells, R. D., & Pandolfo, M. (1998). Inhibitory Effects of Expanded GAA· TTC Triplet Repeats from Intron I of the Friedreich Ataxia Gene on Transcription and Replicationin Vivo. *Journal of Biological Chemistry*, *273*(23), 14588-14595.

Osman, C., Voelker, D. R., & Langer, T. (2011). Making heads or tails of phospholipids in mitochondria. *The Journal of cell biology*, *192*(1), 7-16.

Ovádi, J. (1991). Physiological significance of metabolic channelling. *Journal of theoretical biology*, *152*(1), 1-22.

Oyedotun, K. S., Yau, P. F., & Lemire, B. D. (2004). Identification of the heme axial ligands in the cytochrome b562 of the Saccharomyces cerevisiae succinate dehydrogenase. *Journal of Biological Chemistry*, *279*(10), 9432-9439.

Oyedotun, K. S., Sit, C. S., & Lemire, B. D. (2007). The Saccharomyces cerevisiae succinate dehydrogenase does not require heme for ubiquinone reduction. *Biochimica et Biophysica Acta (BBA)-Bioenergetics*, *1767*(12), 1436-1445.

Papanikolaou, G., Tzilianos, M., Christakis, J. I., Bogdanos, D., Tsimirika, K., MacFarlane, J., ... & Nemeth, E. (2005). Hepcidin in iron overload disorders. *Blood*, *105*(10), 4103-4105.

Paradies, G., Petrosillo, G., Pistolese, M., & Ruggiero, F. M. (2000). The effect of reactive oxygen species generated from the mitochondrial electron transport chain on the cytochrome c oxidase activity and on the cardiolipin content in bovine heart submitochondrial particles. *FEBS letters*, *466*(2-3), 323-326.

Paul, V. D., & Lill, R. (2015). Biogenesis of cytosolic and nuclear iron–sulfur proteins and their role in genome stability. *Biochimica Et Biophysica Acta (BBA)-Molecular Cell Research*, *1853*(6), 1528-1539.

Pecina, P., Houst kova, H., Zeman, J., & Houstek, J. (2004). Genetic defects of cytochrome c oxidase assembly. *Physiological research*, *53*, S213-224.

Perez-Gallardo, R. V., Briones, L. S., Díaz-Pérez, A. L., Gutiérrez, S., Rodríguez-Zavala, J. S., & Campos-García, J. (2013). Reactive oxygen species production induced by ethanol in Saccharomyces cerevisiae increases because of a dysfunctional mitochondrial iron–sulfur cluster assembly system. *FEMS yeast research*, *13*(8), 804-819.

Petrosillo, G., Ruggiero, F. M., Di Venosa, N., & Paradies, G. (2003). Decreased complex III activity in mitochondria isolated from rat heart subjected to ischemia and reperfusion: role of reactive oxygen species and cardiolipin. *The FASEB Journal*, *17*(6), 714-716.

Pfeiffer, K., Gohil, V., Stuart, R. A., Hunte, C., Brandt, U., Greenberg, M. L., & Schägger, H. (2003). Cardiolipin stabilizes respiratory chain supercomplexes. *Journal of biological chemistry*, *278*(52), 52873-52880.

Pufahl, R. A., Singer, C. P., Peariso, K. L., Lin, S. J., Schmidt, P. J., Fahrni, C. J., ... & O'Halloran, T. V. (1997). Metal ion chaperone function of the soluble Cu (I) receptor Atx1. *Science*, *278*(5339), 853-856.

Reedy, C. J., & Gibney, B. R. (2004). Heme protein assemblies. *Chemical reviews*, *104*(2), 617-650.

Richardson, D. R., Lane, D. J., Becker, E. M., Huang, M. L. H., Whitnall, M., Rahmanto, Y. S., ... & Ponka, P. (2010). Mitochondrial iron trafficking and the integration of iron metabolism between the mitochondrion and cytosol. *Proceedings of the National Academy of Sciences*, *107*(24), 10775-10782.

Rodgers, K. R. (1999). Heme-based sensors in biological systems. *Current opinion in chemical biology*, *3*(2), 158-167.

Rodriguez-Manzaneque, M. T., Tamarit, J., Bellı, G., Ros, J., & Herrero, E. (2002). Grx5 is a mitochondrial glutaredoxin required for the activity of iron/sulfur enzymes. *Molecular biology of the cell*, *13*(4), 1109-1121.

Rosca, M. G., Vazquez, E. J., Kerner, J., Parland, W., Chandler, M. P., Stanley, W., ... & Hoppel, C. L. (2008). Cardiac mitochondria in heart failure: decrease in respirasomes and oxidative phosphorylation. *Cardiovascular research*, *80*(1), 30-39.

Rosca, M. G., & Hoppel, C. L. (2009). New aspects of impaired mitochondrial function in heart failure. *Journal of bioenergetics and biomembranes*, *41*(2), 107-112.

Rouault, T. A. (2012). Biogenesis of iron-sulfur clusters in mammalian cells: new insights and relevance to human disease. *Disease models & mechanisms*, *5*(2), 155-164.

Rouhier, N., Couturier, J., Johnson, M. K., & Jacquot, J. P. (2010). Glutaredoxins: roles in iron homeostasis. *Trends in biochemical sciences*, *35*(1), 43-52.

Rutherford, J. C., Jaron, S., & Winge, D. R. (2003). Aft1p and Aft2p mediate iron-responsive gene expression in yeast through related promoter elements. *Journal of Biological Chemistry*, *278*(30), 27636-27643.

Rutter, J., Winge, D. R., & Schiffman, J. D. (2010). Succinate dehydrogenase–assembly, regulation and role in human disease. *Mitochondrion*, *10*(4), 393-401.

Saltzgaber-Müller, J., & Schatz, G. (1978). Heme is necessary for the accumulation and assembly of cytochrome c oxidase subunits in Saccharomyces cerevisiae. *Journal of Biological Chemistry*, *253*(1), 305-310.

Sánchez, L. A., Gómez-Gallardo, M., Díaz-Pérez, A. L., Cortés-Rojo, C., & Campos-García, J. (2019). Iba57p participates in maturation of a [2Fe–2S]-cluster Rieske protein and in formation of supercomplexes III/IV of Saccharomyces cerevisiae electron transport chain. *Mitochondrion*, *44*, 75-84.

Schäfer, E., Dencher, N. A., Vonck, J., & Parcej, D. N. (2007). Three-dimensional structure of the respiratory chain supercomplex I1III2IV1 from bovine heart mitochondria. *Biochemistry*, *46*(44), 12579-12585.

Schägger, H., & Pfeiffer, K. (2000). Supercomplexes in the respiratory chains of yeast and mammalian mitochondria. *The EMBO journal*, *19*(8), 1777-1783.

Schägger, H., & Pfeiffer, K. (2001). The ratio of oxidative phosphorylation complexes I–V in bovine heart mitochondria and the composition of respiratory chain supercomplexes. *Journal of Biological Chemistry*, *276*(41), 37861-37867.

Schilke, B., Williams, B., Knieszner, H., Pukszta, S., D'Silva, P., Craig, E. A., & Marszalek, J. (2006). Evolution of mitochondrial chaperones utilized in Fe-S cluster biogenesis. *Current biology*, *16*(16), 1660-1665.

Schon, E. A., DiMauro, S., & Hirano, M. (2012). Human mitochondrial DNA: roles of inherited and somatic mutations. *Nature Reviews Genetics*, *13*(12), 878.

Schultz, I. J., Chen, C., Paw, B. H., & Hamza, I. (2010). Iron and porphyrin trafficking in heme biogenesis. *Journal of Biological Chemistry*, *285*(35), 26753-26759.

Sharma, A. K., Pallesen, L. J., Spang, R. J., & Walden, W. E. (2010). Cytosolic iron-sulfur cluster assembly (CIA) system: factors, mechanism, and relevance to cellular iron regulation. *Journal of Biological Chemistry*, *285*(35), 26745-26751.

Shaw, G. C., Cope, J. J., Li, L., Corson, K., Hersey, C., Ackermann, G. E., ... & Trede, N. S. (2006). Mitoferrin is essential for erythroid iron assimilation. *Nature*, *440*(7080), 96.

Sheftel, A. D., Wilbrecht, C., Stehling, O., Niggemeyer, B., Elsässer, H. P., Mühlenhoff, U., & Lill, R. (2012). The human mitochondrial ISCA1, ISCA2, and IBA57 proteins are required for [4Fe-4S] protein maturation. *Molecular biology of the cell*, *23*(7), 1157-1166.

Shoubridge, E. A. (2001). Cytochrome c oxidase deficiency. *American journal of medical genetics*, *106*(1), 46-52.

Silman, H. I., Rieske, J. S., Lipton, S. H., & Baum, H. (1967). A new protein component of complex III of the mitochondrial electron transfer chain. *Journal of Biological Chemistry*, *242*(21), 4867-4875.

Sinclair, J., & Hamza, I. (2015). Lessons from bloodless worms: heme homeostasis in C. elegans. *Biometals*, *28*(3), 481-489.

Slater, E. C. (2003). Keilin, cytochrome, and the respiratory chain. *Journal of Biological Chemistry*, *278*(19), 16455-16461.

Solans, A., Zambrano, A., & Barrientos, A. (2004). Cytochrome c oxidase deficiency: from yeast to human. *Preclinica*, *2*, 336-348.

Sono, M., Roach, M. P., Coulter, E. D., & Dawson, J. H. (1996). Heme-containing oxygenases. *Chemical reviews*, *96*(7), 2841-2888.

Soto, I. C., Fontanesi, F., Liu, J., & Barrientos, A. (2012). Biogenesis and assembly of eukaryotic cytochrome c oxidase catalytic core. *Biochimica Et Biophysica Acta (BBA)-Bioenergetics*, *1817*(6), 883-897.

Stanley, I. A., Ribeiro, S. M., Giménez-Cassina, A., Norberg, E., & Danial, N. N. (2014). Changing appetites: the adaptive advantages of fuel choice. *Trends in cell biology*, *24*(2), 118-127.

Stehling, O., & Lill, R. (2013). The role of mitochondria in cellular iron–sulfur protein biogenesis: mechanisms, connected processes, and diseases. *Cold Spring Harbor perspectives in biology*, *5*(8), a011312.

Steinrücke, P., & Ludwig, B. (1993). Genetics of Paracoccus denitrificans. *FEMS microbiology reviews*, *10*(1-2), 83-117.

Stroh, A., Anderka, O., Pfeiffer, K., Yagi, T., Finel, M., Ludwig, B., & Schägger, H. (2004). Assembly of respiratory complexes I, III, and IV into NADH oxidase supercomplex stabilizes complex I in Paracoccus denitrificans. *Journal of Biological Chemistry*, *279*(6), 5000-5007.

Sundaresan, M., Yu, Z. X., Ferrans, V. J., Irani, K., & Finkel, T. (1995). Requirement for generation of H2O2 for platelet-derived growth factor signal transduction. *Science*, *270*(5234), 296-299.

Tasseva, G., Bai, H. D., Davidescu, M., Haromy, A., Michelakis, E., & Vance, J. E. (2013). Phosphatidylethanolamine deficiency in Mammalian mitochondria impairs oxidative phosphorylation and alters mitochondrial morphology. *Journal of Biological Chemistry*, *288*(6), 4158-4173.

Trouillard, M., Meunier, B., & Rappaport, F. (2011). Questioning the functional relevance of mitochondrial supercomplexes by time-resolved analysis of the respiratory chain. *Proceedings of the National Academy of Sciences*, *108*(45), E1027-E1034.

Trumpower, B. L. (2002). A concerted, alternating sites mechanism of ubiquinol oxidation by the dimeric cytochrome bc1 complex. *Biochimica et Biophysica Acta (BBA)-Bioenergetics*, *1555*(1-3), 166-173.

Tsiftsoglou, A. S., Tsamadou, A. I., & Papadopoulou, L. C. (2006). Heme as key regulator of major mammalian cellular functions: molecular, cellular, and pharmacological aspects. *Pharmacology & therapeutics*, *111*(2), 327-345.

Tsou, A. Y., Paulsen, E. K., Lagedrost, S. J., Perlman, S. L., Mathews, K. D., Wilmot, G. R., ... & Lynch, D. R. (2011). Mortality in Friedreich ataxia. *Journal of the neurological sciences*, *307*(1-2), 46-49.

Turrens, J. F. (2003). Mitochondrial formation of reactive oxygen species. *The Journal of physiology*, *552*(2), 335-344.

Vafai, S. B., & Mootha, V. K. (2012). Mitochondrial disorders as windows into an ancient organelle. *Nature*, *491*(7424), 374.

Varanasi, L., & Hosler, J. (2011). Alternative initial proton acceptors for the D pathway of Rhodobacter sphaeroides cytochrome c oxidase. *Biochemistry*, *50*(14), 2820-2828.

Veatch, J. R., McMurray, M. A., Nelson, Z. W., & Gottschling, D. E. (2009). Mitochondrial dysfunction leads to nuclear genome instability via an iron-sulfur cluster defect. *Cell*, *137*(7), 1247-1258.

Vinothkumar, K. R., Zhu, J., & Hirst, J. (2014). Architecture of mammalian respiratory complex I. *Nature*, *515*(7525), 80.

Vives-Bauza, C., Zhou, C., Huang, Y., Cui, M., De Vries, R. L., Kim, J., ... & Magrané, J. (2010). PINK1-dependent recruitment of Parkin to mitochondria in mitophagy. *Proceedings of the National Academy of Sciences*, *107*(1), 378-383.

Wang, Y., Langer, N. B., Shaw, G. C., Yang, G., Li, L., Kaplan, J., ... & Bloomer, J. R. (2011). Abnormal mitoferrin-1 expression in patients with erythropoietic protoporphyria. *Experimental hematology*, *39*(7), 784-794.

Wenz, T., Hielscher, R., Hellwig, P., Schägger, H., Richers, S., & Hunte, C. (2009). Role of phospholipids in respiratory cytochrome bc1 complex catalysis and supercomplex formation. *Biochimica et Biophysica Acta (BBA)-Bioenergetics*, *1787*(6), 609-616.

Whitnall, M., Rahmanto, Y. S., Huang, M. L. H., Saletta, F., Lok, H. C., Gutiérrez, L., ... & Ponka, P. (2012). Identification of nonferritin mitochondrial iron deposits in a mouse model of Friedreich ataxia. *Proceedings of the National Academy of Sciences*, *109*(50), 20590-20595.

Williams, S. L., Valnot, I., Rustin, P., & Taanman, J. W. (2004). Cytochrome c oxidase subassemblies in fibroblast cultures from patients carrying mutations in COX10, SCO1, or SURF1. *Journal of Biological Chemistry*, *279*(9), 7462-7469.

Wrighting, D. M., & Andrews, N. C. (2008). Iron homeostasis and erythropoiesis. *Current topics in developmental biology*, *82*, 141-167.

Xie, Y., Hou, W., Song, X., Yu, Y., Huang, J., Sun, X., ... & Tang, D. (2016). Ferroptosis: process and function. *Cell death and differentiation*, *23*(3), 369.

Xu, N., Cheng, X., Yu, Q., Zhang, B., Ding, X., Xing, L., & Li, M. (2012). Identification and functional characterization of mitochondrial carrier Mrs4 in Candida albicans. *FEMS yeast research*, *12*(7), 844-858.

Yang, W. S., & Stockwell, B. R. (2008). Synthetic lethal screening identifies compounds activating iron-dependent, nonapoptotic cell death in oncogenic-RAS-harboring cancer cells. *Chemistry & biology*, *15*(3), 234-245.

Yang, W. S., SriRamaratnam, R., Welsch, M. E., Shimada, K., Skouta, R., Viswanathan, V. S., ... & Brown, L. M. (2014). Regulation of ferroptotic cancer cell death by GPX4. *Cell*, *156*(1-2), 317-331.

Yankovskaya, V., Horsefield, R., Törnroth, S., Luna-Chavez, C., Miyoshi, H., Léger, C., ... & Iwata, S. (2003). Architecture of succinate dehydrogenase and reactive oxygen species generation. *Science*, *299*(5607), 700-704.

Yuan, X., Fleming, M. D., & Hamza, I. (2013). Heme transport and erythropoiesis. *Current opinion in chemical biology*, *17*(2), 204-211.

Zara, V., Conte, L., & Trumpower, B. L. (2009). Evidence that the assembly of the yeast cytochrome bc1 complex involves the formation of a large core structure in the inner mitochondrial membrane. *The FEBS journal*, *276*(7), 1900-1914.